Dissertation zur Erlangung des Doktorgrades
der Fakultät für Chemie und Pharmazie
der Ludwig-Maximilians-Universität München

Real time observation of TF function on translating ribosomes

Christian Malte Kaiser

aus

Hannover

2006

Erklärung

Diese Dissertation wurde im Sinne von § 13 Abs. 3 bzw. 4 der Promotionsordnung vom 29. Januar 1998 von Herrn Professor Dr. F. Ulrich Hartl betreut.

Ehrenwörtliche Versicherung

Diese Dissertation wurde selbständig, ohne unerlaubte Hilfen erarbeitet.

München, am ....

....

Christian Kaiser

Dissertation eingereicht am	04. April 2006
1. Gutachter:	Professor Dr. F. Ulrich Hartl
2. Gutachter:	PD Dr. Konstanze Winklhofer
Mündliche Prüfung am	24. Mai 2006

DANKSAGUNG

Die vorliegende Arbeit wurde in der Zeit von Oktober 2001 bis April 2006 in der Abteilung Zelluläre Biochemie, Prof. Dr. F. Ulrich Hartl, am Max-Planck-Institut für Biochemie, Martinsried, angefertigt.

Mein besonderer Dank gilt Herrn Prof. Dr. F. Ulrich Hartl für die Betreuung meiner Promotion, für die Überlassung des interessanten Themas und die Bereitstellung ausgezeichneter Arbeitsbedingungen. Seine stete Unterstützung und sein lebendiges Interesse an meiner Arbeit waren die Grundlage für das Gelingen dieser Arbeit.

Frau PD Dr. Konstanze Winklhofer danke ich für die Übernahme des Co-Referats.

Bei den Mitarbeitern der Abteilung Zelluläre Biochemie bedanke ich mich für ihre kollegiale Hilfe und eine gute Arbeitsatmosphäre. Allen voran danke ich Dr. Peter Breuer und Hung-Chun Chang, denen ich mich auch freundschaftlich verbunden fühle.

Besonders herzlich danke ich Dr. José M. Barral für die sehr gute, fruchtbare und außerordentlich freundschaftliche Zusammenarbeit. Durch seine fachliche Kompetenz und seinen Enthusiasmus hat er über die gesamte Zeit meiner Promotion für Motivation und Inspiration gesorgt und so wesentlich zum Gelingen dieser Arbeit beigetragen.

Für Inspiration außerhalb des Labors während meiner Doktorarbeit in München bin ich Helmut Dreschhoff und meinem langjährigen Weggefährten Marian Kalocay dankbar.

Meiner Partnerin Christiane Dreisbusch danke ich von ganzem Herzen für ihre bedingungslose liebevolle Unterstützung, die mich durch die späteren Phasen meiner Promotion getragen hat.

Schließlich danke ich ganz besonders meiner Familie, insbesondere meinem Bruder Philipp Kaiser und meiner Mutter Ilse Kaiser, die nie müde wurde, mich Zeit meines Lebens zu unterstützen. Ohne ihre Hilfe und ihren Rückhalt wäre diese Arbeit nicht möglich gewesen.

CONTENTS

I SUMMARY 1

II INTRODUCTION 4
II.1 Protein structure and principles of protein folding *in vitro* 4
II.2 Protein synthesis and folding in the cell 8
II.3 Molecular chaperones 10
II.4 Chaperone systems in the cytosol 12
  II.4.1 Ribosome-associated chaperones 13
  II.4.2 The Hsp70 system 15
  II.4.3 The chaperonins 17
  II.4.4 Additional chaperone systems 19
II.5 Protein synthesis on the ribosome and early events in *de novo* protein folding .. 21
  II.5.1 The ribosome 21
  II.5.2 Translation and folding 24
  II.5.3 Trigger factor 25
II.6 Aim of this study 33

III MATERIALS AND METHODS 34
III.1 Chemicals 34
III.2 Materials and Instruments 35
III.3 Buffers and Media 36
  III.3.1 Buffers 36
  III.3.2 Media 38
III.4 DNA manipulations 40
  III.4.1 General Procedures 40
  III.4.2 Cloning of TF-expression constructs 41
  III.4.3 Cloning of the TF deletion mutant NC 42
  III.4.4 Cloning of the human titin I27 domain 43
  III.4.5 Site-directed mutagenesis 43
  III.4.6 Generation of linear template DNA for *in vitro* translation reactions 44
III.5 Protein preparative methods 45
  III.5.1 Purification of TF 45
  III.5.2 Purification of TEV protease 46
  III.5.3 Isolation of ribosomes 46
  III.5.4 Site-specific labeling of TF single cysteine mutants 47
  III.5.5 Differential labeling of TF double cysteine mutant proteins 48
III.6 Protein analytical methods 49
  III.6.1 Quantitation of protein concentrations 49
  III.6.2 Quantitation of accessible thiol groups and determination of thiol reactivity ... 49
  III.6.3 SDS-PAGE 50
  III.6.4 Western Blotting 51
  III.6.5 Autoradiography 51
  III.6.6 Protein production in the reconstituted system 52
  III.6.7 Limited proteolysis 52
  III.6.8 Determination of FL specific activity 52

III.7 Fluorescence Measurements 54
III.7.1 General 54
III.7.2 Equilibrium fluorescence measurements 54
III.7.3 Kinetic fluorescence measurements 55
III.7.4 Competition experiments 55
III.7.5 Steady state fluorescence anisotropy measurements 56
III.8 Ribosome tagging 57
III.8.1 Generation of *rpl-FH-tetR* cassettes 57
III.8.2 Chromosomal integration of *rpl-FH-tetR* cassettes 58
III.8.3 P1-transduction 59
III.8.4 Preparation of *E. coli* lysates for analytical ribosome isolations 60
III.8.5 Sedimentation analysis of *E. coli* ribosomes 61
III.8.6 Ribosome pull-downs using anti-FLAG agarose 62
III.8.7 Ribosome pull-downs using magnetic beads 62
III.9 Data Evaluation and Calculations 63
III.9.1 FRET efficiency and distance calculations 63
III.9.2 Determination of Förster distances 64
III.9.3 Calculation of steady state fluorescence anisotropies 66
III.9.4 TF monomer-dimer equilibrium 67
III.9.5 TF-ribosome equilibrium 68
III.9.6 K_D determination from Trp-fluorescence 68
III.9.7 K_D determination from BADAN fluorescence 69
III.9.8 K_D determination from steady state fluorescence anisotropy 70
III.9.9 Calculation of inter-molecular distances 71
III.9.10 Calculation of intra-molecular distances 72
III.9.11 Kinetic evaluation 72
III.9.12 Assignment of the mean hydrophobicity to residues in protein sequences ... 73

IV RESULTS 74
IV.1 TF undergoes a conformational change upon binding to the ribosome 74
IV.2 TF exists predominantly as a dimer when not bound to the ribosome 79
IV.3 Translation of FL results in increased recruitment of TF to the ribosome 85
IV.4 Translation results in increased affinity of TF for the ribosome-nascent chain complex 90
IV.5 Kinetic analysis of TF-ribosome complex dissociation 92
IV.6 TF interacts with its substrate after ribosome departure and does not rebind post-translationally 95
IV.7 The properties of the nascent chain modulate its interaction with TF 98
IV.8 Hydrophobic motifs in the substrate determine TF displacement kinetics 100
IV.9 The ability of a nascent chain to fold co-translationally determines the extent of TF recruitment to the ribosome 103
IV.10 The TF PPIase domain contributes to substrate interaction but is dispensable for the initial binding step 107
IV.11 The ribosomal proteome: Identification of factors that might cooperate with TF or substitute for TF function in a *Δtig* background 113
IV.11.1 Introduction of a FLAG-His_6 epitope tag into genes encoding large ribosomal proteins and assessment of their assembly into intact ribosomes 113
IV.11.2 The FH tag can be introduced into ribosomal protein L17 at the chromosomal level 119
IV.11.3 Additional ribosome-associated proteins can be pulled down under conditions that stabilize ribosome-nascent chain complexes 122

V DISCUSSION 125
V.1 Structural rearrangements within TF upon ribosome binding 125
V.2 Kinetic characterization of the TF-ribosome interaction 128
V.3 TF is recruited to translating ribosomes 129
V.4 TF regulation by the nascent chain 132
V.5 The TF PPIase domain contributes towards substrate binding, but is not essential for TF function 134
V.6 The dynamic cycle of TF function 135
V.7 Factors that work in concert with TF or compensate for its loss of function ... 136

VI REFERENCES 139

VII APPENDICES 155
VII.1 Primer sequences and features 155
VII.2 Plasmid maps and protein sequences 158
VII.3 Abbreviations 162
VII.4 *Curriculum vitae* 164

I SUMMARY

To become biologically active, most proteins need to fold into precise three-dimensional, or native, structures. Molecular chaperones assist the folding of newly synthesized and denatured proteins in acquiring their native state in the crowded intracellular environment. Trigger factor (TF), a 48 kDa protein that is present only in bacteria, is the first chaperone to interact with the nascent polypeptide chain as soon as it emerges from the ribosome. TF has a modular structure comprised of an amino-terminal ribosome binding domain, a middle peptidyl-prolyl isomerase (PPIase) domain and a carboxyl-terminal domain. In its tertiary structure, the carboxyl-terminal domain links the amino-terminal and the PPIase domains and constitutes, together with the amino-terminal domain, a potential substrate binding region. TF binds to the large ribosomal subunit in the vicinity of the ribosomal exit tunnel and is capable of forming homo-dimers while free in solution. The ATP-dependent Hsp70 homolog DnaK, regulated by its co-factors DnaJ and GrpE, acts on nascent polypeptides subsequently to TF. Nucleotide binding has not been observed for TF, and there are no known co-factors that regulate TF function.

In the present study, the mechanism by which TF aids the folding of newly synthesized proteins was investigated utilizing fluorescence spectroscopy techniques. By measuring intra-molecular fluorescence resonance energy transfer (FRET) between exogenous fluorophores attached site-specifically to TF, it was shown that binding to the ribosome causes a conformational aperture within TF. This structural rearrangement may position the substrate-binding region in a state competent to receive the polypeptide nascent chain. Ribosome binding of TF can be followed by means of an environmentally sensitive fluorophore covalently linked to the TF molecule. Conformational compaction and release of TF from non-translating ribosomes were found to occur concomitantly, with a half-time of $t_{1/2} \approx 10$ s. The TF dimer was characterized utilizing the single tryptophan within TF as an endogenous probe and exogenous fluorophores introduced at specific sites, which allowed the measurement of inter-molecular FRET. The protomers within the TF dimer were found to be arranged in a nearly perpendicular fashion, with the proposed substrate binding region occluded in the dimer. These results suggest that TF cycles between an inactive, dimeric form and a ribosome-bound monomeric form in which the substrate binding region is exposed.

The dynamics of TF interactions with ribosomes actively engaged in translation and the resulting nascent polypeptide chains were analyzed utilizing a novel approach involving a reconstituted transcription/translation system. Translation of various model substrates resulted in enhanced ribosome recruitment of TF, indicating that the affinity of TF for ribosome-nascent chain complexes is ~30 fold higher than for vacant ribosomes. The analysis of a TF deletion mutant lacking the PPIase domain revealed that the PPIase domain serves as a secondary substrate binding site, in addition to the main substrate binding region constituted by the amino- and the carboxyl-terminal domains.

During translation of firefly luciferase (FL), a previously characterized TF substrate, the kinetics of ribosome release were found to be unaltered, whereas the conformational compaction event took place with $t_{1/2} \approx 36$ s. The delay in conformational compaction kinetics over ribosome release that was observed during FL translation suggests that TF stays associated with the nascent chain after vacating the ribosomal binding site, thus allowing the loading of another TF molecule onto the same nascent chain. These findings were supported by kinetic analysis of steady state fluorescence anisotropy of fluorescently labeled TF. Translation of substrates other than FL revealed that the half-time of TF molecular compaction correlates well with the occurrence of motifs of high hydrophobicity on the nascent polypeptide chain. TF-substrate interaction is prolonged for nascent chains exposing sequences of high mean hydrophobicity. Moreover, by analyzing the extent of TF recruitment to the ribosomes containing stalled nascent chains that had folded to various degrees, it was found that folding and burial of the hydrophobic elements result in the release of TF from the substrate.

Taken together, the results suggest a model of TF mechanism: In solution, monomeric and dimeric TF are in rapid equilibrium. Ribosome-binding stabilizes the monomeric form and induces a conformational aperture within TF, presumably resulting in proper sub-domain alignment in preparation for interaction with the emerging nascent chain. This activation by ribosome docking topologically restricts the TF chaperone function to nascent polypeptide chains. Without translation, TF goes through a default cycle with a mean residence time on the ribosome of ~10 s before detachment from the ribosome and relaxation to its compact conformation. During translation, interaction with the elongating polypeptide stabilizes the open conformation beyond TF ribosome-detachment. TF remains associated with its substrates for varying periods of time, dependent on their properties. This prevents misfolding events from occurring in its substrates and allows a second TF-molecule to be loaded onto longer nascent chains. TF then dissociates from its substrate either co- or post-translationally and relaxes to its

compact conformation. Dimerization leads to occlusion of the substrate binding region and serves to maintain a pool of TF that can readily be activated by ribosome-binding.

The mechanism suggested in the present study explains the previously observed function of TF in delaying folding and misfolding events relative to translation *in vivo*. It may serve as a paradigm for regulation of nucleotide-independent chaperones. The novel approach developed in the present study provides opportunities to identify and characterize additional factors that may assist in protein folding at the ribosome under a wide variety of conditions, including in the absence of TF.

II INTRODUCTION

II.1 Protein structure and principles of protein folding *in vitro*

Proteins are linear polymers of up to 20 different amino acids (aa). All amino acids contain an amino- and a carboxyl-group covalently linked to a central C_α-atom. In addition, a functional group (or a hydrogen atom) is coupled to the C_α-atom, which is different for each amino acid. In a condensation reaction, amino acids can polymerize to polypeptides (or proteins) *via* the formation of a planar peptide bond. The peptide bonds form what is referred to as the backbone of the protein.

In all organisms of all kingdoms of life, proteins play a pivotal role in all cellular processes, such as maintenance of cellular structure and integrity, inter- and intra-cellular communication, metabolism and transport. To fulfill these functions, proteins must adopt specific three-dimensional structures, which are very diverse, including fibrillar shapes of structural proteins, globular structures of some metabolic enzymes and channels traversing membranes in energy producing systems. The process by which a protein acquires its unique three-dimensional structure is called protein folding.

To describe protein structure, four hierarchical levels are distinguished: The primary structure is the sequence of the different amino acids. The secondary structure refers to common repeating structures found in many proteins. The two most common secondary structural elements are the α-helix and the β-pleated sheet. The tertiary structure describes the overall structure of the folded polypeptide chain, including the arrangements of secondary structural elements. The quaternary structure constitutes the arrangement of subunits in an assembly of two or more proteins.

Many proteins are organized in a modular fashion. These modules are referred to as domains, which are typically 100–300 aa in length, and are structurally and functionally distinct units (Doolittle 1995; Orengo *et al.* 1994). Linking two or more domains on the primary structure level has facilitated the evolution of polypeptides with novel functions (Kummerfeld & Teichmann 2005). Multi-domain proteins occur in all kingdoms of life, although they are more abundant in eukaryotes than in prokaryotes (65% *vs.* 40%, respectively) (Ekman *et al.* 2005).

Pioneering experiments on protein folding were performed in the late 1960's by Anfinsen and co-workers. Purified, denatured Ribonuclease A was shown to be able to regain its native state in solution upon removal of denaturant, as measured by its enzymatic activity, in a spontaneous and unaided fashion (Anfinsen 1972; Anfinsen 1973; Taniuchi & Anfinsen 1969). These experiments demonstrated that the information defining the tertiary structure of a protein is contained within its amino acid sequence. The native tertiary structure is the polypeptide conformation with the lowest free energy. The spontaneous folding process was found to be reversible and occurred on a biologically relevant time scale (Schechter *et al.* 1970).

Usually, folding does not involve the formation or breakage of covalent bonds. Rather, the polypeptide is conformationally flexible through rotation around single bonds. The natively folded structure is stabilized by a multitude of weak interactions, such as hydrogen bonds and hydrophobic and ionic interactions. Considering only the protein backbone, rotation can occur around the axis formed by the C_α and the carboxyl carbon as well as around the axis formed by the C_α and the amino nitrogen, described by the angles Ψ and Φ, respectively. No rotation can occur around the axis formed by the peptide bond due to its planar nature. Thus, the conformation of the backbone can be described by a pair of angles, Ψ and Φ, for each peptide bond. It was found that two of the numerous possible pairs of Ψ and Φ occur with a high frequency in natively folded proteins (Ramachandran & Sasisekharan 1968). These two pairs of angles are referred to as the α- and the β-conformation.

Levinthal performed mathematical calculations regarding the time that would be required for a protein to adopt its native structure if the folding process were a completely random process. If only the two most stable backbone conformations, α and β, are considered, a hypothetical protein of 150 aa in length can adopt $\sim 10^{30}$ different conformations. Taking into account that the fastest possible rate for conformational changes is $\sim 10^{11}$ s^{-1}, it would take the hypothetical protein more than 10^{11} years to reach its native structure (Dinner *et al.* 2000; Levinthal 1969). The discrepancy between the estimated time for random folding and the observed fast folding of proteins is called the Levinthal paradox. It led to the conclusion that a protein cannot fold by sampling the entire available conformational space randomly. Rather, the efficient folding must proceed through transient intermediates, in which local folded elements are stabilized and determine further folding of the polypeptide (Baldwin 1996; Baldwin & Rose 1999; Levinthal 1969; Privalov 1996). These intermediates would greatly reduce the number of possible conformations during folding, defining steps of a folding pathway through the random folding space, and thus allow protein folding to take place on a biologically relevant time scale. Indeed, folding intermediates were observed for various model proteins, such as Apomyoglobulin, Ribonuclease A, Barstar and Lysozyme (Agashe *et al.* 1995; Jamin & Baldwin 1996; Radford *et al.* 1992; Udgaonkar & Baldwin 1990; Wildegger & Kiefhaber 1997).

Several models have been suggested to describe general folding mechanisms (Daggett & Fersht 2003). One of the models, the "hydrophobic collapse" model, suggests that a rapid collapse of the polypeptide chain provides a confined environment for folding to proceed rapidly (Baldwin 1989; Schellman 1955). In the "framework model" (Kim & Baldwin 1982; Kim & Baldwin 1990; Ptitsyn & Rashin 1975), secondary structural elements from first and then coalesce with others to from the final tertiary structure of the native protein. Later, some model proteins were found to fold *via* a simple two-state mechanism, without the formation of intermediate structures, *e.g.* chymotrypsin inhibitor 2 (Jackson & Fersht 1991). The observations made with chymotrypsin inhibitor 2 led to the formulation of a "nucleation condensation" mechanism, which unifies the framework and the hydrophobic collapse models. It suggests that both hydrophobic interactions and secondary structural elements stabilize the transition state (Fersht 1997).

Another example of a two-state folding mechanism is provided by the bacterial immunity protein Im9 (Ferguson *et al.* 1999). Interestingly, the analysis of the structurally highly homologous proteins Im7 and Im9 revealed that small alterations in amino acid sequence can lead to a change in the folding mechanism: Whereas Im9 folds mainly *via* a two state-mechanism, stabilized folding intermediates were observed for Im7 (Ferguson *et al.* 1999; Paci *et al.* 2004). This demonstrated that the folding kinetics depend on the exact polypeptide sequence rather than on the overall stability or tertiary structure of the native protein.

The development of new methodologies that allow monitoring of protein folding *in vitro* has yielded insight into folding mechanisms of various model proteins (Brockwell *et al.* 2000). In combination with the different experimental approaches, Φ-value analysis (Fersht *et al.* 1992) and molecular dynamics simulations (Ferguson & Fersht 2003; Vendruscolo & Dobson 2005) have provided detailed insights into folding mechanism. However, most of the analyses are still limited to relatively small proteins of typically less than 100 aa.

Detailed kinetic analysis, monitoring the folding of several small protein by various techniques, has led to the description of protein folding in terms of an "energy landscape" or "folding funnel" (Baldwin 1995; Radford *et al.* 1992) (see Figure 1). The energy landscape is a three- or multi-dimensional surface representing the free energy of a polypeptide molecule as a function of two or more variables, *e.g.* conformational parameters. Each point on the energy surface represents a conformation of the polypeptide and the corresponding free energy. The native state of a protein, defined as the conformation with the lowest free energy, is thus the lowest point in the energy landscape, or the bottom of the funnel. During folding, the protein follows a route from the rim of the funnel, representing a disordered, denatured state, to the bottom of the funnel. Populated intermediates on the way from the unfolded to the native protein are local minima in the energy landscape (Radford 2000; Schultz 2000; Troullier *et al.* 2000). If the folding polypeptide cannot escape a local minimum, it becomes kinetically trapped and eventually misfolds in an off-pathway reaction. The actual pathway along which a protein folds is dependent on the environment in which the folding reaction takes place.

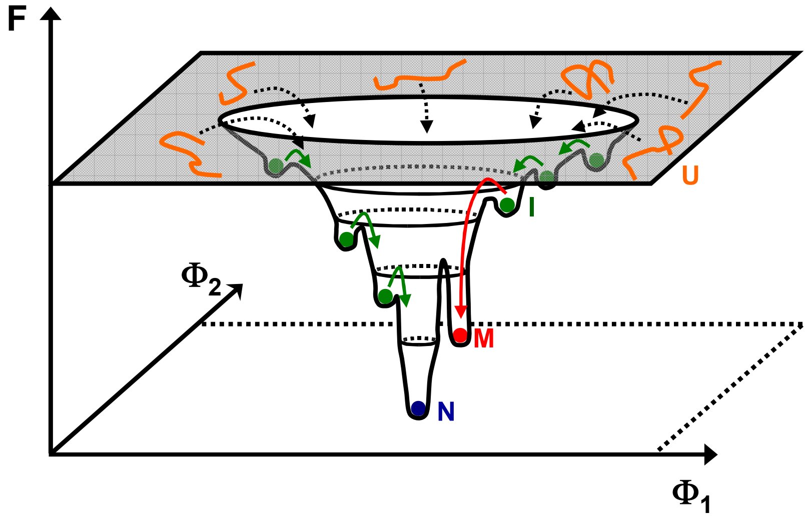

Figure 1: Schematic representation of the free energy landscape of a folding protein.

The free energy (E) is displayed as a function of two reaction coordinates (Φ_1 and Φ_2) which describe the conformation of the folding protein. A multitude of unfolded conformations (U, orange) on the top enter the funnel that contains an almost indefinite number of local energy minima, representing folding intermediates (I, green). The folding protein proceeds then through local minima towards the native conformation (N, blue), which has the lowest free energy. In some local minima, misfolded species may be trapped irreversibly (M, red).
From Schultz 2000, modified.

II.2 Protein synthesis and folding in the cell

In vitro refolding experiments are usually carried out by transferring the purified, unfolded protein from denaturant to non-denaturing solutions that allow folding under well defined conditions, such as temperature, pH, protein concentration and ionic strength and composition. These conditions are optimized for a given protein and can vary greatly from one protein to another. Protein folding in the cell differs in many respects from *in vitro* refolding. The polypeptide is synthesized in a vectorial fashion on the ribosome at a rate of 4 – 20 aa *per* second (Bremer & Dennis 1996; Mathews *et al.* 2000). Thus, not all of the polypeptide sequence becomes available for folding at once, in contrast to *in vitro* refolding. The environment that is met by the newly synthesized polypeptide is a crowded one, with a concentration of ~300 mg/ml of macromolecules, and all proteins (within the same cellular compartment) have to fold under similar conditions. For many proteins, these conditions do not favor productive spontaneous folding, but rather promote unproductive side reactions such as aggregation (Ellis 2001; Hartl 1996).

Most soluble, native proteins contain a hydrophobic core that stabilizes their tertiary structure, since the hydrophilic environment of aqueous solutions favors the clustering and burial of hydrophobic regions. These hydrophobic regions are exposed in unfolded proteins, which can lead to inter-molecular clustering and subsequently to protein aggregation. Although there are molecular machines that are capable of re-solubilizing protein aggregates in the cell (Ben-Zvi & Goloubinoff 2001; Weibezahn *et al.* 2005), aggregation is often irreversible, rendering the aggregated proteins permanently inactive. Thus, there is a competition between productive folding on the one hand and aggregation on the other.

The high intracellular concentration of macromolecules results in changes in the thermodynamic properties of the unfolded polypeptide chains, favoring the aggregation reaction over spontaneous folding. The excluded volume or molecular crowding theory describes how high concentrations of macromolecules affect protein folding and aggregation (Ellis 2001; Minton 2001). The high concentration of solutes, which occupy a large fraction of the available volume, results in increased chemical activities and diffusion coefficients of the solutes. Due to the exclusion of volume, small, compact structures are favored over large, extended ones. Thus, unfolded proteins will tend to compact either intra-molecularly, *i.e.* by folding into a compact native state, or by aggregation. In addition to these volume effects, macromolecules in the cytosol often expose hydrophobic surfaces which promote aggregation. Aberrant folding and aggregation in the cell does not only lead to inactivation of the affected proteins, but can result in severe cellular dysfunction, resulting in, for instance, a number of human diseases (Barral *et al.* 2004).

Over the past two decades, factors have been identified and studied that assist non-native proteins in folding under cellular conditions. This group of molecules is referred to as molecular chaperones (Martin & Hartl 1993). Molecular chaperones interact with non-native polypeptides and prevent their misfolding and aggregation. They contribute towards successful folding to the native structure without providing specific conformational information to the folding process, in agreement with the conclusion reached by Anfinsen that the tertiary structure of a protein is solely determined by its own amino acid sequence (Anfinsen 1973). Importantly, molecular chaperones are not part of the folded, biologically active structure.

II.3 Molecular chaperones

In order to overcome the challenges of protein folding in the crowded intracellular environment, all organisms have evolved a large arsenal of molecular chaperones (Hartl & Hayer-Hartl 2002; Young *et al.* 2004). They contribute both to the *de novo* folding of newly synthesized proteins and to the rescue of stress-denatured existing proteins. Due to the latter function, the expression of many chaperones is up-regulated in response to stress-stimuli, such as elevated temperature or oxidative stress. These chaperones are called heat shock proteins (Hsp's).

Chaperones usually bind their substrates through regions that are normally buried in native proteins, *e.g.* exposed hydrophobic segments and unstructured backbone regions. The burial of these elements in the folded structure prevent chaperones from binding native proteins. Many chaperones act on their substrates in repeated cycles of binding and release, often in a nucleotide-dependent fashion. In this manner, unfolded proteins are prevented from interacting non-productively with each other and from forming aggregates. The formation of kinetically trapped folding intermediates is thus prevented or may even be reversed. Generally, two mechanisms of chaperone action are distinguished: Chaperones may bind their substrate and hold it in a folding-competent state, so that it can fold upon release (*e.g.* Trigger factor (TF) or the Hsp70 chaperones). In contrast, the cylindrical chaperonins, or Hsp60s, sequester their substrates into a central cavity, providing a protected environment in which the protein is allowed to fold. By favoring the productive folding into the native tertiary structure and preventing non-productive side-reactions, molecular chaperones often increase the yield of folding reactions. The rate of the folding reaction is not necessarily increased, in fact, the folding speed often is decreased (Agashe *et al.* 2004). This constitutes a main difference between molecular chaperones and proteins with enzymatic activities in the classical sense.

Catalysis of protein folding is observed in the cases of isomerization reactions. Peptidyl-prolyl isomerases (PPIases) accelerate the folding by catalyzing the often rate limiting step of prolyl-isomerization during protein folding (Schmid 1995; Schmid 2001). Recently, a non-prolyl peptide bond *cis-trans* isomerase activity for DnaK, the bacterial Hsp70 homolog, has been described (Schiene-Fischer *et al.* 2002). Protein disulfide isomerases catalyze disulfide bond formation of proteins in the endoplasmic reticulum of eukaryotic cells and the bacterial periplasm (Freedman *et al.* 2002; Wilkinson & Gilbert

2004). Often, these activities are combined with chaperone functions (Schiene & Fischer 2000).

Transient incorporation of a chaperone into the folded structure of its substrate has been observed in particular cases for peptide-bond *cis-trans* isomerization and disulfide bond formation (Schiene & Fischer 2000; Schiene-Fischer *et al.* 2002). The periplasmic chaperone FimC stays associated with its substrate FimG after folding and regulates its assembly into pilus structures (Vetsch *et al.* 2004). Folding of subtilisin is mediated by its pro-peptide, which acts as an intra-molecular chaperone. After folding, subtilisin stays associated with its chaperone, before the latter one is proteolytically removed to yield the mature enzyme (Shinde *et al.* 1997).

II.4 Chaperone systems in the cytosol

All organisms contain a large arsenal of molecular chaperones that are crucial for efficient protein folding. According to certain properties, chaperones can be grouped into classes of functionally and structurally related proteins. An overview of different chaperone systems involved in *de novo* folding is shown in Figure 2. Depending on the folding properties of the substrate protein, it may require assistance from one or more molecular chaperones or fold in a mostly unassisted manner. The interplay among the different chaperone systems during protein folding is becoming increasingly better understood, leading to the perception that molecular chaperones are organized to form a functional network (Hartl & Hayer-Hartl 2002; Young *et al.* 2004).

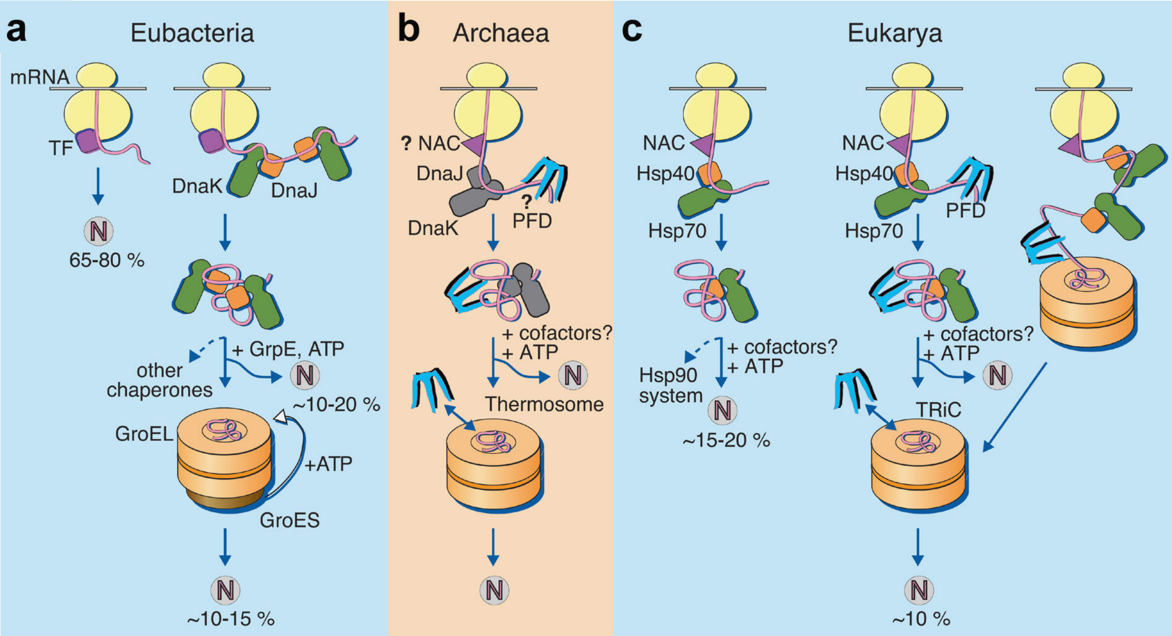
a
Eubacteria
mRNA
TF
N
65-80 %
DnaK
DnaJ
other chaperones
+ GrpE, ATP
N
~10-20 %
GroEL
+ATP
GroES
N
~10-15 %
b
Archaea
? NAC
DnaJ
DnaK
?
PFD
+ cofactors?
+ ATP
N
Thermosome
N
c
Eukarya
NAC
Hsp40
Hsp70
+ cofactors?
+ ATP
Hsp90 system
N
~15-20 %
NAC
Hsp40
PFD
Hsp70
+ cofactors?
+ ATP
N
TRiC
N
~10 %

Figure 2: Chaperone systems involved in de novo protein folding

N: Natively folded protein, NAC: nascent chain associated complex, PFD: prefoldin, TF: Trigger factor. **a.** Eubacteria. Interaction with TF is a general feature of all nascent chains. The majority of proteins (65–80%) fold without further assistance. DnaK assists the remainder of the proteins through one or several cycles of substrate binding and release. Chaperonin substrates are further transferred to GroEL. **b.** Archaea. The DnaK/DnaJ-system is not present in all archaeal species. The occurrence of archaeal NAC and the interaction of PFD with nascent chains has not yet been experimentally verified. **c.** The mammalian cytosol as a paradigm for eukarya. NAC probably interacts with nascent chains. Hsc70 is recruited to the ribosome by the recently discovered zuotin-homolog Mpp11 (not shown). Most proteins fold upon release from these factors. A fraction of the Hsp70 substrates is transferred to Hsp90. PFD mediates the transfer of polypeptides to TRiC co- or post-translationally. From Hartl & Hayer-Hartl, 2002.

II.4.1 Ribosome-associated chaperones

Proteins are synthesized in a vectorial fashion by the ribosome, from which they emerge through an exit tunnel. The elongating protein chain is referred to as the nascent (polypeptide) chain. Before the synthesis of an entire protein or domain is complete, the nascent chain cannot undergo the highly co-operative process of folding. Thus, nascent chains emerging from the ribosome may expose non-native features until synthesis of the protein/domain is complete, which renders them prone to aggregation. Additionally, a high local concentration of nascent chains on polyribosomes further increases the risk of aggregate formation (Frydman 2001).

Ribosome-associated chaperones prevent misfolding and aggregation of newly synthesized proteins. In eubacteria, trigger factor (TF) is the first chaperone to bind to the nascent chain. TF is a 48 kDa chaperone with PPIase activity (Hesterkamp & Bukau 1996). The latter is, however, dispensable for TF chaperone function *in vivo* (Genevaux *et al.* 2004; Kramer *et al.* 2004). TF associates with ribosomes in a 1:1 stoichiometry, mainly through interaction with the ribosomal protein L23 in the vicinity of the ribosomal exit tunnel (Blaha *et al.* 2003; Ferbitz *et al.* 2004; Kramer *et al.* 2002). TF associates with nascent chains independently of proline residues (Patzelt *et al.* 2001) as soon as they emerge from the ribosomal exit tunnel. The cytosolic concentration of TF (~40–50 µM) exceeds that of ribosomes (~30µM) (Bremer & Dennis 1996; Lill *et al.* 1988), so that ribosome-bound TF is in an equilibrium with free TF. The TF-substrate complex dissociates after release from the ribosome (Agashe *et al.* 2004; Hesterkamp *et al.* 1996). A nucleotide-dependent regulation of TF-substrate interaction has not been observed, and TF does not contain regions with similarities to known nucleotide binding domains.

Another bacterial chaperone system that was found to associate with nascent chains is the Hsp70 system DnaK/DnaJ (see below). DnaK interacts with ~15% of nascent polypeptides. This fraction is increased to ~40 % in *E. coli Δtig* cells devoid of TF (Deuerling *et al.* 2003; Deuerling *et al.* 1999; Teter *et al.* 1999), suggesting a functional overlap between TF and the DnaK-system. The functional redundancy of the two systems is further supported by the analysis of bacterial strains carrying gene deletions of these systems: Individual deletions of the *tig* and *dnaK* genes encoding TF and DnaK, respectively, are tolerated and allow cell growth at 37 °C. The combined deletion, however, leads to pronounced protein aggregation in the cytosol and lethality at temperatures above 30 °C (Genevaux *et al.* 2004; Vorderwulbecke *et al.* 2004). Other factors can potentially compensate for the loss of TF and DnaK (Ullers *et al.* 2004;

Vorderwulbecke *et al.* 2004). However, the simultaneous depletion of TF and DnaK results in important mechanistic consequences, apparent in a shift from an efficient post-translational pathway to a rapid, but inefficient co-translational folding mechanism (Agashe *et al.* 2004). In contrast to TF, DnaK is not known to associate specifically with ribosomes. Rather, binding to nascent chains mediates the association of DnaK with ribosome nascent chain complexes (RNC's).

Whereas a gene encoding TF is present in all eubacterial genomes analyzed, no TF homolog has been found in eukarya. Instead, the eukaryotic cytosol contains a heterodimeric complex called NAC (nascent polypeptide associated complex), consisting of αNAC (33 kDa) and βNAC (22 kDa) (Shi *et al.* 1995; Wiedmann *et al.* 1994). NAC has a function similar to TF in that it binds to short nascent chains and dissociates from them upon release from the ribosome (Beatrix *et al.* 2000; Hartl 1996). It appears to be involved in targeting nascent chains to the endoplasmic reticulum (Wiedmann *et al.* 1994). The analysis of a heterologous complex of NAC with prokaryotic ribosomes revealed that a conserved motif within βNAC mediated binding to the ribosome (Wegrzyn *et al.* 2005). Recently, the docking site of NAC could be mapped to the ribosomal protein L25, which is the eukaryotic homolog of L23 in bacteria (Grallath *et al.* 2006). NAC has been observed to prevent aggregation in *in vitro* experiments (Grallath *et al.* 2006), thus exhibiting certain chaperone-like properties.

The eukaryotic model organism *Saccharomyces cerevisiae* contains another hetero-dimer, termed RAC (ribosome associated complex), that associates with RNC's. RAC consists of Ssz1, a member of the Hsp70 family, and the DnaJ-related Hsp40 protein zuotin (Gautschi *et al.* 2001; Gautschi *et al.* 2002; Michimoto *et al.* 2000). Zuotin contains a J-domain for interaction with Hsp70's, and a separate ribosome-binding domain (Yan *et al.* 1998). Zuotin is the partner Hsp40 protein for the Hsp70-class chaperones Ssb1 and Ssb2 (Bukau *et al.* 2000; Yan *et al.* 1998). The Ssb proteins are found both on the ribosome (Nelson *et al.* 1992; Pfund *et al.* 1998) and free in the cytosol (Siegers *et al.* 2003). Mutations in the J-domain of zuotin or the deletion of the *Ssz1* gene, but not an Ssz1 truncated mutant lacking the putative substrate binding domain, result in the same phenotype that is observed upon deletion of the *Ssb* genes, indicating that RAC is required for the recruitment of the Ssb-proteins to the ribosome (Gautschi *et al.* 2002; Hundley, H. *et al.* 2002). Ssz does not appear to be involved in nascent chain binding (Hundley, H. *et al.* 2002) and its function does not seem to rely on ATPase activity (Huang *et al.* 2005). Ssz1 may act as a modulator of zuotin rather than as a chaperone itself (Huang *et al.* 2005).

In mammals, the constitutively expressed heat shock cognate protein (Hsc70), a member of the Hsp70 protein family, has been found to associate with nascent polypeptides and promotes their co-translational folding (Beckmann *et al.* 1990; Eggers *et al.* 1997; Frydman *et al.* 1994), possibly in co-operation with the Hsp40 homologs Hdj1 and Hdj2 (Nagata *et al.* 1998; Terada *et al.* 1997). Hsc70 is probably recruited to the ribosome by the recently identified human zuotin ortholog Mpp11, which illustrates that ribosome-tethered chaperones have been conserved throughout evolution (Hundley, H. A. *et al.* 2005).

II.4.2 The Hsp70 system

Members of the Hsp70 family of proteins are found in all bacteria and eukaryotes as well as in some, but not all archaea (Hartl & Hayer-Hartl 2002; Laksanalamai *et al.* 2004; Leroux 2001; Young *et al.* 2004). They are located in the cytosol in both bacteria and eukaryotes as well as in eukaryotic organelles, *e.g.* mitochondria and the endoplasmic reticulum. The most thoroughly studied *E. coli* Hsp70 is DnaK. It plays a central role in the modulation of the σ^{32} mediated heat shock response in *E. coli*, which is the best characterized example of heat shock regulated protein expression (Lund 2001). Eukaryotic organisms usually contain several cytosolic Hsp70 proteins. The yeast *S. cerevisiae* contains four free cytosolic Hsp70 proteins (Ssa1 to 4). Higher eukaryotes have a constitutively expressed Hsp70 homolog (Hsc70) in addition to the stress-inducible form.

Hsp70's bind to stretches of extended polypeptides rich in hydrophobic residues, usually exposed only in non-native proteins, *via* hydrogen-bonds with the peptide backbone and hydrophobic interactions with the side-chains. In this manner, aggregation and misfolding of the substrate polypeptide is prevented. Substrate binding and release occur in an ATP-dependent fashion, modulated by accessory proteins or co-factors.

Hsp70 chaperones are monomeric proteins of ~70 kDa in size, composed of a ~45 kDa amino terminal ATPase domain and a ~25 kDa carboxyl-terminal polypeptide binding domain. The structures of the individual domains of DnaK have been solved separately (Harrison *et al.* 1997; Zhu *et al.* 1996), and recently, the structure of a full-length Hsp70 homolog, bovine Hsc70, has been determined (Jiang *et al.* 2005), providing detailed structural insight into inter-domain interactions important for Hsp70 chaperone function.

The mechanism of Hsp70 function is best understood for the DnaK system (Hartl & Hayer-Hartl 2002; Mayer & Bukau 2005; Naylor & Hartl 2001) (see Figure 3). In the

ATP-bound state, the substrate binding cleft is in an open conformation, allowing rapid substrate association and dissociation. The affinity of the DnaK-ATP-complex for substrate is relatively low. Hydrolysis of ATP to ADP leads to large structural rearrangements within DnaK, resulting in closing of the substrate binding pocket and stable substrate association. The cycling of DnaK between an ATP-bound state with low affinity and an ADP-bound state with high affinity for the substrate is modulated by DnaJ and GrpE co-factors. DnaJ, a monomeric 41 kDa protein of the Hsp40 class, binds to DnaK through its amino-terminal J-domain and stimulates the ATPase activity of DnaK, enhancing stable peptide binding. DnaJ contains a carboxyl-terminal binding site for hydrophobic peptides and can thus deliver unfolded proteins to DnaK. GrpE acts as a nucleotide exchange factor on DnaK, inducing the rapid release of ADP from DnaK. Rebinding of ATP to DnaK leads to decreased affinity and release of the substrate, completing the DnaK functional cycle (see Figure 3).

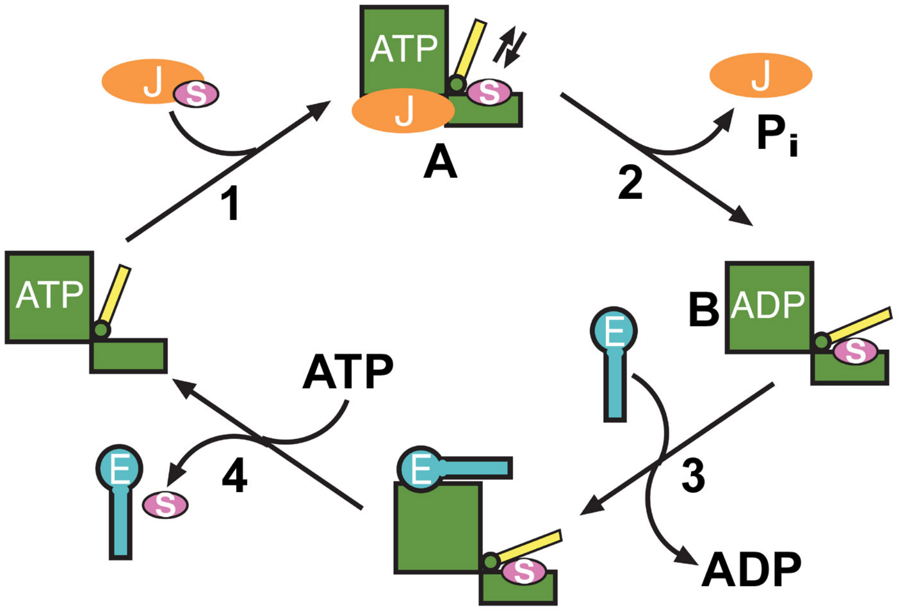

Figure 3: The reaction cycle of the DnaK/DnaJ-system.

J: DnaJ, E: GrpE, S: substrate protein. The ATPase domain (square) and the substrate binding domain (rectangle) of DnaK are colored in green, the α-helical latch in yellow. **(1)** Unfolded substrate protein alone can bind to the DnaK in the ATP-bound state (not shown) or is transferred from DnaJ. The DnaK-DnaJ-substrate-ATP complex **(A)** has low substrate affinity, allowing rapid substrate exchange. This complex is probably very transient, since DnaJ stimulates ATP-hydrolysis, leading to release of DnaJ and inorganic phosphate **(2)**. In the ADP-bound state **(B)**, the latch is closed and the substrate is stably bound. Binding of GrpE **(3)** to the DnaK-substrate-ADP complex leads to ADP-release. Upon rebinding of ATP to DnaK **(4)**, the latch opens up and GrpE as well as the substrate are released from DnaK. Modified from Hartl & Hayer-Hartl, 2002.

Eukaryotic Hsp70 homologs work by a mechanism similar to that of DnaK. They co-operate with DnaJ-like co-chaperones, such as the Hsp40-proteins Ydj1 and Sis1 in yeast or Hdj1 and Hdj2 in mammals, that stimulate their ATPase activity (Young *et al.* 2004). In contrast, no eukaryotic GrpE homolog has been identified. Instead, the structurally unrelated BAG1 and its homologs (Snl1 in yeast) act as nucleotide exchange factors on Hsc70 (Hohfeld & Jentsch 1997; Sondermann *et al.* 2001; Young *et al.* 2003). The mammalian co-chaperone HIP (Hsp70 interacting protein) stabilizes the ADP-bound form of Hsc70, antagonizing BAG1 function (Hohfeld *et al.* 1995). HspBP1 in mammals, or Fes1 in *S. cerevisiae*, is another eukaryotic protein that acts as a nucleotide exchange factor for eukaryotic Hsp70 homologs (Kabani *et al.* 2002). The recently solved structure of HspBP1 in complex with the Hsp70 ATPase domain revealed that HspBP1 is structurally and mechanistically distinct from GrpE and BAG1 (Shomura *et al.* 2005).

II.4.3 The chaperonins

The chaperonins are large oligomeric assemblies with a molecular mass of ~800 kDa (Bukau & Horwich 1998; Hartl & Hayer-Hartl 2002; Naylor & Hartl 2001). They consist of two double ring structures, in which each ring encloses a central cavity. The chaperonins are classified into two subgroups. The Group I chaperonins, also referred to as Hsp60's, are present in eubacteria and eukaryotic organelles, such as mitochondria and chloroplasts. They consist of two homo-heptameric rings which form a barrel-shaped structure and cooperate with heptameric co-factors of the Hsp10 class. Group II chaperonins, found in the eukaryotic cytosol and in archaea, are topologically related to Group I chaperonins, but share only distant sequence homology. They are composed of two rings containing eight subunits each and do not require Hsp10-like co-factors. Chaperonins act by capturing non-native polypeptides through hydrophobic interactions and subsequently releasing them into a central hydrophilic cavity in an ATP-regulated manner. Thus, chaperonins provide a protected folding environment, a mechanism fundamentally different from the one exerted by members of the Hsp70 family or TF.

The *E. coli* chaperonin system, GroEL and its co-factor GroES, has been analyzed in great detail both structurally and biochemically. GroEL consists of two homo-heptameric rings of 57 kDa subunits, which are stacked back to back and form a barrel-like structure (Braig *et al.* 1994; Langer *et al.* 1992). The subunits harbor an equatorial domain with ATPase activity and an apical substrate binding domain, which are connected by a hinge-like domain. The inter-subunit contacts are formed by the equatorial domain. Binding of ATP and the heptameric GroES co-factor, consisting of identical 10 kDa subunits, results in large structural rearrangements within the GroEL ring. The GroEL rings, termed *cis*- and *trans*-rings, are coupled by negative allostery, such that both rings cannot exist in the same nucleotide-bound state simultaneously (Hartl & Hayer-Hartl 2002).

The GroEL/GroES reaction cycle (Bukau & Horwich 1998; Hartl & Hayer-Hartl 2002) (see Figure 4) is initiated by binding of a non-native protein to the apical domain of a GroEL *trans* ring that is free of nucleotide and GroES. Subsequently, binding of seven molecules of ATP in the same ring induces large structural rearrangements: The apical domains twist up and outward, allowing GroES to bind to them and leading to release of the substrate into the central cavity. The cavity volume increases simultaneously, and the cavity surface changes its properties from hydrophobic to hydrophilic. Concomitant with these rearrangements, GroES and ADP are released from the former *cis* ring. The substrate is allowed to fold in the sequestered environment of the GroEL cavity during ATP hydrolysis for ~10 s. Binding of unfolded substrate, ATP and GroES to the vacant ring results in release of ADP, GroES and the substrate from the opposite ring. If the substrate failed to acquire its native structure, it can rebind and participate in another cycle of binding and release. GroEL/GroES can encapsulate substrates up to a molecular weight of

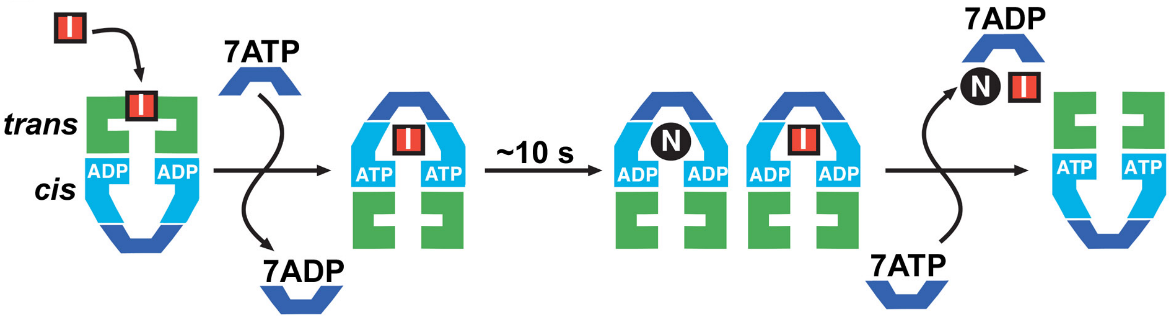

Figure 4: The reaction cycle of the GroEL/GroES-system.

I: folding intermediate; N: natively folded protein. The GroEL trans ring is shown in green, the cis ring in light blue. GroES is colored blue. Binding of the folding intermediate at the apical domains of the trans ring is followed by binding of GroES and seven molecules of ATP to the same ring, leading to release of the substrate into the GroEL/GroES cavity. Simultaneously, ADP and GroES dissociate from the opposite ring. The substrate is allowed to fold inside the now hydrophilic cavity for ~10 s, before ATP hydrolysis leads to binding of GroES and ATP to the opposite ring and release of ADP, GroES and the substrate. Within one cycle, both N and I accumulate, and I rapidly rebinds.
From Hartl & Hayer-Hartl, 2002.

~60 kDa. The folding of some polypeptides larger than 60 kDa can proceed without encapsulation by binding to the GroEL *trans* ring, opposite the one with bound GroES (Chaudhuri *et al.* 2001).

GroEL is thought to act at a later stage in protein folding than TF and the DnaK system. In contrast to the latter, it recognizes compact folding intermediates (Hayer-Hartl *et al.* 1994). The substrate set of GroEL is more restricted than that of TF and DnaK, and has been investigated in detail recently (Kerner *et al.* 2005). Certain folds composed of combinations of α-helices and β-strands, such as the TIM barrel domain, are enriched among the native structures of GroEL substrates, reflecting special assistance for these complex domains from the chaperonin during their folding.

The mechanism and substrate set of Group II chaperonins is less well defined than that of GroEL. Group I and Group II chaperonins share a similar topology in that they are composed of oligomeric double-rings. The chaperonin of the eukaryotic cytosol is termed TRiC (TCP1 Ring Complex) or CCT (Chaperonin Containing TCP1). TRiC consists of two hetero-oligomeric rings of eight orthologous subunits each. The archaeal Group II chaperonin, referred to as the thermosome, consists of up to three different subunits, which form octameric or nonameric rings. An α-helical segment in their apical domains, absent in GroEL, is thought to function as a built-in lid (Ditzel *et al.* 1998; Klumpp *et al.* 1997). TRiC was initially identified due to its requirement for the folding of actin and tubulin, abundant proteins in the eukaryotic cytosol (Sternlicht *et al.* 1993; Yaffe *et al.* 1992). A recently described class of substrate proteins is constituted by the WD40-repeat proteins (Siegers *et al.* 2003). The archaeon *Methanosarcina mazei* was found to contain both a Group I and a Group II chaperonin (Klunker *et al.* 2003) and might offer an opportunity to investigate substrate preferences of the two families in detail.

II.4.4 Additional chaperone systems

In addition to the cytosolic chaperone systems described above, a large number of other cellular factors assist in the folding of newly-synthesized or stress-denatured proteins, often in co-operation with the Hsp70 system or the chaperonins. Compartments other than the cytosol, such as the endoplasmic reticulum in eukaryotes or the periplasm in bacteria, harbor their own unique inventory of specialized molecular chaperones. These will not be discussed further here.

Small heat-shock proteins, which are often found associated with inclusion bodies in *E. coli*, are stress-inducible molecular chaperones that bind unfolded proteins, preventing their aggregation and facilitating their refolding by ATP-dependent chaperones (Ehrnsperger *et al.* 1997; Narberhaus 2002; Van Montfort *et al.* 2001). The eubacterial proteins IbpA and IbpB are members of this class of proteins. Small heat shock proteins of the eukaryotic cytosol include Hsp12 and Hsp42 as well as the mammalian α-crystallins.

The Clp (Hsp100) proteins constitute a subfamily of AAA proteins. They participate in the re-solubilization of aggregated proteins in cooperation with the DnaK chaperone system or the protein degradation machinery (Glover & Lindquist 1998; Mogk & Bukau 2004; Schirmer *et al.* 1996; Weibezahn *et al.* 2005).

Prefoldin, also called Gim (genes involved in microtubule biogenesis) complex or GimC (Geissler *et al.* 1998; Vainberg *et al.* 1998), is a hetero-oligomeric complex of two α and four β subunits that is found in the cytosol of eukaryotes and archaea. Its structure resembles the shape of a jellyfish with six α-helical coiled-coil structures protruding from a β-barrel body (Siegert *et al.* 2000). GimC is able to stabilize non-native proteins, both co- and post-translationally, and transfer them to the chaperonin (Leroux *et al.* 1999).

Eukaryotic Hsp90 is a member of the ATP-dependent, homo-dimeric Hsp90 family of chaperones (Young *et al.* 2004). Similar to the Hsp70-system, the ATPase activity of Hsp90 regulates substrate binding and release, but the biochemical mechanism of Hsp90 is not yet fully understood. In contrast to chaperones of the Hsp70 class, it appears to act at a later stage of the folding process on more compact folding intermediates of a variety of proteins, including transcription factors, regulatory kinases and other signaling and structural proteins (Pratt & Toft 2003; Richter & Buchner 2001; Young *et al.* 2001). Hsp90 often works together with the cytosolic Hsp70 family member Hsc70, forming the Hsc70–Hsp90 machinery, which is regulated by diverse co-factor proteins. A feature often found in these co-factors is a tetratricopeptide repeat (TPR) clamp domain that mediates interaction with Hsp90, Hsc70, or both. An example of such a co-chaperone is the mammalian Hsp-organizing protein (HOP), which has two independent TPR clamp domains and co-ordinates the action of Hsc70 and Hsp90 (Young *et al.* 2004; Young *et al.* 2003). The wide variety of co-factor proteins allows the Hsc70-Hsp90 system to operate in diverse functional contexts (Young *et al.* 2003).

II.5 Protein synthesis on the ribosome and early events in *de novo* protein folding

II.5.1 The ribosome

Proteins are synthesized by the ribosome (Nierhaus & Wilson 2004), a large assembly of RNA and protein belonging to the functional class of polymerases, which translates the information encoded in the messenger RNA (mRNA) into an amino acid sequence. The molecular weight of ribosomes ranges from 2.5×10^6 Da in prokaryotes to 4.5×10^6 Da in higher eukaryotes. Ribosomal RNA (rRNA) constitutes two thirds of the ribosomal mass, whereas the remaining third consists of ribosomal proteins (r-proteins). The ribosome is composed of a large and a small subunit, with sedimentation coefficients of 50S and 30S, respectively, for the bacterial ribosome, which associate on the mRNA to form the active 70S particle. The 50S (or large) subunit contains one molecule each of 5S and 23S rRNA, named according to their sedimentation coefficients. In addition to rRNA, the 50S subunit contains about 35 different r-proteins, termed RPL's (ribosomal proteins of the large subunit), most of them in single copy. The 30S (or small) ribosomal subunit is composed of one molecule of 16S rRNA and 22 r-proteins, called RPS's (ribosomal proteins of the small subunit) (Nierhaus & Wilson 2004).

In the year 2000, high resolution crystal structures of both ribosomal subunits became available (Ban *et al.* 2000; Schluenzen *et al.* 2000; Wimberly *et al.* 2000). Subsequently, additional ribosomal structures have been determined, including one of the entire *E. coli* ribosome (Schuwirth *et al.* 2005). These structures provided insight into the mRNA decoding mechanism (Ogle & Ramakrishnan 2005) and the catalysis of peptide bond formation at the atomic level (Moore & Steitz 2003; Steitz 2005), revealing that the peptidyl-transferase center of the ribosome is composed entirely of RNA. Also, the understanding of the structure and function of many ribosomal proteins has benefited enormously from the availability of ribosomal crystal structures. Due to their tight interaction with rRNA, most ribosomal proteins exhibit tertiary structures not present in other proteins and are unstable in solution by themselves, which makes their characterization a challenging undertaking (Brodersen & Nissen 2005). Co-crystal structures of ribosomal subunits with various substrates or inhibitors, antibiotics and associated proteins have shed light on many aspects of ribosomal function and translation in molecular detail (Auerbach *et al.* 2004; Baram & Yonath 2005; Nilsson & Nissen 2005; Schlunzen *et al.* 2005; Steitz 2005; Yonath 2005).

The large ribosomal subunit forms a compact, monolithic structure (see Figure 5). The proteins are mostly located on the surface, whereas the core of the ribosome consists almost exclusively of RNA. This subunit is formed by a central, massive core with a medial elongated feature and two lateral protuberances, called stalks (L1 and L7/L12 stalk). The peptidyl-transferase center (Moore & Steitz 2003; Steitz 2005) and the ribosomal exit tunnel are located within this subunit (Jenni & Ban 2003). The small subunit is traditionally subdivided into a "head", a "neck" and a "body" region. It contains the decoding center (Ogle *et al.* 2001; Ogle *et al.* 2002), as well as the proteins S1, S7 and S11 responsible for tethering the mRNA to the ribosome, which, in the translating state, is tightly wrapped around the "head"-region (Yusupova *et al.* 2001).

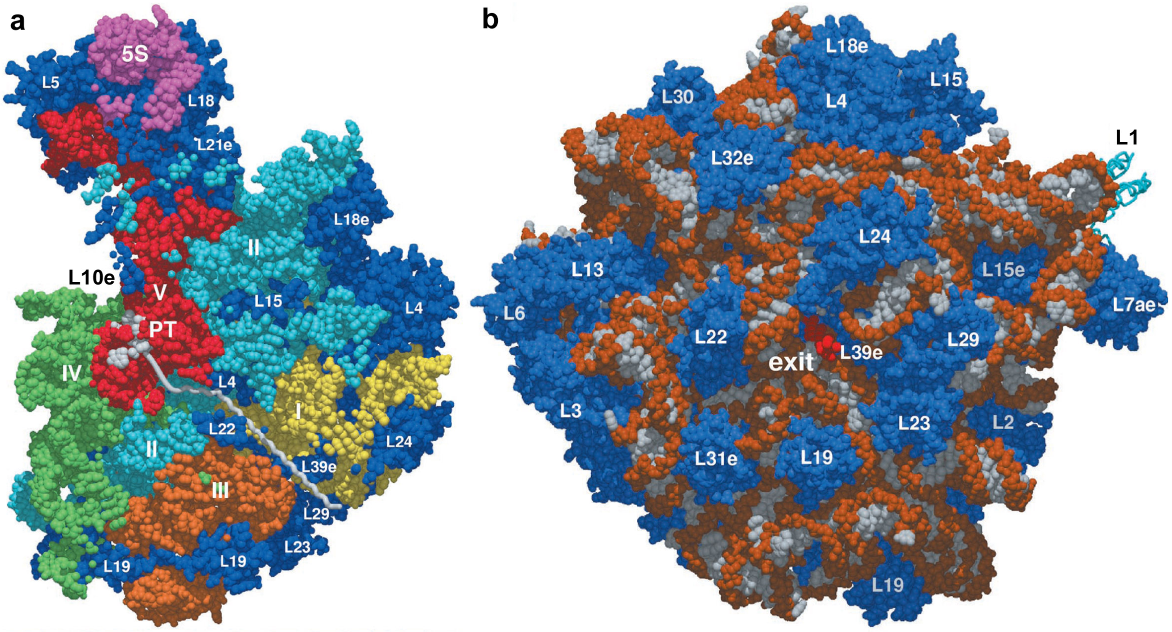

Figure 5: Structure of the large ribosomal subunit.

PT: peptidyl-transferase center. **a.** Cross-section through the large ribosomal subunit from H. marismortui along the entire length of the ribosomal exit tunnel. A ribbon representation of α-helical polypeptide has been modeled inside the exit tunnel (gray). Backbone atoms of rRNA and ribosomal proteins are shown in spacefilling representation. Color coding of the 23S rRNA is according to domains (**I**: yellow, **II**: light blue, **III**: orange, IV: green, V: red). 5S rRNA is colored in pink and proteins in blue. The tunnel surface is made mostly or rRNA, with some contributions from ribosomal proteins. **b.** Spacefilling representation of the large ribosomal subunit with the tunnel exit in the center. The rRNA backbone is colored orange and the bases gray. In red, a modeled polypeptide is shown exiting the tunnel. Proteins are colored blue, with L19, L22, L23, L24, L29, and L31e encircling the tunnel exit. From Nissen *et al.*, 2000 (pdb-code *1FFK*).
]

The ribosomal exit tunnel, through which the nascent polypeptide chain travels as it is elongating, traverses the large ribosomal subunit from the peptidyl-transferase center to the tunnel exit which is studded with the r-proteins L19, L22, L23, L24, L29, and L31e in the 50S subunit from the archaeon *Haloarcula marismortui* (Nissen *et al.* 2000) (see Figure 5). The tunnel surface is constituted mainly by the 23S rRNA with contributions from the non-globular domains of the ribosomal proteins L4, L22 and L39e (Nissen *et al.* 2000). It is ~100 Å long and has a diameter of 10–20 Å at its narrowest constriction (Ban et al. 2000; Nissen et al. 2000; Yusupov et al. 2001). So far, no other clearly continuous channel has been identified leading from the peptidyl-transferase center to the ribosome exterior, thus, all nascent peptides are expected to emerge from the ribosome *via* this exit tunnel.

The tunnel surface is largely hydrophilic and does not expose any large hydrophobic patches that would constitute a binding site for hydrophobic sequences in the nascent chain (Nissen *et al.* 2000). Thus, the tunnel has been considered to be rather inert and not to interact specifically with elongating nascent proteins. Recent evidence showed that the translation of the SecM polypeptide leads to stalling of translation (Nakatogawa & Ito 2001), demonstrating that the nature of the nascent chain may have regulatory impact on the peptidyl transferase activity of the ribosome. Suppressor mutations in the 23S rRNA and the ribosomal protein L22 alleviated this effect, demonstrating that it is based on specific interactions of the nascent chain with components of the wall of the exit tunnel (Nakatogawa & Ito 2002).

Results from limited proteolysis experiments obtained in the late 1960's indicated that 30–40 aa of a ribosome-bound nascent chain are protected from proteolytic degradation (Blobel & Sabatini 1970; Malkin & Rich 1967). Considering a tunnel length of ~100 Å, these results suggest that the nascent polypeptide resides within the exit tunnel in an extended conformation, consistent with the relatively small diameter of the tunnel, which would not be expected to accommodate structures more complex than an α-helix. Recent results, however, indicated that certain nascent chains may form partially compacted structures within the ribosomal channel (Lu & Deutsch 2005; Woolhead *et al.* 2004). Observations by cryo-electron microscopy revealed dynamic properties of the exit tunnel: Translation of model polypeptides led to an expansion in volume of the exit tunnel, possibly allowing the compaction of the nascent chain before it exits the ribosomal tunnel (Gilbert *et al.* 2004). Folding within the ribosomal exit tunnel has so far been observed only for trans-membrane proteins. Most soluble proteins are expected to emerge from the ribosome in an unfolded state, where they encounters the crowded environment of the cytosol as well as ribosome-tethered molecular chaperones that guide their folding to the native state.

II.5.2 Translation and folding

Protein folding *per se* is a spontaneous process, driven by the minimization of the free energy of the system. Thus, a polypeptide sequence will have the propensity to start folding as soon as it emerges from the ribosomal exit tunnel. During translation, the amino terminus of the nascent chain emerges first from the interior of the ribosome, and more of the polypeptide sequence becomes available sequentially as peptide elongation proceeds. Productive folding, however, requires the sequence of at least an entire protein domain to be available, and folding is usually fast compared to the rate of translation. If the folding of the nascent polypeptide begins before the synthesis of a domain is completed, there is a risk of misfolding, *i.e.* the irreversible formation of non-native intra-molecular contacts, which is further enhanced by the crowded environment that the nascent polypeptide encounters in the cytosol. These difficulties have to be overcome by the action of molecular chaperones.

Two different mechanisms have evolved to promote efficient folding of newly synthesized proteins. The eukaryotic chaperone machinery allows efficient sequential domain folding during translation, demonstrated by the analysis of artificial two-domain fusion-proteins (Netzer & Hartl 1997). Co-translational domain-wise folding occurs in the prokaryotic cytosol as well (Nicola *et al.* 1999), but with a greatly reduced efficiency when compared to eukaryotes (Netzer & Hartl 1997). Instead, domain folding is delayed relative to translation in bacteria, or may be entirely post-translational for some proteins (Agashe *et al.* 2004). It has been shown that both TF and DnaK improve the folding yield of two multi-domain proteins, firefly luciferase (FL) and *E. coli* β-galactosidase, by delaying their folding and promoting a post-translational mechanism. In the absence of these chaperones, rapid, but inefficient co-translational folding was observed (Agashe *et al.* 2004).

Individual classes of chaperones as well as the translational machinery are conserved to a high degree among prokaryotes and eukaryotes. Yet, important differences affecting the coupling of translation and folding may reflect different selective pressures. Rapid, co-translational domain-folding in eukaryotes, facilitated by relatively low translation rates of ~3–8 aa/s (Bremer & Dennis 1996; Mathews *et al.* 2000) and a specialized chaperone machinery, may have allowed the evolution of readily foldable modular proteins with novel functions by random gene fusion (Netzer & Hartl 1997). In contrast, bacteria may have been able to achieve short generation times through higher translation rates (~12–22 aa/s) and the evolution of chaperones that promote robust post-translational folding (Agashe *et al.* 2004; Chang *et al.* 2005; Hartl & Hayer-Hartl 2002), such as the uniquely bacterial TF.

II.5.3 Trigger factor

TF was originally identified by Wickner and co-workers in 1987 as a ribosome-associated, essential component of the secretion machinery of *E. coli*. *In vitro* experiments, analyzing the translocation of the bacterial outer membrane protein OmpA through the inner membrane, suggested that TF stabilized the precursor, proOmpA, in a loosely folded conformation and promoted its translocation (Crooke *et al.* 1988; Crooke *et al.* 1988; Crooke & Wickner 1987). Cloning of the corresponding gene, termed *tig*, allowed the construction of *E. coli* strains harboring the *tig* gene under the control of an exogenous promoter (Guthrie & Wickner 1990). Depletion of TF in these cells did not result in a defect of OmpA-secretion, showing that TF was not required for this process. Instead, reduced TF levels were observed to promote filamentation of the cells, indicating defects in cell division, probably through secondary effects (Guthrie & Wickner 1990). Work from different laboratories in the following years led to the recognition of TF as a general ribosome-associated molecular chaperone (Hesterkamp *et al.* 1996; Stoller *et al.* 1995; Valent *et al.* 1995).

The *tig* gene is not induced upon heat shock, thus, TF is not considered a heat shock protein. Rather, TF levels seem to be regulated according to cell growth rates, similar to components of the transcription/translation machinery (Griffiths *et al.* 1995; Guthrie & Wickner 1990; Lill *et al.* 1988; Pedersen *et al.* 1978). The *tig* gene is not essential for survival in an *E. coli* wild type background. Combined deletion with the *dnaK* gene results synthetic lethality at temperatures above 30 °C (Deuerling *et al.* 1999; Teter *et al.* 1999). All bacterial genomes sequenced to date contain a *tig* homolog. Even *Mycoplasma genitalium*, that has the smallest bacterial genome known and lacks GroEL, contains a gene encoding TF (Bang *et al.* 2000; Fraser *et al.* 1995).

The *E. coli* TF protein is composed of 432 aa and has a calculated molecular weight of 48.2 kDa. It is composed of three subdomains (see Figure 6): An amino-terminal

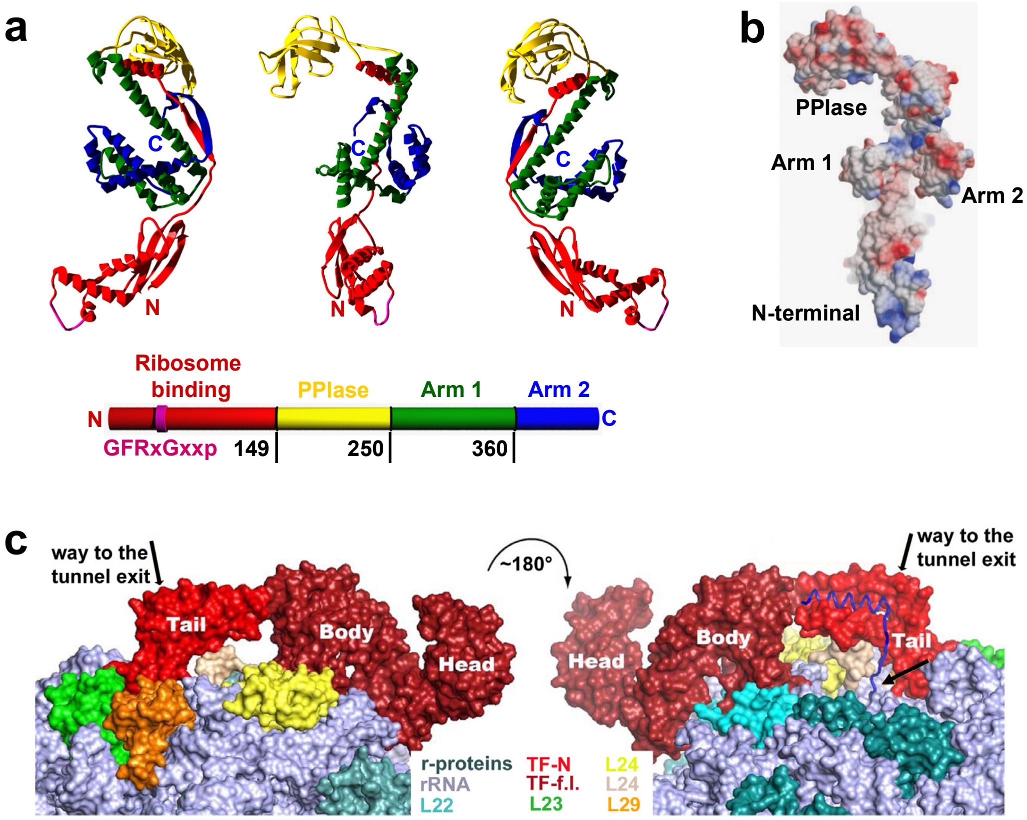
a
C
N
C
N
C
N
Ribosome binding
PPIase
Arm 1
Arm 2
N
C
GFRxGxxp
149
250
360
b
PPIase
Arm 1
Arm 2
N-terminal
c
way to the tunnel exit
~180°
way to the tunnel exit
Tail
Body
Head
Head
Body
Tail
r-proteins
rRNA
L22
TF-N
TF-f.l.
L23
L24
L24
L29

Figure 6: Structure of TF and assumed positioning on the ribosome.

N: amino-terminus, C: carboxyl-terminus, TF-N: TF amino-terminal ribosome binding domain, TF-f.l.: full-length TF **a.** Ribbon representation of the full-length TF structure (pdb-code *1w26*, chain A, Ferbitz *et al*. 2004). The three images are related by rotation around the vertical long axis by ~90°. The amino-terminal domain is colored red, the middle PPIase domain yellow, the Arm 1 and Arm 2 of the carboxyl-terminal domain are shown green and blue, respectively. The TF signature motif is colored in magenta. The domain arrangement along the primary structure is shown schematically with the same color coding in the bottom panel. Numbers indicate the position of the domain boundaries. **b.** Surface representation of TF in a orientation similar to that in the middle panel of **(a).** The coloring corresponds to the electrostatic potential (blue: positive; red: negative). The crevice, surrounded by the protrusions (Arm 1 and 2) exposes hydrophobic patches on the surface, colored white. **c.** Modeling of full-length *E. coli* TF (Body, Head; dark red) onto the ribosome based on the co-crystal structure of the amino-terminal TF-domain of *D. radiodurans* TF (Tail; red) in complex with its 50S ribosomal subunit. Ribosomal proteins (r-proteins) and rRNA are colored as indicated. A modeled nascent chain emerging from the exit tunnel (indicated by black arrows) is shown in blue. The loop-extension of L24 (shown in gold; with the globular domain in yellow) encroaches on the hydrophobic crevice.
The ribbon diagrams in (**a**) were generated with DeepView/Swiss PDB-viewer and rendered with Pov-Ray. (**b**) from Ferbitz *et al*. 2004. (**c**) from Schlunzen *et al.* 2005.

domain that mediates ribosome binding, followed by a central PPIase domain with homology to the immunophilins of the FK506 binding protein (FKBP) family, and a carboxyl-terminal domain that, based on the analysis of deletion mutants (Hesterkamp *et al.* 1997), had been proposed to be the major substrate binding domain. TF associates with non-translating ribosomes in a salt-sensitive manner, whereas the association with translating ribosomes is salt-resistant (Hesterkamp *et al.* 1996).

The structure of the isolated ribosome binding domain of TF (TF-BD) was solved in 2003 (Kristensen & Gajhede 2003). It revealed an elongated α + β-structure consisting of a four-stranded anti-parallel β-sheet flanked by two long α-helices (see Figure 7). One of the α-helices is strongly kinked at a position close to the loop connecting the two α-helices. This loop contains the TF "signature motif", Gly_{43}-Phe-Arg-x-Gly-x-x-Pro_{50}, constituting the main ribosome-binding region in TF (Kramer *et al.* 2002). The TF FRK/AAA mutant, where residues 44–46 were replaced with alanine, showed a severe reduction in its ability to bind to the ribosome (Kramer *et al.* 2002). Mutational analysis revealed that TF binds to the ribosomal protein L23, since mutation of the conserved glutamate at position 18 in the *E. coli* L23 to alanine or glutamine severely reduced TF-binding (Kramer *et al.* 2002).

The substrate specificity of the TF PPIase resembles that of the FKBP-type of PPIases (Callebaut & Mornon 1995; Stoller *et al.* 1995). Limited sequence similarity with other PPIases of the FKBP family and the inability of the inhibitors FK506 and cyclosporin A to abolish the TF PPIase activity led to the suggestion that the TF PPIase represents a new family of this class of enzymes (Stoller *et al.* 1995). Neither TF mutants that carry point mutations in the PPIase domain, inactivating its enzymatic function, nor deletion of the entire domain affected the ability of TF to complement the synthetic lethality of a combined deletion of *tig* and *dnaK*. Thus, PPIase activity appears not to be essential for TF function (Genevaux *et al.* 2004; Kramer *et al.* 2004).

Although it was proposed to be involved in substrate binding (Hesterkamp *et al.* 1997), the function of the carboxyl-terminal domain remained enigmatic until the structure of full-length *E. coli* TF was solved in 2004 (Ferbitz *et al.* 2004) (see Figure 6). This domain forms a backbone-like structure, separating the amino-terminal ribosome-binding domain from the PPIase "head", which are at opposite ends of the molecule. The carboxyl-terminal domain forms, encompassed by two protrusions or arms, a central crevice that exposes a hydrophobic surface (see Figure 6), consistent with its role as the substrate binding domain. The structure of a carboxyl-terminally truncated version of TF from

Vibrio cholerae was determined independently (Ludlam *et al.* 2004), exhibiting many of the features observed in the *E. coli* TF structure.

The crystal structure of full-length TF in complex with the ribosome has not been solved to date. However, crystal structures of the amino-terminal TF-BD with the large ribosomal subunit from bacteria and archaea have allowed to model full-length TF onto the ribosome (Baram *et al.* 2005; Ferbitz *et al.* 2004; Schlunzen *et al.* 2005), suggesting its probable position. All of these models predict that the hydrophobic crevice of TF is oriented towards the exit tunnel and thus would be accessible to the emerging nascent chain (see Figure 6).

In the earliest of these models, built from a co-crystal structure of the amino-terminal 144 aa of *E. coli* TF in a heterologous complex with the 50S subunit from the archaeon *H. marismortui*, TF was proposed to crouch over the ribosomal exit tunnel. The resulting "cradle"-shaped space was suggested to provide a confined space large enough to accommodate compactly folded domains of up to ~15 kDa in size, allowing their co-translational folding in a protected environment (Ferbitz *et al.* 2004). This model, however, was afflicted with major uncertainty, since only 35 out of 144 residues of the TF-BD could be visualized, whereas the other residues could not be assigned to the experimentally-determined electron density. In addition, due to the absence of TF in all archaeal genomes sequenced to date, the heterologous complex provided incomplete insight into TF-ribosome interactions.

Subsequently, two structures of a homologous complex of the TF-BD and the 50S subunit from the eubacterium *Deinococcus radiodurans* were solved, revealing the molecular details of the interaction between the ribosome and this TF domain (Baram *et al.* 2005; Schlunzen *et al.* 2005). The predominant contacts that mediate ribosome binding of TF are established by the flexible loop region of TF, that is located between helices α1 and α2 and contains the TF signature motif. This region contacts the ribosomal protein L23 and ribosomal RNA. Residues at the side of the loop also contact the ribosomal protein L29, although to a minor extent (Schlunzen *et al.* 2005). This is consistent with L29 not being essential for TF-ribosome interactions (Kramer *et al.* 2002). In addition, helix α2 contacts an extended loop structure of L24 (Schlunzen *et al.* 2005) (see Figure 6). The revealed interactions position TF in a way that the hydrophilic surface of the 4-stranded β-sheets faces away from the ribosome towards the solvent, whereas the hydrophobic surface at the opposite site of the β-sheet faces the ribosomal exit tunnel (Baram *et al.* 2005; Schlunzen *et al.* 2005).

A reorientation of helix α2 in the ribosome-bound state (see Figure 7) enables the interaction of TF with L24. In the ribosome-bound state, the carboxyl-terminal end of helix α2 is shifted away from the β-sheet structure of the TF-BD, as compared to the situation with unbound TF. This conformational rearrangement causes the binding loop to adopt a more open conformation. In addition, this loop is folded back towards helix α2 in the ribosome-bound conformation, resulting in a hooked conformation of the loop (Schlunzen *et al.* 2005).

In the structure of free TF (Ferbitz *et al.* 2004), helix α2 is packed against the 4-stranded β-sheet of the TF-BD, stabilized mainly by hydrophobic interactions. The shift in the position of the helix by 40° that is observed in the ribosome-bound structure leads to a separation of these structural elements and an increase in area of the hydrophobic surface on the β-sheet that is oriented towards the polypeptide exit tunnel (Baram *et al.* 2005; Schlunzen *et al.* 2005). The structural rearrangements within the amino-terminal TF-BD open up a tunnel-like structure with highly hydrophobic walls, that is aligned with the ribosomal exit tunnel on one side and with the hydrophobic crevice of the TF body on the other (Schlunzen *et al.* 2005) (see Figure 7). These observations suggest that ribosome

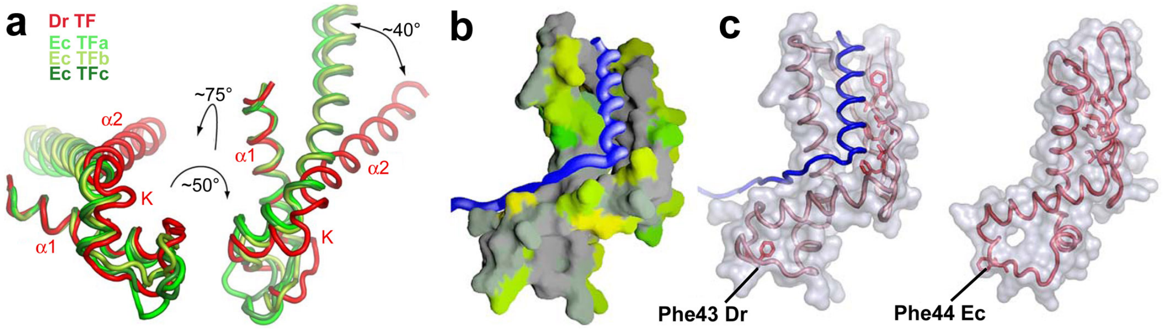

Figure 7: Conformational rearrangements in the TF ribosome binding domain.

Dr: *D. radiodurans*, Ec: *E. coli*, K: kink in helix α2. **a.** Superposition of the loop region of ribosome-bound TF from *D. radiodurans* (red) with each of the three molcecules (a, b and c, in different shades of green) found in the asymmetric unit of the unbound amino-terminal TF-BD from *E. coli* (Kristensen & Gajhede 2003). The two orientations shown are related by rotation as indicated. Helix α2 of the ribosome-bound *D. radiodurans* TF-BD is shifted by ~40° when compared to the free *E. coli* TF. **b.** Surface representation of the ribosome bound amino-terminal domain of *D. radiodurans* TF. An α-helical nascent peptide is modeled into the conduit. Hydrophobic regions on the surface are shown in gray, polar regions in green/orange. **c.** Left: same as **b.**, but with a transparent surface and a backbone representation in red. Right: same representation of the free *E. coli* TF-BD. The hydrophobic channel is present only in the ribosome-bound structure, where the universally conserved Phe43-residue and the neighboring residues are flipped into the hydrophobic loop-region compared to the structure of the free *E. coli* TF.
From Schlunzen *et al.* 2005.

binding induces the formation of a conduit in the TF amino-terminal domain that could guide the nascent chain towards the hydrophobic crevice.

The docking of the full-length TF onto the ribosome-bound TF-BD from *D. radiodurans* TF resulted in a model in which the overall orientation of TF was similar to the one described by Ferbitz *et al.* The interaction between helix α2 and L24, however, was not visible in the heterologous complex, because the L24 from *H. marismortui* lacks the loop extension that contacts α2 (Ferbitz *et al.* 2004; Schlunzen *et al.* 2005). The L24 loop is relatively disordered in the native *D. radiodurans* 50S structure, but appears to be stabilized in the complex with the TF amino-terminal domain. In the resulting model, the space confined by the molecular cradle is substantially reduced by the L24 extension, such that a globular domain of ~15 kDa cannot be accommodated (see Figure 6). The loop extension of L24 from *E. coli* is slightly larger than in *D. radiodurans*. The crevice in the homologous complex of *E. coli* TF with its 50S ribosomal subunit is thus expected to exhibit at least the same restriction in space, rendering the occurrence of co-translational folding within the proposed cradle very unlikely (Schlunzen *et al.* 2005).

In vitro experiments have shed light on the dynamics of the TF-ribosome interactions (Maier *et al.* 2003). Both the association and the dissociation of the TF-ribosome complex were found to be rather slow processes, with an average lifetime of ~30 s for the complex at 20 °C (Maier *et al.* 2003), significantly longer than the lifetime of a complex between TF and model substrates in solution (~100 ms) (Maier *et al.* 2001). The dissociation constants (K_D) of TF complexes with vacant, *i.e.* non-translating ribosomes, and free substrates are ~1 µM (Maier *et al.* 2003; Patzelt *et al.* 2002) and ~100µM (Maier *et al.* 2001), respectively. Free TF forms dimers in solution (Patzelt *et al.* 2002), with reported K_D's for self-association in the range of 1.8 µM to 18 µM (Maier *et al.* 2003; Patzelt *et al.* 2002). Recently, the analysis of carboxyl-terminal truncation mutants showed a reduction in their ability to dimerize, indicating an involvement of the carboxyl-terminal domain in dimer formation (Zeng *et al.* 2005). In addition to the fact that a single TF amino-terminal domain is bound to the large ribosomal subunit in the three complexes thus far observed (Baram *et al.* 2005; Ferbitz *et al.* 2004; Schlunzen *et al.* 2005), biochemical evidence also suggests that the ribosome-bound species is a monomer (Patzelt *et al.* 2002), although neutron scattering analysis suggested dimeric TF to be bound on the ribosome (Blaha *et al.* 2003).

In vitro, TF can be cross-linked to nascent chains as short as 57 residues (Hesterkamp *et al.* 1996). It can act as a shield since it protects ribosome-bound nascent chains against proteolytic degradation, although it is not clear how general this function is with regard to the characteristics of the nascent chain (Hoffmann *et al.* 2006; Tomic *et al.* 2006). The interaction of TF with free substrate polypeptides in solution, without the context of translation, is rather weak (Maier *et al.* 2001; Patzelt *et al.* 2001), which renders the identification of TF-binding sites on the substrate difficult. Using a membrane-bound peptide array, a binding motif was identified consisting of 8 aa enriched in basic and aromatic residues (Patzelt *et al.* 2001). Binding to these peptides was attributed to the TF PPIase domain. In light of the recent structural information, it appears likely that the PPIase domain does not constitute the main substrate binding site (Ferbitz *et al.* 2004). The finding that structural rearrangements occur within TF upon association with the ribosome (Baram *et al.* 2005; Schlunzen *et al.* 2005) suggests that ribosome binding may promote binding of TF to its substrate nascent polypeptide in addition to creating a high local concentration of TF at the ribosomal exit site.

In vitro refolding experiments have shown a function of TF in preventing aggregation and promoting the refolding of certain denatured model proteins (Kramer *et al.* 2004; Liu *et al.* 2005; Liu & Zhou 2004; Maier *et al.* 2001), leading to different hypotheses regarding TF mechanisms. Due to an excess of TF molecules compared to ribosomes in the cell, a significant fraction of TF is clearly not ribosome-associated, and this fraction could potentially exert a chaperone function on free substrates. The discovery that ribosome-binding leads to conformational changes and the exposure of hydrophobic binding surfaces, at least within the amino-terminal domain (see Figure 7), suggests that the chaperone function of free TF may be distinct from the mechanism by which ribosome-bound TF assists the folding of newly synthesized proteins.

In vivo experiments showed that, under laboratory conditions, deletion of the *tig* gene alone does not result in any apparent growth defects or protein aggregation. In the absence of TF, an increased fraction of newly synthesized proteins interacts with DnaK, indicating a functional overlap of these two systems (Deuerling *et al.* 2003; Teter *et al.* 1999). Combined deletion of the *tig* and *dnaK* genes, however, causes protein aggregation at all growth temperatures tested and synthetic lethality at temperatures of 30 °C or more (Agashe *et al.* 2004; Genevaux *et al.* 2004; Vorderwulbecke *et al.* 2004). Ribosome binding is crucial for TF function, since mutations in the ribosomal protein L23 that abolish TF binding are also lethal in the absence of DnaK (Kramer *et al.* 2002). The synthetic lethality of a combined deletion of *tig* and *dnaK* can, in part, be suppressed by adaptation of the cells and enhanced expression of other factors that may prevent bulk protein aggregation, *e.g.* the GroEL/GroES system (Genevaux *et al.* 2004; Vorderwulbecke *et al.* 2004). Similarly, overexpression of SecB, a component of the *sec* pathway of protein secretion, was shown to suppress the phenotypes of cells lacking TF and DnaK (Ullers *et al.* 2004).

The contributions of the individual domains towards TF function *in vivo* has been analyzed by the ability of TF deletion mutants to rescue the temperature sensitive phenotype of the *E. coli* MC4100 *ΔtigΔdnaKdnaJ* strain (Genevaux *et al.* 2004; Kramer *et al.* 2004). A TF mutant in which the entire PPIase domain has been deleted behaved essentially as wild type, indicating that the PPIase domain is dispensable for the TF function associated with cell survival. It appears to be less clear, however, whether the amino-terminal TF-BD alone (or together with the PPIase domain) is sufficient to complement TF function in the absence of DnaK. Kramer *et al.* reported complementation of the synthetic lethality phenotype for both of these constructs, whereas Genevaux *et al.* did not observe rescue with constructs of almost the identical sequence (Genevaux *et al.* 2004; Kramer *et al.* 2004). However, the presence of amino-terminal ribosome-binding domain was found to be strictly required for TF function in all cases (Genevaux *et al.* 2004; Kramer *et al.* 2004).

II.6 Aim of this study

Recently, the mechanistic importance of TF chaperone function in *de novo* protein folding has been highlighted by the analysis of multi-domain protein folding *in vivo* (Agashe *et al.* 2004). The TF crystal structure provided insight into the domain organization of the chaperone and suggested functional implications (Ferbitz *et al.* 2004). However, little is known about the biochemical mechanism by which TF assists the folding of newly synthesized proteins. The structure of the TF amino-terminal domain in complex with the large ribosomal subunit revealed changes in the tertiary structure (Baram *et al.* 2005; Schlunzen *et al.* 2005). Thus, characterization of substrate interactions with full-length TF in the context of translation seemed highly desirable. To provide such information constitutes the main goal of this study.

The large mass of TF and the tight packing of large ribosomal subunits in the crystals thus far obtained may prevent co-crystallization of full-length TF in complex with the ribosome for X-ray structural studies. Therefore, alternative approaches must be employed to investigate this interaction. The only well characterized functional mutant of TF is the FRK/AAA version, deficient in ribosome binding (Kramer *et al.* 2002). Also, nucleotide- or co-factor-dependent regulation of TF has not been reported. Thus, arrest of TF in a defined functional state, which would make it amenable to classical biochemical characterization, is difficult. Fluorescence-based techniques have therefore been applied in this study to characterize the interaction of TF with the ribosome and with its nascent chain substrates. Furthermore, the application of these spectroscopic techniques to a cell-free transcription/translation system (Shimizu *et al.* 2005) allowed the detailed observation of TF activity in real time during translation of various substrate proteins. The results obtained in this study suggest a dynamic functional cycle for TF, representing a paradigm of ATP-independent chaperone regulation.

III MATERIALS AND METHODS

III.1 Chemicals

Unless otherwise stated, chemicals were from **Sigma-Aldrich** (Steinheim, Germany) of "*pro analysi*" grade.

Amersham Pharmacia Biotech (Freiburg, Germany): ECL plus detection kit

BioMol (Hamburg, Germany): IPTG; HEPES

BioRad (Munich, Germany):

- Ethidium bromide
- Bradford Protein Assay

Boehringer Mannheim (Mannheim, Germany): Proteinase K

Difco (Heidelberg, Germany):

- Bacto Tryptone
- Bacto Yeast Extract
- Bacto Agar

Merck (Darmstadt, Germany): ampicillin

New England Biolabs (Frankfurt a.M., Germany):

- Restriction endonucleases
- T4 ligase

Post Genome Institute (Tokyo, Japan): PURE system II classic translation system

Promega (Mannheim, Germany):

- *Taq* polymerase
- Luciferase Assay System (#E1501)

Roche (Basel, Switzerland):

- Benzonase
- Complete protease inhibitor
- EDTA-free protease inhibitor
- DNase I, RNase free
- Shrimp Alkaline Phosphatase (SAP)

Schleicher & Schuell (Dassel, Germany): Protran Nitrocellulose Transfer Membrane

III.2 Materials and Instruments

Abimed (Langenfeld, Germany): Gilson Pipetman 2, 10, 20, 100, 200 and 1000

Amersham Pharmacia Biotech (Freiburg, Germany):

- EPS 300 electrophoresis power supply
- FPLC chromatography systems
- ÄKTA Explorer 100 chromatography system
- HiTrap Chelating column, 5ml
- HiPrep Desalting column
- NAP-5 Sephadex G25 desalting columns

Amicon (Beverly, MA, USA): concentration devices (Centriprep, Centricon)

Avestin (Mannheim, Germany): EmulsiFlex C5 homogenizer

Beckman (Munich, Germany):

- DU 640 UV/VIS Spectrophotometer
- Avanti J-25 centrifuge with rotors JLA 10.500 and JA 25.50
- Optima LE 80k ultracentrifuge with rotors SW28 Ti, SW 41 Ti, SW 55 Ti

Biometra (Göttingen, Germany): T3 PCR-Thermocycler

BioRad (Munich, Germany):

- MiniProtean 2 electrophoresis chamber
- Tank blot system
- Gene Pulser Xcell electroporation device with Gene Pulser electroporation cuvettes

Branson Ultrasonics (Danbury, CT, USA): Sonifier Cell Disruptor B15

Dynal/Invitrogen (Karlsruhe, Germany): Dynabeads Protein A coupled magnetic beads

Eppendorf (Hamburg, Germany):

- 5415C and 5417R centrifuges
- Thermomixer Comfort

Fisher Scientific (Schwerte, Germany): Accumet Basic pH meter

Fuji (Tokyo, Japan) : FLA 2000 Phosphorimager

Hampton Research (Aliso Viejo, CA, USA):

- VDX Plate with sealant
- 22 mm Siliconized Square cover slides

Mettler Toledo (Gießen, Germany) : AG285 and PB602 balances

Millipore (Eschborn, Germany):

- Millex SV Filter Units, pore size 0.22 μM
- Steritop GP Filter Units, pore size 0.22 μM
- MilliQ plus deionization system

New Brunswick Scientific (Nürtingen, Germany): Innova 4430 incubator

Raytest (Straubenhardt, Germany): AIDA version 2.31 gel imaging software

Savant (Strasbourg, France): SGD 2000 slab gel dryer

III.3 Buffers and Media

III.3.1 Buffers

5x SDS-PAGE sample buffer	
10x DNA loading buffer	2 g/l Orange G 2 g/l Bromophenol Blue 2 g/l Xylene cyanol FF 0.37 g/l EDTA di-sodium salt di-hydrate 500 g/l sucrose
10I-buffer	50 mM sodium-PO$_4$ pH 8.0 300 mM NaCl 10 mM imidazole 10% glycerol
25T-buffer	25 mM Tris-HCl, pH 7.6 at 4 °C 100 mM NaCl
50H-buffer	50 mM HEPES-KOH
50P-buffer	50 mM sodium-PO$_4$ pH 8
Buffer A	20 mM Tris-HCl, pH 7.5 at 4 °C 10.5 mM Mg acetate 100 mM NH$_4$Cl 0.5 mM EDTA 3 mM β-mercapto ethanol
Buffer B	20 mM Tris-HCl, pH 7.5 at 4 °C 10.5 mM Mg acetate 500 mM NH$_4$Cl 0.5 mM EDTA 3 mM β-mercapto ethanol

Buffer C	10 mM Tris-HCl, pH 7.5 at 4 °C 10.5 mM Mg acetate 500 mM NH_4Cl 0.5 mM EDTA 7 mM β-mercapto ethanol
Buffer E	10 mM Tris-HCl, pH 7.5 at 4 °C 10 mM Mg acetate 60 mM NH_4Cl 3 mM β-mercapto ethanol
Citrate buffer	100 mM citric acid pH adjusted to 5.5 with NaOH
Luciferase Dilution Buffer	25 mM Tris-phosphate pH 7.8 2 mM DTT 2 mM CDTA 10% glycerol 1% Triton X-100 1 mg/ml BSA
MC buffer	100 mM $MgSO_4$ 5 mM $CaCl_2$
PBS	137 mM NaCl 2.68 mM KCl 10.1 mM Na_2HPO_4 1.76 mM NaH_2PO_4 pH adjusted to 7.4 with HCl
Ribosome Spec-buffer	25 mM Tris-HCl pH 7.4 10 mM $MgCl_2$ 100 mM NH_4Cl

SDS-PAGE electrophoresis buffer	50 mM Tris-HCl pH 8.3 380 mM glycine 0.1% (w/v) SDS
TAE-buffer	242 g/l Tris base 57.1 ml/l acetic acid 50 mM EDTA
TBST	25 mM Tris-HCl, pH 7.2 150 mM NaCl
TBST	25 mM Tris-HCl, pH 7.2 150 mM NaCl 0.1% Tween 20
TEV Storage buffer	20 mM Tris-HCl pH 8.0 100 mM NaCl 1 mM DTT 0.5 mM EDTA 10% glycerol

III.3.2 Media

LB medium	10 g/l bacto tryptone 5 g/l bacto yeast extract 5 g/l NaCl pH adjusted to 7.4 with NaOH
LB agar	16 g/l bacto agar dissolved in LB medium

SOC medium	20 g/l bacto tryptone 5 g/l bacto yeast extract 5 g/l NaCl 2.5 mM KCl pH adjusted to 7.4 with NaOH after autoclaving, supplemented with 10 mM $MgCl_2$ 20 mM glucose
Top agar	10g/l bacto tryptone 1g bacto yeast extract 8g bacto agar 8g NaCl after autoclaving, supplemented with 2 ml 1M $CaCl_2$ 5 ml 20% glucose

III.4 DNA manipulations

III.4.1 General Procedures

Unless indicated otherwise, all molecular biology procedures were performed as described by Sambrook *et al.*, 1989.

Gel extraction of DNA fragments, purification of PCR products and clean up of digested DNA fragments was achieved by immobilization of DNA on a silica-based membrane, removal of contaminants and subsequent elution in 10 mM Tris-HCl, pH 8 (elution buffer, EB) using commercially available kits (Wizard SV Gel and PCR Clean-Up System, Promega). Plasmid DNA was isolated from *E. coli* DH5α using the same principle (Wizard SV Miniprep System, Promega).

Double stranded-DNA was quantitated spectrophotometrically assuming that 1 A_{260} unit corresponds to 50 µg double stranded DNA.

Ehe I endonuclease was from Fermentas, all other endonucleases were from New England Biolabs (NEB).

Unless stated otherwise, *Pfu* turbo polymerase (Stratagene) was used to amplify DNA fragments with specific primers. PCR reactions were set up in the buffer supplied by the manufacturer without additional Mg^{2+} and contained 10 pmol of each primer, 10 pmol of each dNTP and 2.5 units of the polymerase in a volume of 50 µl. Denaturation during the PCR cycle was at 95 °C, annealing was at 50 °C and the elongation temperature was 72 °C unless indicated otherwise. After an initial denaturation of 2 min, 34 cycles of 30 s denaturation, 30 s annealing and elongation for a variable time were conducted.

Colony PCR was performed using *Taq* polymerase with primers specific for promoter and terminator sequences on the plasmid of interest. A typical reaction mix contained 5 pmol of each primer, 5 pmol of each dNTP, 2.5 mM $MgCl_2$ and 1 unit of *Taq* polymerase. A colony of DH5α cells transformed with the plasmid of interest was picked with a sterile pipet tip and first swirled in the PCR reaction mix before used to inoculate LB medium. The temperature profile for colony PCR was the same as for regular PCR reactions except that an initial denaturation step of 5 min was used.

Agarose gel electrophoresis for the analysis of DNA fragments was performed using a Horizon 58 electrophoresis chamber (Whatman) with an EPS 300 power supply (Pharmacia Biotech) operated at constant voltage (90 V). Agarose gels were prepared in TAE buffer containing 1 – 2% agarose and 1 µg/ml ethidium bromide for visualization of double stranded DNA.

The integrity of the open reading frame (ORF) of all plasmids was verified by Dye Terminator Cycle Sequencing performed by Sequiserve (Vaterstetten, Germany).

For bacterial growth, LB medium was used. When indicated, the medium was supplemented with 100 µg/ml ampicillin (LB^{Amp}), 30 µg/ml kanamycin (LB^{Kan}), 170 µg/ml chloramphenicol (LB^{Cam}) or 50 µg/ml tetracycline (LB^{Tet}).

Chemically competent *E. coli* DH5α and BL21(DE3)*gold* cells were prepared by the calcium phosphate method (Sambrook *et al.* 1989). For transformation of plasmid DNA, chemically competent cells were mixed with DNA and incubated 15 min on ice. Cells were subjected to a heat shock by incubation at 42 °C for 90 sec and placed on ice before resuspension in unsupplemented LB medium. Prior to plating on LB-agar, cells were allowed to recover at 37 °C for 1 h.

For the preparation of electro-competent *E. coli* cells, a culture was grown in 5 ml LB-medium to an OD_{600} of 0.6 – 0.8. Cells were harvested and subjected to three successive washes with sterile water. Cells were resuspended in water, mixed with DNA and incubated on ice for 15 min. Electroporation was performed using Gene Pulser cuvettes with an electrode gap of 0.2 cm (Biorad) and a GenePulser Xcell device (Biorad). Settings for resistance, capacitance and voltage were 200 Ω, 25 µFd and 2.5 kV, respectively. Immediately after electroporation, cells were resuspended in 800 µl SOC medium and allowed to recover for 1 h prior to plating.

Vector maps of all plasmids generated are given in Appendix VII.2.

III.4.2 Cloning of TF-expression constructs

pPROEX-HTa-based plasmids were generated for protein overproduction. The ORF of the various TF versions was inserted into this backbone in a way that the encoded protein was preceded by an amino-terminal His_6 sequence and a TEV protease recognition site.

The ORF of full-length TF was amplified by PCR from *E. coli* K12 genomic DNA using primers TFP1B (forward) and TFP4 (reverse; for primer sequences, see Appendix VII.1). TF1B was 5'-phosphorylated. Elongation was allowed to proceed for 90 s *per* cycle. For carboxyl-terminal truncations of TF consisting of the amino-terminal 112 and 148 residues, reverse primers TFP2 and TFP3 were used, respectively. In this case, the elongation time was 1 min. The specificity of the reaction and the correct size of the products was confirmed by agarose gel electrophoresis. The PCR products were purified and eluted in 75 µl EB. The purified PCR products were digested with *Sal I* endonuclease, subjected to a DNA clean up step and eluted in 30µl EB.

For preparation of the backbone, ~7.5 µg pPROEX-HTa plasmid (Invitrogen) were digested with *Ehe* I and *Sal* I endonucleases and dephosphorylated using Shrimp Alkaline Phosphatase (SAP, Roche). The DNA was purified and eluted in 30 µl EB.

For ligation of the *Sal* I-cut, 5'-phosphorylated insert into the *Ehe* I, *Sal* I cut pPROEX-HTa, 3 µl insert and 1 µl vector were incubated with 400 units of T4 ligase (NEB) in a volume of 20 µl. In a control reaction, water was added instead of insert. Incubation was carried out in a thermocycler running the following temperature profile: 20 min at 20 °C, followed by 99 cycles of 2 min each at 12 °C, 18 °C and 24 °C, and finally 60 min at 20 °C.

Half of the ligation reaction was transformed into chemically competent DH5α cells. Cells were plated on LB^{Amp}-agar. Transformants were allowed to form colonies overnight at 37 °C. Single colonies were used to inoculate LB^{Amp} medium and grown overnight at 37 °C. Cells were harvested and plasmid DNA was isolated. Presence of an insert of the correct size was confirmed by restriction analysis using *Sty* I and *Sal* I endonucleases.

III.4.3 Cloning of the TF deletion mutant NC

Plasmids encoding the NC proteins were generated in collaboration with Hung-Chun Chang. An expression construct for the production of a TF variant lacking the central PPIase domain was generated in a two-step procedure: First, a DNA fragment encoding the carboxyl-terminal part of TF (residues 244 to 432) was amplified by PCR using primers Not-TFC (forward) and XbaI-stop-TFC (reverse) with plasmid pCKTF3B as a template (see Appendices VII.1 and VII.2). The resulting fragment was cloned into the pPROEX-HTa *via NotI*- and *XbaI*-endonuclease sites, resulting in plasmid pTFC.

In the second step, a DNA fragment encoding the amino-terminal domain of TF (residues 1 to 150) was amplified using primers TFP1B (forward) and SpeNot-TFN (reverse) with pCKTF3B as a template, resulting in a 5'-phosphorylated DNA fragment. This fragment was cloned into pTFC *via NotI*- and *XbaI*-endonuclease sites, resulting in the expression plasmid pTFNC. This plasmid encodes a TF version in which residues 151 to 243 are deleted and replaced by a flexible linker with the amino acid sequence

GTSAAAG. The ORF is preceded by a sequence encoding a His$_6$-tag and a TEV protease cleavage site. This protein is referred to as NC.

For the generation of an R14C-mutant of NC, primers TFP1B and SpeNot-TFN were used in a PCR with template DNA encoding the TF R14C mutant (pCKTF8) (see Appendix VII.2). The resulting DNA fragment encoding the amino-terminal residues of TF with the R14C mutation was cloned into pTFC as described above. In a similar way, the NC R14C T150C double cysteine mutant was generated, except that primers TFP1B and SpeNot-TFN150C were used on pCKTF8 template DNA. The primer SpeNot-TFN150C introduced the T150C mutation into the PCR-product. The plasmids encoding the cysteine mutants are referred to as pTFNC_R14C and pTFNC_R14C-T150C. The sequences of the primers utilized for the generation of the NC-plasmids are given in Appendix VII.2.

III.4.4 Cloning of the human titin I27 domain

The ORF of domain I27 of human titin was amplified by PCR from plasmid pTitin (obtained from Sladjana Tomic, MPI for Biochemistry, Martinsried, Germany) using primers I27 F-NdeI and I27 R-SpeI (see Appendix VII.1). The PCR-product was ligated into the vector pCH25 (Chang *et al.*, 2005) *via NdeI*- and *SpeI* endonuclease sites. The resulting plasmid pCH25Titin encodes the I27-domain followed by a 25 amino acid flexible linker -TS(GGGGS)$_4$AAA- and an ORF encoding GFP. Plasmid pCH25Titin was generated in collaboration with Hung-Chun Chang.

III.4.5 Site-directed mutagenesis

Site-directed mutagenesis was used to introduce single cysteine codons into the otherwise cysteine-free *E. coli* TF ORF and for mutagenesis of *T. thermophilus* TF yielding the FRP/AAA mutant. To this end, primers were designed containing the desired mutation flanked by sequences complementary to the template. These complementary stretches encompassed ~10 residues upstream and ~20 residues downstream of the site of mutagenesis. The primers also introduced an endonuclease restriction site to allow selection of positive clones by restriction digestion analysis. Primer sequences and characteristics are listed in Appendix VII.1.

10 pmol of each primer were mixed with 20 ng of template DNA in a regular PCR reaction. Elongation was allowed to proceed at 68 °C for 11 min. This lower temperature

was chosen to enhance the fidelity of the polymerase. The correct size of the PCR products was verified by agarose gel electrophoresis.

After amplification, template DNA was digested by the addition of 1.5 µl *Dpn* I endonuclease directly to the PCR reactions and incubation at 37 °C for 1 h. The *Dpn* I recognition sequence GATC occurs with high frequency and needs to be methylated for *Dpn* I to cleave DNA. Therefore, *Dpn* I cleaves only template plasmid DNA that was methylated by the host cell, but not the unmethylated PCR product. *Dpn* I was inactivated by incubation at 65 °C for 20 min. 5 µl of the *Dpn* I treated PCR reaction were transformed into DH5α chemically competent cells. Cells were plated on LB-agar containing 100 µg/ml ampicillin. Transformants were allowed to form colonies overnight at 37 °C. Single colonies were used to inoculate LB^{Amp} medium and grown overnight at 37 °C. Cells were harvested and plasmid DNA was isolated.

Presence of the restriction site introduced by the specific primers for site directed mutagenesis was verified by restriction digestion analysis. Positive clones were verified by DNA sequencing.

III.4.6 Generation of linear template DNA for in vitro translation reactions

Linear DNA templates for protein production in the reconstituted system were generated by PCR using *Taq* polymerase. Fragments of the titin I27 domain were amplified directly from pCH25Titin using T7-uni as the forward primer and a suitable reverse primer (see Appendix VII.1). The resulting products contained all the regulatory elements necessary for *in vitro* translation, such as the T7-promoter and a ribosomal binding site.

FL fragments for *in vitro* translations were generated in a two-step PCR process. In the first reaction, a part of the FL ORF was amplified with specific primers (see Appendix VII.1). The forward primer contained an extension at the 5'-end of the coding sequence that added an adapter sequence and an initiator codon to the ORF. The second PCR was performed with the same reverse primer as the first reaction, but with the Universal Primer as the forward primer, binding at the adapter sequence. The Universal Primer introduced the necessary regulatory sequences upstream of the ORF. All PCR products were subjected to gel purification before they were used as templates DNA for protein production in the reconstituted system.

III.5 Protein preparative methods

III.5.1 Purification of TF

pPROEX-based plasmids harboring the ORF of the various TF versions were transformed into *E. coli* BL21(DE3)*gold* chemically competent cells. Cells were plated on LB^{Amp}-agar. Transformants were allowed to form colonies overnight at 37 °C. Colonies were used to inoculate 200 ml of LB^{Amp} medium. The culture was grown to an OD_{600} of ~4 at 37 °C with vigorous agitation. This culture was diluted into fresh LB^{Amp} medium supplemented with 1 mM IPTG and incubated for 2 h at 37 °C with agitation. The culture was chilled on ice-water.

Cells were harvested by centrifugation in an JLA 10.500 rotor (Beckman) for 4 min at 8000 rpm, 4 °C. Cells were resuspended in PBS, pelleted again, and the pellet was frozen in liquid nitrogen.

For cell lysis, cells were thawed and resuspended in ~50 ml PBS. Cell lysis was achieved by 4 to 5 passages through an Emulsiflex C5 homogenizer (Avestin) operated at 10000 – 15000 psi. The lysate was cleared by centrifugation at 40,000 *g*, 4 °C for 30 min.

The cleared lysate was applied at a flow rate of 1 ml/min to a 5 ml HiTrap Chelating column (Amersham) pre-charged with Ni^{2+} and equilibrated in PBS. The column was washed with PBS and subsequently with 10 mM and 25 mM imidazole in PBS until a stable baseline was reached. Bound His_6-tagged protein was eluted with 300 mM imidazole in PBS. The peak fractions were pooled and passed through a HiPrep Desalting column (Amersham) equilibrated in PBS.

For the removal of the amino-terminal His_6 sequence, the desalted protein in PBS was incubated with TEV protease in the presence of 2 mM DTT. After efficient cleavage, the protein was again desalted into PBS as described and passed through a regenerated 5 ml HiTrap Chelating column charged with Ni^{2+} and equilibrated in PBS. In this final step, the cleaved His_6-tag fragments, uncleaved His_6-TF and the His_6-tagged TEV protease were retained by the Ni^{2+}-NTA resin. The flow through, containing pure TF wihout the N-terminal His_6-tag, was collected and concentrated 20- to 30-fold by ultrafiltration using Amicon Ultra-15 Centrifugal Filter Units (Millipore). The purified protein was shock-frozen in liquid nitrogen in small aliquots and stored at –80 °C.

III.5.2 Purification of TEV protease

The plasmid pETEV encoding a His_6-tagged version of the mature protease from Tobacco Etch Virus (TEV protease) in a pET-backbone was transformed into *E. coli* BL21(DE3)*gold* cells. Transformants were plated on LB^{Kan}-agar. LB^{Kan} medium was inoculated with multiple colonies of these transformants, and the culture was grown to saturation overnight at 37 °C. 4 l of LB^{Kan} medium were inoculated with this overnight culture to an OD_{600} of ~0.1, and the culture was grown at 37 °C to an OD_{600} of 0.4. The culture was then cooled to 18 °C and allowed to grow for additional 90 min. IPTG was added to 0.4 mM, and expression was allowed to proceed for ~16 h at 18 °C before the culture was cooled on ice-water. Cells were harvested, resuspended in ~100 ml 10I-buffer and frozen in liquid nitrogen.

The cell suspension was thawed slowly with occasional vortexing. After thawing, the suspension was supplemented with 0.5 mg/ml lysozyme, 0.1% Triton X-100 and 100 U/ml Benzonase and incubated for 30 min at 4 °C with constant agitation. The suspension was sonicated in 4 aliquots, 4 times for 30 s *per* aliquot using a Branson Sonifier with a microtip at full duty. The lysate was cleared by centrifugation for 40 min at 40,000 *g* at 4 °C.

The cleared lysate was applied at 1 ml/min to a 5 ml HiTrap Chelating column charged with Ni^{2+} ions equilibrated in 10I-buffer. The column was washed with 10I-buffer and 20 mM imidazole in the same buffer. Elution of the recombinant protein was achieved with 200 mM imidazole in the same buffer. Peak fraction of the eluate were pooled and dialyzed against 100 volumes of TEV Storage buffer. Aliquots were flash-frozen in liquid nitrogen and stored at –80 °C.

III.5.3 Isolation of ribosomes

E. coli strain MC4100 with a deletion in the gene encoding TF, MC4100 *Δtig*, was obtained from P. Geneveaux (Departement de Biochimie Medicale, Centre Medical Universitaire, Geneve, Switzerland). Ribosomes were isolated from *E. coli* MC4100 *Δtig* according to published procedures (Spedding 1990).

E. coli MC4100 *Δtig* cells were plated on LB-agar containing 17 µg/ml chloramphenicol (Cam). Colonies were allowed to form colonies overnight at 37 °C. A single colony was used to inoculate LB^{Cam} medium, which was grown to saturation overnight at 37 °C. This starter culture was diluted 1:100 into 6 l of unsupplemented LB medium. The culture was grown at 37 °C to an OD_{600} of ~0.5. The culture was allowed to cool slowly to 15 °C and then chilled on ice water. All subsequent steps were performed either on ice or at 4 °C.

Cells were harvested by centrifugation, resuspended in Buffer A and pelleted again. The cell pellet was flash-frozen in liquid nitrogen and stored at –80 °C, yielding typically 15 g wet weight of cells.

Cells were thawed and resuspended in 50 ml Buffer A and lysed by three passages through an Emulsiflex C5 homogenizer (Avestin) operated at 10,000 – 15,000 psi. The lysate was cleared by centrifugation at 30,000 *g*, 4 °C for 30 min. The top three fourths of the cleared lysate were recovered. Portions of the cleared lysate were layered over an equal volume of 1.1 M sucrose in Buffer B and centrifuged for 15 h at 100,000 *g*. The supernatant was decanted and the clear pellet was gently rinsed with Buffer A. The pellet was dissolved in Buffer A by gentle agitation for 1 h and subjected to a second cushion centrifugation as described. The pellet was dissolved in Buffer C, and ribosomes were sedimented by centrifugation at 100,000 *g* for 16 h. The pellet was resuspended in Buffer E yielding, ~500 A_{260} units/ml and dialyzed against Buffer E (3 changes of ~500 volumes over several hours each). Small aliquots of purified ribosomes were flash-frozen in liquid nitrogen and stored at –80 °C.

III.5.4 Site-specific labeling of TF single cysteine mutants

Dyes for site-specific labeling utilized in this study were 6-bromoacetyl-2-dimethyl-aminonaphthalene (BADAN), 7-diethylamino-3-(4'-maleimidylphenyl)-4-methylcoumarin (CPM) and fluorescein-5-maleimide. Desalting steps in the course of site-specific labeling procedures were performed using Sephadex G-25 desalting columns (Nap-5 columns, Amersham Pharmacia Biotech).

Typically, ~75 nmol of TF single cysteine mutant protein were incubated with 150 nmol tris-(2-carboxyethyl)phosphine (TCEP) in 150 µl PBS for 10 min at 25 °C to completely reduce cysteine thiol groups. A 4-fold molar excess of the fluorescent dye (as the maleimide derivative) and 400 µl 20 mM Tris-HCl, pH 7.5 were added. The reaction was allowed to proceed for 90 min at 25 °C in the dark. β-mercapto-ethanol (β-ME) was added to a final concentration of 10 mM to quench the reaction. Excess dye and β-ME were removed by desalting the protein into PBS. The eluate was concentrated to ~500 µl and desalted into PBS again. The eluate was concentrated 2- to 3-fold, and small aliquots of labeled protein were flash-frozen in liquid nitrogen and stored at –80 °C in the dark.

III.5.5 Differential labeling of TF double cysteine mutant proteins

For differential labeling of TF double cysteine mutant proteins, the protein stock solution in PBS was diluted 1:10 into PBS pH 6.4. 50 nmol of protein were mixed with a two-fold molar excess of CPM and incubated 45 s at 15 °C. β-ME was added to a final concentration of 10 mM to quench the reaction. Excess dye and β-ME were removed by desalting the labeled protein into PBS. The protein was incubated with 1 ml (bed volume) of Thiol Sepharose 4B (Amersham) for 90 min in the cold. The beads were washed three times with one bed volume each of PBS, and the bound protein was eluted in three subsequent steps with 500 µl 100 mM dithio-threitol (DTT) for 20 min each. The eluted fractions were pooled, concentrated to ~500 µl by ultrafiltration and desalted into PBS. The eluate was split into two aliquots of 480 µl each. To one aliquot, 150 nmol fluorescein-5-maleimide in 2.5 µl dimethyl-formamide (DMF) was added, to the other, 2.5 µl DMF were added. After incubation for 90 min at 25 °C, the reactions were desalted into PBS, concentrated two-fold and desalted into PBS again. After a final two- to three-fold concentration step, small aliquots were frozen in liquid nitrogen and stored at –80 °C in the dark.

III.6 Protein analytical methods

III.6.1 Quantitation of protein concentrations

Purified, unmodified proteins were quantitated by absorbance spectroscopy at 280 nm in 6 M Guanidine-HCl, 20 mM Na-PO_4, pH 6.5 using calculated extinction coefficients (Gill & von Hippel 1989). Extinction coefficients were ε_{280nm}(TF) = 15,930 $M^{-1}cm^{-1}$ for TF and ε_{280nm}(NC) = 8,960 $M^{-1}cm^{-1}$ for NC.

Modified proteins were quantitated in a colorimetric assay (Bio-Rad Protein Assay, BioRad) based on the method of Bradford (Bradford 1976). As a reference, a calibration curve with the respective unmodified protein was prepared.

Ribosomes were quantitated spectrophotometrically assuming that 1 A_{260} unit corresponds to 23 pmol of ribosomes when measured in Ribosome Spec-buffer (Spedding *et al.*). This corresponds to an extinction coefficient of $\varepsilon_{260nm} = 4.348 \times 10^7$ M^{-1} cm^{-1}. As a criterion for purity, the A_{260}/A_{280} ratio was determined, which is ≥ 1.8 for clean ribosomes.

III.6.2 Quantitation of accessible thiol groups and determination of thiol reactivity

Quantitation of total and accessible thiol groups in the TF-cysteine mutants was performed as described (Riddles *et al.* 1983). Briefly, the cysteine-containing protein was incubated with 5,5'-dithiobis-(2-nitrobenzoic acid) (DTNB; Ellman's reagent). Reaction of DTNB with free thiols yields a mixed disulfide and a free 2-nitro-5-thiobenzonate anion (TNB^{2-}) in a 1:1 stoichiometry. TNB^{2-} exhibits a strong absorbance at around 410 nm. The amount of TNB^{2-} can be quantitated, thus allowing the calculation of reactive thiols present in the sample.

For quantitation of total thiol groups, the assay was performed under denaturing conditions. A dilution of the TF cysteine mutant (10 µM final) was prepared in PBS containing 2% SDS. DTNB was added to a final concentration of 350 µM, and absorbance at 410 nm was followed over time. The amount of TNB^{2-} ions released during the reaction was calculated using an extinction coefficient of $\varepsilon_{410\,nm}$ (TNB^{2-}) = 13,600 $M^{-1}cm^{-1}$. For the quantitation of accessible thiol groups in the native protein, the reaction was repeated omitting SDS from the buffer.

The reaction of the coumarin-derivative CPM with thiols can be monitored in real-time, because underivatized CPM is virtually non-fluorescent, whereas the thiol-adduct exhibits fluorescence when excited at ~395 nm. To determine the reaction kinetics of CPM towards the cysteines introduced into TF, TF single or double cysteine mutants were diluted to 15 µM in PBS. CPM was added to a final concentration of 30 µM, and fluorescence was followed over time (λ_{exc} = 393 nm, λ_{em} = 482 nm).

III.6.3 SDS-PAGE

For SDS-PAGE, a discontinuous electrophoresis system under denaturing, reducing conditions was used (Laemmli 1970). Samples were prepared for SDS-PAGE by the addition of 5x SDS-PAGE sample buffer and heating to 96 °C for 5 min prior to loading onto the gel.

Stacking gels contained 4% polyacrylamide and separating gels 12% or 15% (see Table 1). Ammonium-peroxo-disulfate (APS) and N,N,N',N'-Di-(dimethylamino)-ethane (TEMED) were added immediately before casting the gels. Electrophoresis was carried out at constant current (40 mA *per* gel) in SDS-PAGE electrophoresis buffer.

	separating gel		**stacking gel**
% acrylamide (AA)	**12**	**15**	**4**
30 % AA, 0.8 % bis-AA	8 ml	10 ml	1.3 ml
1.5 M Tris-HCl, pH 8.8	5 ml	5 ml	–
0.5 M Tris-HCl, pH 6.8	–	–	2.5 ml
10 % SDS	0.2 ml	0.2 ml	0.1 ml
H_2O	1.8 ml	–	6.1 ml
TEMED	10 µl	10 µl	5 µl
APS	50 µl	50 µl	100 µl

Table 1: Composition of stacking and separating gels for SDS-PAGE

After electrophoresis, gels were stained with Coomassie Staining Solution (0.1% Coomassie Brilliant Blue R-250, 30% methanol, 10% acetic acid) and destained with 50% methanol, 12% acetic acid.

If a more sensitive detection was required, protein bands were visualized by silver staining. After electrophoresis, gels were fixed first in 50% methanol, 12% acetic acid (2 × 30 min), then in 50% ethanol (3 × 20 min). After incubation in 200 mg/ml $NaS_2O_3 \cdot 5\ H_2O$ for 1 min, gels were rinsed with water twice. Gels were incubated for 20 min in 2 g/l $AgNO_3$, 375 µl/l formaldehyde and rinsed with water. Gels were developed in 60 g/l

$Na_2CO_3 \cdot 5\ H_2O$. To stop the developing process, gels were transferred into 10% acetic acid and incubated for 10 min. For storage, gels were equilibrated in 1% acetic acid and stored at 4 °C.

III.6.4 Western Blotting

Immuno-blotting was performed according to Towbin *et al.* (1979). After separation by SDS-PAGE, proteins were transferred onto a nitrocellulose membrane in a tank blot system (BioRad). Transfer was achieved at constant current (400 mA) for 1 h in transfer buffer (25 mM Tris, 192 mM glycine, 20% methanol, pH 8.4). After transfer, the membrane was blocked by incubation with 5% (w/v) dry milk in TBST for ~1 h at room temperature (RT) or overnight at 4 °C. All subsequent washing and incubation steps were carried out in TBST. The membrane was washed three times and incubated with the primary antibody for 1 h at RT. After washing the membrane three times, it was incubated with the HRP-coupled secondary antibody for 1 h at RT. The membrane was washed three times. For visualization by enhanced chemiluminescence, the ECLplus Western Blotting Detection System (Amersham Pharmacia) was used, and the membrane was exposed to a BioMax film (Kodak).

Primary antibodies used were rabbit anti-L23 serum (from Andreas Kolbeck, MPI for Biochemistry, Martinsried, Germany; diluted 1:5,000) and the monoclonal anti-FLAG M2 antibody (Sigma; diluted 1:2000). If the anti-FLAG M2 antibody was used, TBS was used instead of TBST, omitting the Tween 20 from the buffer. HRP-coupled goat anti-rabbit IgG (Transduction Laboratories) or goat anti-mouse IgG (Sigma) were used as secondary antibodies at a dilution of 1:2,000.

III.6.5 Autoradiography

Radiolabeled proteins were separated by SDS-PAGE. After electrophoresis, gels were fixed in 50% methanol, 12% acetic acid, briefly rinsed in water and dried on Whatman paper in a Slab Gel Dryer SGD 2000 (Savant) for 1 h at 72 °C. Dried gels were exposed to a phospho-imaging plate (Fuji) for 12 – 36 h. The imaging plate was analyzed using an FLA 200 imaging system (Raytest). Band intensities were quantified using the AIDA software version 2.31 (Raytest).

III.6.6 Protein production in the reconstituted system

The transcription/translation system (PURESYSTEM classic II, Post Genome Institute Co., Ltd; Japan) was reconstituted according to the manufacturers instructions. Template DNA was added to a final concentration of 10 ng/µl. For spectroscopic measurements, the reaction volume was 150 µl, and the reaction was supplemented with labeled TF at a final concentration of 250 nM unless otherwise indicated. If the translated product were to be visualized by autoradiography, 3 µl ^{35}S-methionine (Amersham; 1000 Ci/mmol, 15 mCi/ml) were included in a 150 µl reaction.

III.6.7 Limited proteolysis

Ribosome-nascent chain complexes of the titin I27 domain either alone or with a carboxyl-terminal extension of 50 amino acids were produced in the reconstituted system by the addition of appropriate linear template DNA. The reaction volume was 150 µl, containing 3 µl ^{35}S-methionine to obtain radio labeled translation products. The reaction was allowed to proceed for 45 min at 30 °C. The reactions were cooled to 0 °C, supplemented with 7.5 µg/ml (corresponding to 250 nM) Proteinase K (Boehringer Mannheim) and incubated on ice. At the indicated time points, 25 µl of the reaction were removed and supplemented with phenyl-methyl-sunfonyl fluoride (PMSF) to a final concentration of 1 mM. To each sample, RNase A (Qiagen, Hilden, Germany) was added to a final concentration of 100 µg/ml to digest tRNA moieties. An equal volume of 5x SDS-PAGE sample buffer was added to each sample. Samples were separated by SDS-PAGE and radio labeled bands were visualized by autoradiography.

III.6.8 Determination of FL specific activity

Pyrococcus pyralis firefly luciferase (FL) was translated from plasmid pLuc in the reconstituted system supplemented with 5 µM TF and 1 µl ^{35}S-methionine. In a control reaction, buffer without protein was added. The reaction was allowed to proceed for 45 min at 30 °C before it was placed on ice. To measure luciferase enzymatic activity, an aliquot of the reaction was diluted 1:250 in Luciferase Dilution Buffer. 2 µl of the 1:250 dilution were mixed with 48 µl Luciferase Assay Buffer (Luciferase Assay System #E1501, Promega) and luminescence was measured immediately using an EG&G Berthold Lumat LB 9507 luminometer. To quantitate the amount of protein produced in the translation reaction, an aliquot of the reaction was diluted 1:4 in 2x SDS-PAGE sample buffer, and equal amounts of all samples were subjected to SDS-PAGE and autoradiography. Specific FL activity was calculated by dividing the enzymatic activity by the corresponding band intensity.

III.7 Fluorescence Measurements

III.7.1 General

All buffers used in spectroscopic measurements were sterile filtered (2 µm filtering devices) and degassed. Spectra and kinetic traces were collected on a Fluorolog 3 fluorometer (Jobin Yvon) at 30 °C. For all measurements, a background sample was prepared containing all the components that were present in the sample with unlabeled instead of labeled TF. The background values were subtracted from the values obtained with samples containing labeled TF. The slits of the excitation and emission beam were adjusted to yield a maximum of ~10^6 cps for TF-B or donor-only samples. To correct for fluctuations in the excitation light source, the reference signal (R) was recorded in addition the actual signal (S) during all fluorescence emission measurements. For evaluation, the quotient of S/R was used.

III.7.2 Equilibrium fluorescence measurements

Emission spectra were acquired with increments in emission wavelength of 1 nm and an integration time of 0.25 s *per* data point. At least three scans per measurement were accumulated and averaged.

Measurements with TF-B were performed at a concentration of 250 nM labeled protein. The fluorophore was excited at 397 nm, and emission spectra were collected from 410 to 600 nm.

Samples for inter-molecular FRET measurements contained 250 nM donor-labeled TF and 1 µM acceptor labeled TF. For a donor-only sample, 1 µM unlabeled instead of acceptor labeled protein was used. The donor was excited at 397 nm, and fluorescence emission was recorded from 410 to 650 nm. Measurements without ribosomes were done in PBS. If ribosomes were to be included, the labeled proteins were mixed in PBS in a volume of 30 µl, ribosomes (dissolved in Buffer E) were added to the indicated concentrations and Buffer E was added to a final volume of 150 µl. Samples containing ribosomes were incubated for 20 min at 30 °C before the fluorescence measurements were performed, to allow equilibrium formation.

Intra-molecular FRET measurements were performed in a similar manner to the inter-molecular FRET measurements, except that the samples contained 250 nM of either donor-only or donor and acceptor labeled TF.

III.7.3 Kinetic fluorescence measurements

For measuring changes in fluorescence of labeled TF during translation, the components of the reconstituted system were mixed with labeled TF in the absence of template DNA. For intra-molecular FRET measurements, 250 nM of either donor-only (TF-C) or donor and acceptor labeled TF (TF-CF) was added. Unless otherwise indicated, the derivatized R14C E326C TF version was utilized in these experiments. For inter-molecular FRET-measurements, 250 nM donor labeled and 1 µM either unlabeled or acceptor labeled TF were added. Both donor and acceptor fluorophores were coupled to position 326 for these measurements. For the analysis of TF ribosome recruitment, 250 nM TF derivatized with BADAN at position 14 was utilized.

The reactions were incubated at 30 °C for 3 min before template DNA was added to start the translation reaction. The reaction was transferred into a cuvette pre-warmed to 30 °C, and fluorescence was followed over time. Data points (S, R and S/R) were collected every second with an integration time of 1 s. Excitation and emission wavelengths were 397 nm and 500 nm for TF-B and 397 nm and 460 nm for FRET measurements, respectively.

III.7.4 Competition experiments

For competition experiments with vacant ribosomes, 250 nM labeled TF (TF-B or TF-C/TF-CF) were mixed with ribosomes in Buffer E, and an equilibrium was allowed to form at 30 °C within 20 min. 140 µl of this reaction were mixed with 4.5 µl competitor, typically at 650 µM, resulting in a final competitor concentration of 20 µM. Immediately after mixing, fluorescence was followed over time at a time interval of 0.5 s between data points and an integration time of 0.5 s. Excitation and emission wavelengths were the same as indicated in the previous section.

For the displacement of TF during translation, a reaction with the reconstituted translation system was prepared in a volume of 150 µl and incubated at 30 °C until fluorescence reached a plateau and protein production took place at a constant rate (35 to 45 min after the addition of plasmid). 140 µl of the translation reaction were then used in the competition experiment as described above.

III.7.5 Steady state fluorescence anisotropy measurements

Steady state fluorescence anisotropy measurements were performed in collaboration with Dr. José M. Barral. Steady state fluorescence anisotropy measurements were conducted on an LS 50 B spectro-fluorometer (Perkin Elmer). For equilibrium measurements and TF-ribosome recruitment during translation, the anisotropy was measured continuously. For displacement kinetics, $\boldsymbol{I}_{||}$ and $\boldsymbol{I}_{\perp}$ were measured in separate reaction duplicates, and the anisotropy was calculated according to Eq. 10.

III.8 Ribosome tagging

In order to introduce a FLAG-His$_6$ (FH) epitope tag into the large ribosomal subunit of *E. coli* MC4100, a recently described recombination system for the generation of gene deletions in *E. coli* was utilized (Datsenko & Wanner 2000). This system is based on the phage λ Red recombinase system, consisting of the genes *γ*, *β* and *exo*. These genes were cloned into a plasmid under the control of an arabinose inducible promoter to allow their regulated expression in *E. coli* (plasmid pKD46, Datsenko & Wanner 2000). This plasmid is a temperature sensitive replicon allowing its easy elimination from the host. When the Red recombinase genes are expressed, the efficiency of homologous recombination is drastically enhanced. Originally described for utilization in chromosomal gene disruption, this system was used in the present study to introduce the coding sequence of an FH epitope tag together with a tetracycline resistance gene (*tet*^{R}) into the chromosome of the *E. coli* strain MC4100.

III.8.1 Generation of *rpl-FH-tet*^{R} cassettes

A synthetic oligonucleotide encoding the FH epitope tag (FHfw) was mixed with a complementary oligonucleotide (FHrv) at equimolar concentrations (60 µM each). The oligonucleotides were designed such that, in addition to the complementary central sequence, they contained overhangs that resulted in the formation of cohesive ends after annealing. For annealing, the mixed oligonucleotides were heated to 96 °C for 5 min and allowed to slowly cool down to room temperature. By this procedure, a double stranded oligonucleotide was generated encoding the FH tag with cohesive ends at the 5'- and the 3'-termini compatible with cohesive ends resulting from *Not* I and *Xho* I restriction digestion, respectively.

pET22b(+) was digested with *Not* I and *Xho* I endonucleases and dephosphorylated with SAP. The annealed oligonucleotide encoding the FH epitope tag was ligated into this backbone as described above, yielding plasmid pFH.

The open reading frame (ORF) of the tetracycline resistance gene (*tet*^{R}) was amplified by PCR from plasmid pBR322 (Bolivar *et al.* 1977) using primers tetP1 and tetP2 (see Appendix VII.1). Since the resistance cassette was intended to be inserted into existing operons, a promoter for *tet*^{R}-gene expression was not considered necessary. The PCR product was gel purified, digested with *Hind* III and *Nco* I endonucleases and ligated into plasmid pFH that had been digested with the same enzymes and dephosphorylated with SAP. The resulting plasmid is referred to as pFH-tet.

Stretches of ~500 bp downstream of the rpl-ORF of interest were amplified by PCR from *E. coli* K12 genomic DNA using primer pairs rplP3 and rplP4, where rpl is L13, L17, L20 or L22. The PCR products were digested and inserted into the plasmid pFH-tet downstream of the tet^R-ORF via *Nco* I and *Xba* I endonuclease sites, yielding plasmids pFH-tet-13, pFH-tet-17, pFH-tet-20 and pFH-tet-22. Positive clones were verified by DNA sequencing.

Using primer pairs rplP1 and rplP2, the ORFs encoding L13, L17, L20 and L22 together with ~500 bp of upstream flanking sequences were amplified by PCR from *E. coli* K12 genomic DNA. Products for L13, L17 and L20 were digested with *Xba* I and *Eco* RI, the product for L22 was digested with *Xba* I and *Sac* I, and the digested products were ligated *via* the same sites into pBAD18 (Guzman *et al.* 1995). No positive clones could be obtained for L22, indicating interference with survival of the host cell. The resulting plasmids were pL13, pL17 and pL20.

The inserts of plasmids pFH-tet-13, pFH-tet-17 and pFH-tet-20 were released by restriction digestion with *Xho* I and *Xba* I endonucleases, gel-purified and ligated *via* the same sites into pL13, pL17 and pL20, respectively. The resulting plasmids are referred to as pL13FH, pL17FH and pL20FH. *E. coli* cells transformed with pL13FH showed impaired growth rates. This plasmid was not used in further experiments.

III.8.2 Chromosomal integration of $rpl\text{-}FH\text{-}tet^R$ cassettes

The insert of plasmid pL17FH was amplified by PCR using the primer-pair L17P1 – L17P4. The template was digested with *Dpn* I endonuclease, and the PCR product was gel-purified twice and eluted in 50 µl of sterile water.

E. coli M4100 cells were transformed with pKD46 and plated on LB^{Amp}-agar. Transformants were allowed to form colonies overnight at 30 °C. A single colony was used to inoculate 50 ml LB^{Amp}. A culture was grown at 30 °C to an OD_{600} of ~0.1 before arabinose was added to a final concentration of 0.02% (w/v). The culture was further grown at 30 °C to an OD_{600} of 0.8, arabinose was added to a final concentration of 0.2% and the culture was grown for another 10 min. Cells from 5 ml of this culture were harvested by centrifugation and rendered electrocompetent as described above.

The cell pellet was resuspended in 50 µl of the purified PCR product and incubated 15 min on ice. Cells were subjected to electroporation and resuspended in SOC medium. After incubation at 37 °C with gentle shaking at 300 rpm for 1 h, one third of the cells was plated on LB^{Tet}-agar and incubated at 37 °C overnight. A single colony was picked and resuspended in 50 µl LB medium. 10 µl of the suspension was plated on either LB^{Amp}- or LB^{Tet}-agar. After overnight incubation at 37 °C, colonies appeared only on LB^{Tet}-, not on LB^{Amp}-agar. A single colony was used to inoculate 5 ml of LB^{Tet} medium, and a culture was grown overnight at 37 °C to saturation. A glycerol stock of this culture was prepared by mixing 600 µl of this culture with 300 µl sterile glycerol. The stock was flash-frozen in liquid nitrogen and stored at –80 °C.

The resulting strain is referred to as CK1 (*E. coli* MC4100 *rplQ::rplQ-FH-tet*^{R}). Loss of the pKD46 plasmid was verified by streaking *E. coli* CK1 cells from the glycerol stock on different selective media at 30 °C. Growth was observed only upon selection for tetracycline resistance and cells failed to grow on ampicillin selective medium.

III.8.3 P1-transduction

For the transduction of the *rplQ-FH-tet*^{R} allele into a TF-deficient strain, P1-phage transduction was performed (Miller 1992) with CK1 as the donor- and *E. coli* MC4100 *Δtig* (Genevaux *et al.* 2004) as the recipient strain.

For the preparation of a P1 lysate from the donor strain, 5 ml LB medium supplemented with 5 mM $CaCl_2$ were inoculated with a single colony of the donor strain and grown to an OD_{600} of 0.2 – 0.3. The culture was infected with 5×10^7 plaque forming units (pfu) of wild type P1 phage. The culture was further grown until it cleared (indicating cell lysis), which usually happened within 3 h. The lysate was mixed with 100 µl chloroform. The lysate was cleared by centrifugation at 4,500 *g* for 10 min, and the supernatant was transferred into a sterile tube. The P1 lysate was mixed with 100 µl chloroform and stored a 4 °C.

For determination of the phage titer of the P1 lysate prepared from strain CK1, a culture of WT *E. coli* MC4100 cells was grown at 37 °C in a volume of 1 ml to an OD_{600} of 0.8. Cells were collected by centrifugation and resuspended in 1 ml MC buffer. Dilutions of the P1 lysate of $1{:}10^6$ and $1{:}10^8$ were prepared in sterile water. 100 µl aliquots of resuspended cells were mixed with 100 or 10 µl of the $1{:}10^6$ dilution or 100 µl of the $1{:}10^8$ dilution of the P1 lysate and incubated at 37 °C for 15 min. Each aliquot of the infected cells was mixed with 5 ml top agar that had been melted and allowed to cool to 50 °C. The top agar was immediately layered on top of LB-agar plates pre-warmed to 37°C and distributed evenly on the surface without introducing air bubbles. After the top agar had solidified, plates were incubated overnight at 37 °C to allow bacterial growth and plaque formation. The titer of the P1 lysate was determined by counting the number of plaques *per* plate (each plaque corresponding to one pfu) and correcting for dilution factors.

For the genetic transduction using the P1 lysate prepared from the donor strain, a culture of the recipient strain was grown to an OD_{600} of 0.8. Cells were harvested by centrifugation and resuspended in MC buffer to yield 10^9 cells *per* ml, assuming that 1 OD_{600} unit corresponds to 8×10^8 cells. Resuspended cells were incubated at 37 °C for 20 min or at 30 °C for 40 min. 100 µl of the suspension (corresponding to 10^8 cells) were mixed with 10^7 pfu of the P1 lysate prepared from the donor strain and incubated for 30 min at 37 °C or 1 h at 30 °C. 100 µl of citrate buffer were added to abolish further infection and the cells were spread on LB-agar supplemented with the appropriate antibiotic to select for clones that had received the resistance gene from the donor strain. Positive clones were selected and a glycerol stock was prepared as described above. The resulting strain is referred to as CK3 (*E. coli* MC4100 *Δtig rplQ::rplQ-FH-tet*^{R}).

III.8.4 Preparation of E. coli lysates for analytical ribosome isolations

For the preparation of lysates, cultures of different *E. coli* strains were grown in LB medium. If the FH-tagged ribosomal protein was plasmid-encoded (plasmids pL17FH or pL20FH), the medium was supplemented with 0.2% arabinose to induce gene expression from the plasmid. Cells were grown at 37 °C to an OD_{600} of 0.4 – 0.6.

For preparation of ribosomes enriched in ribosome-nascent chain complexes, the culture was supplemented with 200 µg/ml chloramphenicol before if was poured onto crushed ice that had been cooled to –20 °C. In this case, all buffers used in the following procedures contained 200 µg/ml chloramphenicol. If vacant ribosomes were to be enriched, puromycin was added to a concentration of 50 µg/ml, and the culture was incubated at 15 °C for 15 min. At this temperature, translation elongation is favored over initiation. If these conditions were applied, all buffers used in the following steps contained 50 µg/ml puromycin.

The culture was chilled on ice water, and cells were harvested by centrifugation. All subsequent steps were performed at 4 °C or on ice. Cells were washed once with Buffer A and resuspended in 1/50 of the original culture volume in this buffer. Lysozyme was added to a final concentration of 750 µg/ml, and samples were frozen by placement in a –80 °C freezer for at least one hour before they were thawed in ice water, which resulted in cell lysis.

RNase-free DNase I (Roche) was added to 50 U/ml, and the lysate was incubated 30 min on ice. The lysate was cleared by centrifugation at 20,000 *g* for 30 min, and the top three fourths of the cleared lysate were recovered.

III.8.5 Sedimentation analysis of E. coli ribosomes

To confirm the incorporation of FH-tagged ribosomal proteins into the 70S ribosome, ribosomes from lysates of different *E. coli* strains were isolated by sedimentation through a sucrose cushion. Ribosomes were further analyzed by separation on a 10 – 40% sucrose gradient.

~1.7 ml of the cleared lysate prepared as described in the previous section were layered onto a cushion of 2.5 ml 0.9 M sucrose in Buffer A. Ribosomes were sedimented by centrifugation for 2 h at 300,000 *g*. The ribosomal pellet was rinsed with 750 µl Buffer A and dissolved in Buffer A by gentle agitation to yield an absorbance of A_{260} = 25. For SDS-PAGE and immuno-blot analysis, 75 µl of this sample were incubated with 2 µg/ml RNase A for 15 min at room temperature, and 20 µl 5× SDS-PAGE sample buffer were added.

For further separation of ribosomes, gradients of 10 – 40% sucrose in Buffer A were prepared in SW28 centrifuge tubes (Beckman) with a short cap by tilted tube rotation using a Gradient Master (BioComp) running a 2-step program consisting of step 1: 2 min 50 s, angle 52 °, speed 25; step 2: 36 s, angle 75 °, speed 22. 10 A_{260} units of the dissolved ribosomal pellet were layered on top of the gradient, and separation was achieved by centrifugation for 15 h at 45,000 *g*. The gradient was fractionated from top to bottom into fractions of ~1.3 ml using an AutoDensiFlow gradient fractionator (LabConco UniEquip) connected to a LKB UV-M II absorbance detector (Pharmacia).

From the fractions displaying the highest absorbance at 260 nm, total protein was precipitated after treatment with 2 µg/ml RNase A (Qiagen) for 15 min at room temperature. Precipitation of total protein was achieved by the addition of tri-chloro acetic acid (TCA) to a final concentration of 13% (w/v) and incubation for 5 min at −20 °C and 30 min on ice. Precipitated protein was collected by centrifugation at 20,000 *g* for 15 min. The pellet was resuspended in 50 µl 250 mM Tris-base, and 13 µl 5× SDS-PAGE sample buffer were added.

Samples were subjected to SDS-PAGE. For Coomassie-blue staining, 0.1 ODml of the cleared lysate, 25 µl of the ribosomal sample from cushion centrifugation and 30 µl of the processed gradient fractions were loaded. For immuno-blotting, one tenth of these amounts was loaded.

III.8.6 Ribosome pull-downs using anti-FLAG agarose

For the pull-down of ribosomes containing FH-tagged ribosomal proteins, the agarose-based anti-FLAG M2 Affinity Gel (Sigma) was used. The matrix was equilibrated in Buffer TMN, and 100 µl of beads were incubated with 5 A_{260}-units of cleared lysate for 60 min at 4 °C with constant gentle agitation. Beads were sedimented at 2,000 *g* for 1 min and washed three times with 200 µl of Buffer TMN. Bound material was eluted with 150 µg/ml FLAG peptide (Sigma) in TBS buffer.

III.8.7 Ribosome pull-downs using magnetic beads

For the pull-down of ribosomes with magnetic beads, anti-FLAG monoclonal antibody M2 was bound to Protein A-coupled beads (Dynabeads, Dynal). 125 µl of magnetic beads were equilibrated with PN-buffer. Separation of the beads from buffer was achieved by placing on a MPC-S Magnetic Particle Concentrator (Dynal) for 1 min and aspirating the buffer. Beads were resuspended in 100 µl PN-buffer and 25 µl anti-FLAG M2 antibody (Sigma) were added (~115 µg of protein). After incubation for 45 min at 25 °C, the liquid was removed and the beads were washed three times with Buffer TMN.

To 50 µl of the beads, 10 A_{260}-units of lysate were added in a volume of 100 µl. After 90 min incubation at 4 °C with constant agitation, beads were separated from the liquid and washed three times with Buffer TMN. Elution of bound material was achieved in three subsequent elution steps with 50 µl 250 µg/ml FLAG-peptide (Sigma) in TBS.

III.9 Data Evaluation and Calculations

III.9.1 FRET efficiency and distance calculations

Fluorescence resonance energy transfer (FRET) occurs when the excited-state energy is transferred from an initially excited donor (D) to an acceptor (A). The efficiency of transfer for a given D – A pair is dependent on the distance separating these two fluorophores, with a half-maximal transfer efficiency at a distance of R_0, the Förster distance. The rate constant of energy transfer, k_T, is given by

$$\mathbf{k_T = \frac{1}{\tau_D} \cdot \left(\frac{R_0}{r}\right)^6} \quad \text{(Eq. 1)}$$

with τ_D being the decay time of the donor in the absence of acceptor and r corresponding to the D – A distance. The efficiency of transfer, E_{FRET}, is the fraction of all photons absorbed by the donor that are transferred to the acceptor, given by

$$\mathbf{E_{FRET} = \frac{k_T}{\tau_D^{-1} + k_T}} \quad \text{(Eq. 2).}$$

E_{FRET} can also be determined in steady state fluorescence measurements. In this case, the transfer efficiency is given by the relative fluorescence intensities of the donor in the absence (F_D) and presence (F_{DA}) of acceptor. Given that labeling with the acceptor is complete, the transfer efficiency E_{FRET} is

$$\mathbf{E_{FRET} = 1 - \frac{F_{DA}}{F_D}} \quad \text{(Eq. 3).}$$

Combining equations 1, 2 and 3 yields the correlation of transfer-efficiency E_{FRET} with the distance between the fluorophores:

$$\mathbf{E_{FRET} = \frac{R_0^6}{R_0^6 + r^6}} \quad \text{(Eq. 4a)}$$

or

$$\mathbf{r = R_0 \cdot \sqrt[6]{\frac{1 - E_{FRET}}{E_{FRET}}}} \quad \text{(Eq. 4b).}$$

Thus, from the measured transfer-efficiencies, the distance r separating D and A can be calculated, if the Förster distance (R_0) for a particular combination of D and A is known.

For all FRET-measurements, the donor was CPM and the acceptor was fluorescein. Probes were covalently attached to TF site-specifically *via* cysteine residues engineered at the indicated positions (see above).

III.9.2 Determination of Förster distances

The distance between the donor and acceptor at which energy transfer with half-maximal efficiency if observed is referred to as the Förster distance (R_0). It is given (in Angstroms) by

$$R_0 = 9.87 \cdot 10^3 \left(\frac{\kappa^2 Q_D J(\lambda)}{n^4} \right)^{\frac{1}{6}} \quad \text{(Eq. 5)}$$

with κ being the orientation factor, Q_D the quantum yield of the donor, J(λ) the overlap integral and n the refractive index of the sample. Usually, a value of 1.4 is used for proteinacious solutions (Lakowicz 1999). Since, in most cases, the orientation between the donor and acceptor transition dipole moments cannot be determined for protein-bound fluorescent dyes, a value of $k^2 = 2/3$, reflecting random orientation, is usually applied (Lakowicz 1999).

The quantum yield, Q, of a fluorescent compound can be determined by comparison with a characterized standard of known quantum yield. It is the given by

$$Q = Q_R \cdot \frac{I}{I_R} \cdot \frac{A_R}{A} \cdot \frac{n^2}{n_R^2} \quad \text{(Eq. 6),}$$

where Q_R is the quantum yield of the standard, I is the integrated fluorescence emission, A is the absorption at the excitation wavelength and n is the refractive index. The index R refers to the standard.

The quantum yield of CPM-labeled TF single cysteine mutants in PBS was determined using quinine sulfate (QS) as a standard. All spectra of QS were acquired in 0.1 M H_2SO_4. Fluorescence emission spectra of 250 nM CPM-labeled TF and 5 μM QS from 375 to 660 nm at an excitation wavelength of 366 nm were collected and numerically integrated. The absorption at 366 nm was measured for 50 μM QS and 10 μM CPM-labeled TF. The quantum yield of QS at excitation at 366 nm is 0.53 (Lakowicz 1999). All CPM-labeled TF variants displayed virtually the same quantum yield of 0.693.

The overlap integral J(λ) is determined by the spectral overlap of donor emission and acceptor absorption. It is given by

$$J(\lambda) = \frac{\int_0^\infty \varepsilon_A(\lambda)\, \lambda^4\, F_D(\lambda)\, d\lambda}{\int_0^\infty F_D(\lambda)\, d\lambda} \quad \text{(Eq. 7),}$$

where $\varepsilon_A(\lambda)$ is extinction coefficient spectrum of the acceptor and $F_D(\lambda)$ is the emission spectrum of the donor normalized to unity.

To determine the extinction coefficient spectrum of fluorescein labeled TF variants, absorbance spectra were acquired to calculate $\varepsilon_A(\lambda)$ according to

$$\varepsilon(\lambda) = \frac{A(\lambda)}{c \cdot d} \quad \text{(Eq. 8)},$$

where $A(\lambda)$ is the absorbance at the wavelength λ, c is the molar concentration and d is the path length (in cm).

Fluorescence emission spectra were collected for CPM-labeled TF single cysteine mutants. The peak value was normalized to the value of $\varepsilon_A(\lambda_{max})$. R_0 for combinations of all single donor- and acceptor-labeled TF versions were calculated according to Eq. 5. An overview over the Förster distances determined for the various combinations of donor- and acceptor-positions as well as of the parameters used to calculate those is given in Table 2.

D – A pair (positions)	Q_D	$J(\lambda)$ (10^{-13} Å^6)	F_D	R_0 (Å)
14 – 14	0.401	1.51	4457160	45.8
14 – 150	0.401	1.56	4674161	46.0
14 – 326	0.401	1.38	4351988	45.1
150 – 14	0.462	1.59	4676896	47.3
150 – 150	0.462	1.63	4709775	47.4
150 – 326	0.462	1.47	4566539	46.6
326 – 14	0.453	1.58	4491121	47.1
326 – 150	0.453	1.64	4904594	47.3
326 – 326	0.453	1.45	4385148	46.4
average				46.6 ± 0.81

Table 2: Calculation of Förster distances for various donor acceptor pairs within TF.

D: donor; A: acceptor; Q_D: quantum yield of the donor; $J(\lambda)$: normalized overlap integral; F_D: integrated donor fluorescence; R_0: Förster distance.

III.9.3 Calculation of steady state fluorescence anisotropies

If a fluorophore is irradiated with light linearly polarized in the z-direction, maximum absorption of photons is observed if transition dipole moment ($\vec{\mu}_A$) is parallel to the vector of the electric field ($\vec{E}_z$) of the incoming light. For the majority of the fluorophore molecules, these two vectors are not parallel, but rather form an angle θ_A. The extent of absorption I_z is then proportional to

$$I_z \propto (\vec{\mu}_A \cdot \vec{E}_z)^2 \propto \langle \cos^2 \Theta_A \rangle \quad \text{(Eq. 9)},$$

with $<\cos^2\theta_A>$ being an average of all orientations. Thus, I_z becomes large for small θ_A angles and maximal for $\theta_A = 0$. This preference for small θ_A angles is called photo-selection.

If fluorescence is emitted, it occurs with a transition dipole moment $\vec{\mu}_F$, which usually is different from $\vec{\mu}_A$. Fluorescence emission is detected perpendicularly to the direction of the incoming beam. With polarizers in the path of the emitted light beam, the fractions of light polarized parallel ($I_{||}$) or perpendicular ($I_\perp$) relative to the incoming beam are detected. The anisotropy is the given by

$$A = \frac{I_{||} - I_\perp}{I_{||} + 2 \cdot I_\perp} \quad \text{(Eq. 10).}$$

The denominator ($I_{||} + 2I_\perp$) equals the total fluorescence intensity. Because of the photo-selection and other constraints, the theoretical limits for anisotropy values are $-0.2 \leq A \leq 0.4$ (Winter & Noll 1998).

Anisotropy data were acquired on an LS50B fluorometer (Perkin Elmer) equipped with polarizers. For slow kinetics, the built-in procedure for anisotropy measurements was used, collecting data-points every ~8 sec. For faster kinetics, $I_{||}$ and $I_\perp$ were measured in separate reactions, and the anisotropy was calculated according to Eq. 10. As a fluorescent probe, CPM was attached to TF at position E326C. Anisotropy measurements were conducted by Dr. J. M. Barral.

III.9.4 TF monomer-dimer equilibrium

TF can self-associate to form homo-dimers, as described by the equilibrium-equation

$$\mathbf{2\,TF} \xleftrightarrow[\mathbf{K_D}]{} \mathbf{TF_2} \quad \text{(Eq. 11)}$$

with the dissociation constant K_D being

$$K_D = \frac{\left(c_{eq}(TF)\right)^2}{c_{eq}(TF_2)} \quad \text{(Eq. 12),}$$

where $c_{eq}(TF)$ and $c_{eq}(TF_2)$ are the equilibrium concentrations of the TF monomer and dimer, respectively. The total protomer concentration of TF $c_t(TF)$ is then

$$c_t(TF) = c_{eq}(TF) + 2 \cdot c_{eq}(TF_2) \quad \text{(Eq. 13),}$$

which yields

$$c_{eq}(TF_2) = \frac{1}{2} \cdot \left(c_t(TF) + c_{eq}(TF)\right) \quad \text{(Eq. 14).}$$

Substituting for $c_{eq}(TF_2)$ in Eq. 12 yields

$$K_D = 2 \cdot \frac{\left(c_{eq}(TF)\right)^2}{c_{eq}(TF) + c_{eq}(TF)} \quad \text{(Eq. 15).}$$

Solving this equation for the equilibrium concentration of monomeric TF results in the quadratic expression:

$$0 = c_{eq}(TF) + \frac{1}{2} \cdot K_D \cdot c_{eq}(TF) - \frac{1}{2} \cdot K_D \cdot c_t(TF) \quad \text{(Eq. 16)}$$

with the relevant solution being:

$$c_{eq}(TF) = -\frac{K_D}{4} + \sqrt{\frac{K_D^2}{16} + \frac{1}{2} \cdot K_D \cdot c_t(TF)} \quad \text{(Eq. 17).}$$

The equilibrium concentration of dimers can then be calculated from $c_{eq}(TF)$ and $c_t(TF)$ using Eq. 14.

III.9.5 TF-ribosome equilibrium

TF associates with ribosomes in an equilibrium reaction that can be described as

$$\mathbf{TF} + \mathbf{rib} \xleftrightarrow[K_D]{} [\mathbf{TF}\text{-}\mathbf{rib}] \quad \text{(Eq. 18)}$$

with

$$K_D = \frac{c_{eq}(TF) \cdot c_{eq}(rib)}{c_{eq}(TF\text{-}rib)} \quad \text{(Eq. 19)},$$

where c_{eq}(TF), c_{eq}(rib) and c_{eq}(TF–rib) are the equilibrium concentrations of TF, ribosomes and the TF-ribosome complex, respectively, and K_D is the equilibrium constant for TF-ribosome complex dissociation. The equilibrium concentrations of TF and ribosomes can be expressed in terms of the respective total concentrations and the equilibrium concentration of the TF-ribosome complex:

$$c_{eq}(TF) = c_t(TF) - c_{eq}(TF - rib) \quad \text{(Eq. 20a)}$$

$$c_{eq}(rib) = c_t(rib) - c_{eq}(TF - rib) \quad \text{(Eq. 20b)}$$

with c_t(TF) and c_t(rib) being the total concentrations of TF and ribosomes, respectively. Solving this equation for c_{eq}(TF–rib) results in a quadratic expression with the relevant solution being:

$$c_{eq}(TF\text{-}rib) = \frac{c_t(TF) + c_t(rib) + K_D}{2} - \sqrt{\left(\frac{c_t(TF) + c_t(rib) + K_D}{2}\right)^2 - c_t(TF) \cdot c_t(rib)}$$

(Eq. 21)

The concentration of ribosome-bound TF, c_{bound}(TF), equals the concentration of TF-ribosome complexes, c_{eq}(TF–rib). Therefore, the fraction of TF that is bound by ribosomes is

$$f_{bound} = \frac{c_{bound}(TF)}{c_t(TF)} = \frac{c_{eq}(TF - rib)}{c_t(TF)} \quad \text{(Eq. 22)}$$

III.9.6 K_D determination from Trp-fluorescence

Emission spectra of TF Trp-fluorescence were acquired at various TF concentration and the emission intensity at 345 nm was quantitated. To calculate the K_D of the TF monomer-dimer equilibrium from the measured Trp-fluorescence, it was assumed that the observed fluorescence intensity F_{obs} is an average of the intensity of the monomer, F_m, and that of the dimer, F_d, weighed by the fraction of monomer and dimer, f_m and f_d:

$$F_{obs} = f_m \cdot F_m + f_d \cdot F_d = f_m \cdot F_m + (1 - f_m) \cdot F_d \text{ (Eq. 23).}$$

The fraction of monomeric TF, f_m, is given by the equilibrium concentration of monomeric TF c_{eq}(TF) and the total TF-concentration c_t(TF):

$$f_m = \frac{c_{eq}(TF)}{c_t(TF)} \text{ (Eq. 24).}$$

According to the TF monomer-dimer equilibrium equation, f_m can then be expressed in terms of the K_D and the total TF-concentration c_t(TF)

$$f_m = \frac{c_{eq}(TF)}{c_t(TF)} = \frac{-\frac{K_D}{4} + \sqrt{\frac{K_D^2}{16} + \frac{1}{2} \cdot K_D \cdot c_t(TF)}}{c_t(TF)} \text{ (Eq. 25).}$$

Thus, if this term is substituted for f_m in Eq. 23, F_{obs} can be expressed as a function of the total TF-concentration with the K_D, F_m and F_d as parameters.

III.9.7 K_D determination from BADAN fluorescence

For a given K_D, the fraction of TF that is associated with ribosomes can be calculated according to Eq. 21 and 22. Assuming that free TF-B exhibits the fluorescence F_{free} and ribosome-associated TF fluoresces with F_{bound}, the maximum decrease in fluorescence ΔF^{max}, that is observed if all of the TF-B is ribosome-associated, can be expressed as

$$\Delta F^{max} = F_{free} - F_{bound} \text{ (Eq. 26),}$$

or, normalized to the fluorescence of free TF-B, with the relative change in fluorescence ΔF_{rel} being:

$$\Delta F_{rel}^{max} = \frac{\Delta F^{max}}{F_{free}} = \frac{1}{F_{free}} \cdot (F_{free} - F_{bound}) = 1 - \frac{F_{bound}}{F_{free}} \text{ (Eq. 27).}$$

Normalization is adequate in this case, since fluorescence is expressed in relative units, depending, for instance, on the instrumentation utilized. The observed TF-B fluorescence F^{obs} can be expressed as a linear function of f_{bound} (see Eq. 22):

$$F^{obs} = F_{free} - \Delta F^{max} \cdot f_{bound} \text{ (Eq. 28),}$$

or, normalized to F_{free},

$$F_{rel}^{obs} = 1 - \Delta F_{rel}^{max} \cdot f_{bound} \text{ (Eq. 29).}$$

Rearranging Eq. 29 yields

$$\mathbf{f_{bound}} = \frac{\mathbf{1 - F_{rel}^{obs}}}{\mathbf{\Delta F_{rel}^{max}}} \text{ (Eq. 30).}$$

If the total concentrations of ribosomes and TF ($c(rib)_t$ and $c(TF)_t$) are known, the dissociation constant K_D can be calculated from f_{bound} using Eq. 19. The concentration of the TF-ribosome complex is given by

$$\mathbf{c_{eq}(TF - rib) = c_t(TF) \cdot f_{bound}} \text{ (Eq. 31).}$$

Combining Eq. 20a and 20b with Eq. 19 and substituting according to Eq. 31 yields

$$\mathbf{K_D} = \frac{\mathbf{(c_t(TF) - c_{eq}(TF - rib)) \cdot (c_t(rib) - c_{eq}(TF - rib))}}{\mathbf{c_{eq}(TF - rib)}} \text{ (Eq. 32a)}$$

$$= \frac{\mathbf{(c_t(TF) - c_t(TF) \cdot f_{bound}) \cdot (c_t(rib) - c_t(TF) \cdot f_{bound})}}{\mathbf{c_t(TF) \cdot f_{bound}}} \text{ (Eq. 32b)}$$

$$= \mathbf{c_t(TF) \cdot f_{bound} + c_t(rib) \cdot \frac{1}{f_{bound}} - c_t(TF) - c_t(rib)} \text{ (Eq. 32c)}$$

This equation allows the calculation of K_D from the total concentrations and the fraction of TF that is present in a complex with ribosomes.

III.9.8 K_D determination from steady state fluorescence anisotropy

The K_D from steady state fluorescence anisotropy measurements can be calculated in a similar way as from BADAN fluorescence. In this case, the measured value does not have to be normalized since anisotropy measurements yield absolute values. The observed anisotropy, A_{obs}, is a weighed average of the anisotropy of the free (A_{free}) and the bound form (A_{bound}) of TF-C:

$$\mathbf{A_{obs} = (1 - f_{bound}) \cdot A_{free} + f_{bound} \cdot A_{bound}} \text{ (Eq. 33),}$$

where f_{bound} is the fraction of TF-C that is present in a complex with the ribosome. f_{bound} can then be calculated by rearranging Eq. 33:

$$\mathbf{f_{bound}} = \frac{\mathbf{A_{obs} - A_{free}}}{\mathbf{A_{bound} - A_{free}}} \text{ (Eq. 34).}$$

The dissociation constant can then be calculated according to Eq. 32c.

III.9.9 Calculation of inter-molecular distances

0.25 µM donor-labeled TF were mixed with 1µM acceptor-labeled or unlabeled TF. Emission spectra from 410 to 600 nm were collected at an excitation wavelength of 397 nm. The FRET efficiency was calculated according to Eq. 4b, in which a corrected E'_{FRET} was used instead of E_{FRET} to compensate for the effects described in the following paragraphs.

At a total TF concentration of 1.25 µM, dimer formation is not complete. The fraction of TF that is dimeric can be calculated using Eq. 14 and 17. To calculate the fraction of TF protomers that exists as a dimer (f_{dimer}), the protomer concentration $c_P(TF_2)$ has to be used:

$$c_P(TF_2) = 2 \cdot c(TF_2) \quad \text{(Eq. 35)},$$

because each dimer consists of two protomers. Thus, at a total TF concentration of $c(TF)_T$ = 1.25 µM and a K_D of 1 µM, the fraction of protomers within a dimer is

$$f_{dimer} = \frac{c_P(TF_2)}{c_t(TF)} = 0.55 \quad \text{(Eq. 36)}$$

At the concentrations of donor and acceptor utilized, not every dimer is a hetero-dimer of a donor- and an acceptor-labeled protomer. Generally, for an n-mer composed of A and D present at concentrations c_A and c_D, which oligomerize with the same affinity, the probability P_k of finding an n-mer containing k molecules of A is given by

$$P_k = \binom{n}{k} x_A^{\,2} (1 - x_A)^{(n-k)} \quad \text{(Eq. 37)}$$

with

$$\binom{n}{k} = \frac{n!}{k!\,(n-k)!} \quad \text{(Eq. 38) and}$$

$$x_A = \frac{c_A}{c_A + c_D} \quad \text{(Eq. 39)}$$

In the case of a dimer n = 2, therefore

$$P_2 = P_{AA} = x_A^{\,2} \quad \text{(Eq. 40)}$$

$$P_1 = P_{DA} = 2x_A - 2x_A^{\,2} \quad \text{(Eq. 41)}$$

$$P_0 = P_{DD} = (1 - x_A)^2 \quad \text{(Eq. 42)}$$

For the inter-molecular FRET analysis, one has to correct for the fact that donor-containing dimers can be either homo-dimers (D-D) or hetero-dimers (D-A), because only in the latter ones does FRET occur. With $x_A = 0.8$, the probabilities are $P_{DD} = 0.04$ and $P_{DA} = 0.32$. Therefore, the fraction of D-A dimers relative to all D-containing dimers is

$$\mathbf{f_{DA} = \frac{P_{DA}}{P_{DA} + P_{DD}} = 0.89} \quad \text{(Eq. 43).}$$

Taking into account incomplete dimerization and the formation of donor-labeled homo-dimers, the corrected FRET-efficiency E'_{FRET} is

$$\mathbf{E'_{FRET} = E_{FRET}^{obs} \cdot \frac{1}{f_{dimer} \cdot f_{DA}} = E_{FRET}^{obs} \cdot \frac{1}{0.55 \cdot 0.89}} \quad \text{(Eq. 44).}$$

E'_{FRET} was used to calculate the inter-molecular distances according to Eq. 4b.

III.9.10 Calculation of intra-molecular distances

Intra-molecular distances of TF in solution were calculated using Eq. 3 and 4b. For the calculation of intra-molecular distances within ribosome-associated TF, the FRET efficiency observed was corrected for the fact that under the conditions used, only a fraction of TF was ribosome-associated.

Since $f_{bound} < 1$, the observed FRET efficiency reflects an average of distances in ribosome-bound and free TF. The observed FRET efficiency is therefore an average of FRET efficiencies of the free and the ribosome-bound form of TF weighed by the fraction of TF that is ribosome associated:

$$\mathbf{E_{FRET}^{obs} = f_{bound} \cdot E_{FRET}^{bound} + (1 - f_{bound}) \cdot E_{FRET}^{free}} \quad \text{(Eq. 45)}$$

with observed FRET efficiency $E_{FRET}{}^{obs}$, and $E_{FRET}{}^{free}$ and $E_{FRET}{}^{bound}$ as the FRET efficiencies of free and bound TF, respectively. This yields

$$\mathbf{E_{FRET}^{bound} = \frac{1}{f_{bound}} \cdot (E_{FRET}^{obs} - E_{FRET}^{free}) + E_{FRET}^{free}} \quad \text{(Eq. 46)}$$

as the corrected FRET efficiency for ribosome-bound TF. f_{bound} can be calculated according to Eq. 21 and Eq. 22 from the total concentrations of TF and ribosomes and the dissociation constant of the TF-ribosome complex. The intra-molecular distance is then calculated according to Eq. 4b using the corrected FRET efficiency.

III.9.11 Kinetic evaluation

Competition experiments were analyzed kinetically by assuming a pseudo-first order mechanism. The data were fitted to a three parameter single exponential function

$$\mathbf{y} = \mathbf{y}_0 + \mathbf{a} \cdot \mathbf{e}^{-\mathbf{b} \cdot \mathbf{x}} \quad \text{(Eq. 47)},$$

where y_0 represents the initial value (or y-offset), a is the amplitude and b the time constant. The time constant is correlated to the half-time by the simple relation

$$\mathbf{t}_{1/2} = \frac{\ln(2)}{\mathbf{b}} \quad \text{(Eq. 48)}.$$

III.9.12 Assignment of the mean hydrophobicity to residues in protein sequences

For hydrophobicity calculations, the hydropathy scale by Roseman was used (Roseman 1988). The values for the individual amino acids are listed in Table 3. The average mean hydrophobicity h_n for each residue n in a protein consisting of L residues over a window of w residues was calculated according to

$$\mathbf{h}_n = \frac{1}{\mathbf{w}} \cdot \sum_{i=n-a}^{n+a} \mathbf{h}_i \quad \text{(Eq. 49)}$$

with $\mathbf{a} = \frac{\mathbf{w}}{2} - 0.5$ (Eq. 50) and $\mathbf{a} \le \mathbf{n} \le \mathbf{L} - \mathbf{a}$ (Eq. 51).

Amino acid	ΔG (kJ/mol)
Ala	-0.39
Arg	3.95
Asn	1.91
Asp	3.81
Cys	-0.25
Gln	1.3
Glu	2.91
Gly	0
His	0.64
Ile	-1.82
Leu	-1.82
Lys	2.77
Met	-0.96
Phe	-2.27
Pro	-0.99
Ser	1.24
Thr	1
Trp	-2.13
Tyr	-1.47
Val	-1.3

Table 3: Hydrophobicity scale according to Roseman (Roseman 1988).

IV RESULTS

IV.1 TF undergoes a conformational change upon binding to the ribosome

Differential labeling with donor and acceptor chromophores at specific positions within a protein molecule allows the observation of intra-molecular fluorescence resonance energy transfer (FRET). From the efficiency of transfer (E_{FRET}), the distances between these positions can be determined (Stryer 1968). A way to introduce fluorophores at specific sites within proteins is *via* the attachment of thiol-reactive dyes to cysteine-residues engineered at the desired position(s).

Positions in the TF molecule that appeared suitable for the introduction of fluorophores were selected based on the TF crystal structure (Ferbitz *et al.* 2004) (Figure 8). A residue was considered suitable if it exhibited a low degree of conservation

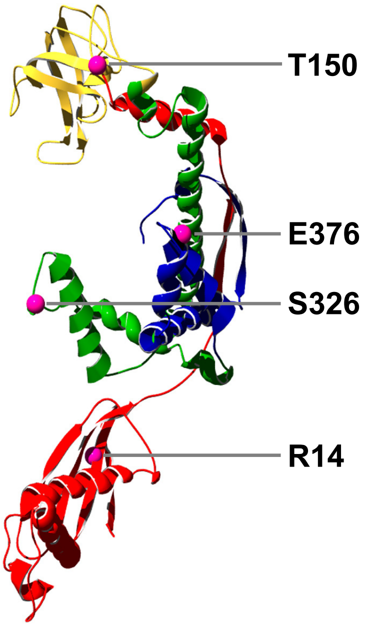

Figure 8: Positions for the introduction of exogenous chromophores were based on the TF crystal structure.

The ribbon diagram of the TF crystal structure (pdb-code *1w26*; Ferbitz *et al.* 2004) is color coded according to the subdomains, with the amino-terminal domain (residues 1 – 149) shown in red, the PPIase domain (150 – 250) in yellow, arm 1 (251 – 360) in green and arm 2 (361 – 432) in blue. As a pre-requisite for thiol-derivatization of the exogenous chromophores onto the TF molecule, the following residues were mutated to cysteine: R14, T150, S326 and E376 (as indicated). The C_{α}-atoms of these residues are represented as magenta spheres to highlight their positions throughout the TF molecule.

among TF-variants from different species and a rather hydrophilic, solvent exposed side-chain. Additionally, the positions were chosen to be distributed over the different subdomains of the TF-molecule. The residues that were selected for the introduction of cysteines were R14 in the amino-terminal domain, T150 in the PPIase domain, E326 in tip1 and S376 in tip 2. A TF R14C mutant was generated, and the mutation was combined with either of the three of the above cysteine mutations, yielding the double cysteine mutants R14C T150C, R14C E326C and R14C E376C.

The double cysteine mutant proteins were purified and differentially labeled with CPM as the donor and fluorescein as the acceptor fluorophore (see Materials and Methods). Emission spectra of the labeled double cysteine mutants are shown in Figure 9 a. The fluorescence emission at ~460 nm was normalized to the emission in the absence of

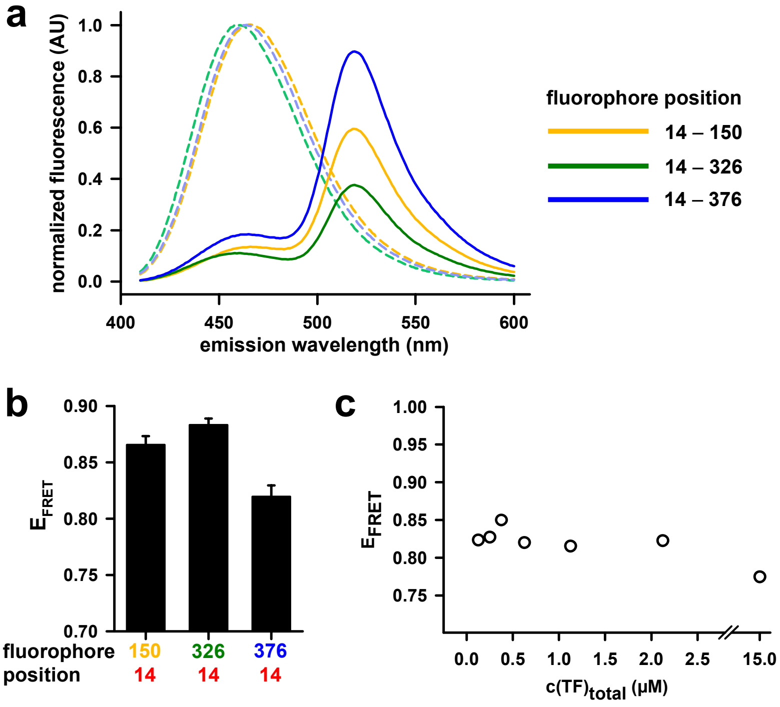

Figure 9: Intra-molecular FRET within TF labeled with fluorescence donor and acceptor pairs.

a. Fluorescence emission spectra of differentially labeled TF versions. Spectra in the presence of acceptor are shown as solid lines in yellow, green and blue for the donor-acceptor pairs 14 – 150, 14 – 326 and 14 – 376, respectively. All spectra are normalized to the emission maximum of the respective donor-only spectrum (broken lines). **b.** FRET efficiencies observed with the donor and acceptor pair at various positions. Measurements correspond to averages of at least three experiments, with standard deviations. **c.** Efficiency of intra-molecular FRET between positions 14 and 326 in the presence of excess unlabeled TF. E_{FRET} was determined for 250 nM differentially labeled TF in the presence of various concentrations of unlabeled TF, as indicated. The FRET efficiency does not vary over a wide range of TF concentrations, indicating that energy transfer occurs intra-molecularly.

acceptor. The presence of the acceptor led to a pronounced decrease in donor fluorescence for all of the above combinations. The calculated transfer efficiencies between the different positions are displayed in Figure 9b. E_{FRET} remained essentially unchanged when unlabeled TF was included at concentrations as high as 15 µM (60-fold excess over labeled TF, Figure 9 c). This demonstrates that the energy transfer takes place in an intra-molecular fashion. Furthermore, the formation of TF-dimers (see below) at elevated concentrations does not alter these distances, suggesting that dimerization is not associated with a TF conformational change.

From the observed transfer efficiencies, the distances between the different positions were calculated. The distances corresponded to 34, 33 and 36 Å between position 14 and positions 150, 326 and 376, respectively. For the pair at positions 14 and 150, the distance derived from intra-molecular FRET measurements varies considerably from the one determined from the TF crystal-structure (Ferbitz *et al.* 2004), which corresponds to more than 70 Å.

Having established that FRET can be observed between the different TF subdomains within a molecule, it was investigated whether any conformational changes occur upon binding of TF to the ribosome. The spectral properties of the exogenous fluorophores utilized allow fluorescence measurements to be conducted in the presence of ribosomes, which, due to their high absorbance in the UV-region, interfere with spectroscopic measurements at wavelengths shorter than ~300 nm. Fluorescence emission spectra of 250 nM labeled TF in the absence and presence of 2 µM ribosomes are shown in Figure 10 a – c. For all combinations of label positions, E_{FRET} was markedly reduced when ribosomes were present, correlating with an increase in distance between these positions (Figure 10d). This observation suggests that upon binding to the ribosome, TF adopts a more extended conformation than in solution, perhaps more closely resembling that of the crystal structure. A comparison of the distances derived from fluorescence spectroscopy to those from the crystal structure is given in Table 4.

Taken together, the data indicate that in solution, TF adopts a structure that is significantly more compact than the one in the crystal structure. Upon ribosome binding, there is an increase in distance between the positions of the labels, reflecting a conformational change within TF. This is displayed in a schematic fashion in Figure 10 e.

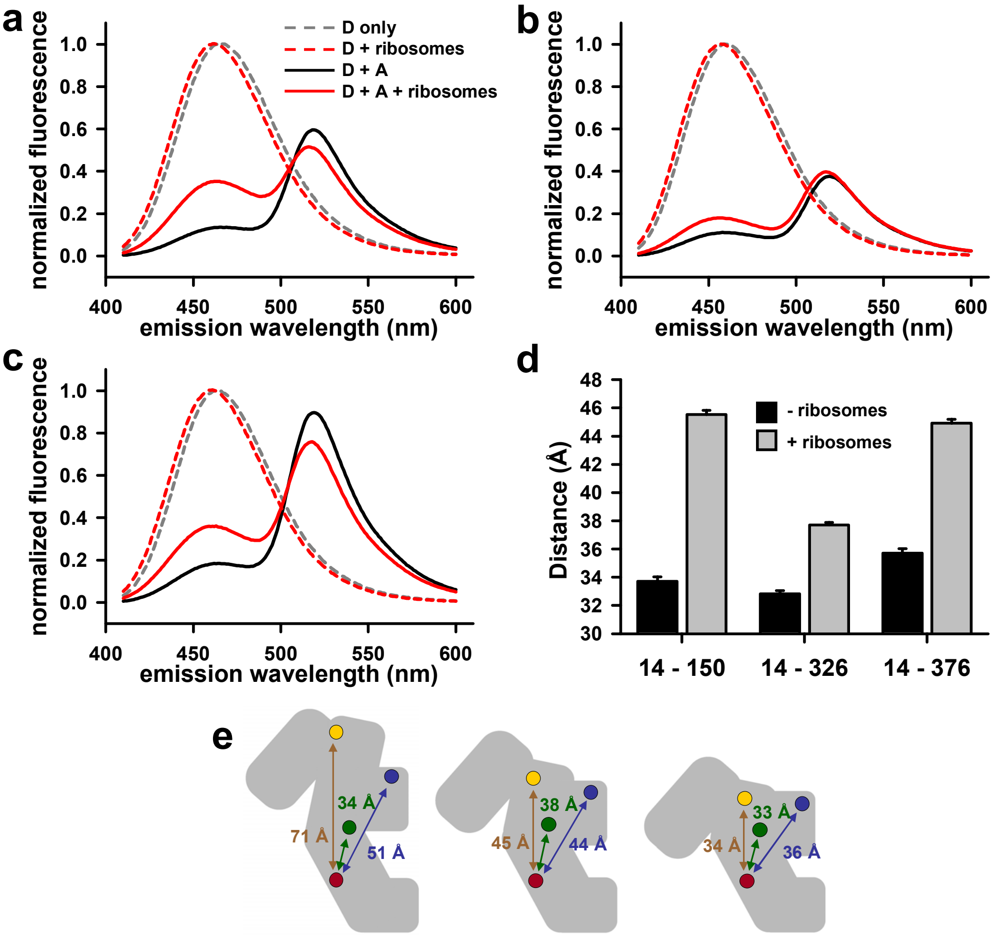

Figure 10: TF undergoes a conformational change upon binding to the ribosome.

a – **c.** Fluorescence emission spectra of differentially labeled TF in the absence and presence of ribosomes. Spectra of 250 nM differentially labeled TF with the donor – acceptor pairs at positions 14 – 150 (**a**), 14 – 326 (**b**) and 14 – 376 (**c**) were acquired in the absence (black lines) or presence (red lines) of 2 µM ribosomes. The spectra were normalized to the maximum emission of analogous donor-only labeled samples (broken lines). Presence of ribosomes causes an increase in donor fluorescence at ~460 nm with a concomitant decrease in acceptor fluorescence at ~510 nm. **d.** Distances derived from intra-molecular FRET measurements (see Materials and Methods) for the free (black bars) and the ribosome-bound forms (grey bars) of TF. The largest increase in distance upon ribosome binding is observed between positions 14 and 150. Measurements correspond to averages of at least three experiments, with standard deviations. **e.** Comparison of distances derived from the crystal structure and from intra-molecular FRET-measurements. TF is drawn as a grey silhouette viewed from a similar angle as the structure representation in Figure 8. The probes at positions 14, 150, 326 and 376 are represented as filled circles colored red, yellow, green and blue, respectively. Arrows are drawn to scale according to the distances from the crystal structure (left panel) and the distances derived from intra-molecular FRET measurements in the presence (middle panel) and absence (right panel) of ribosomes.

D – A pair (positions)	D – A distances (r)		Δr	C_α-distances (1w26)
	– ribosomes	+ ribosomes		
14 – 150	33.7 Å	45.3 Å	11.6 Å	73 Å
14 – 326	32.8 Å	37.5 Å	4.7 Å	45/49 Å
14 – 376	35.7 Å	44.8 Å	9.0 Å	39/43 Å

Table 4: Distances derived from intra-molecular FRET measurements and from the crystal structure of E. coli TF.

D: donor; A: acceptor; r: FRET-derived distance. For each combination of donor and acceptor positions, the distances calculated from E_{FRET} are listed. Δr indicates the difference in distance between the same positions in free and ribosome-bound TF. The C_α distances were calculated from the coordinates of the *E. coli* TF structure (pdb-code *1w26*) (Ferbitz *et al.* 2004), which vary in part for the two protomers in the asymmetric unit.

IV.2 TF exists predominantly as a dimer when not bound to the ribosome

Previous studies have demonstrated that purified TF undergoes self-association to form homo-dimers as observed by analytical ultracentrifugation and gel filtration analysis. The reported dimer dissociation constants vary significantly, from 1.8 to 18 µM (Maier *et al.* 2003; Patzelt *et al.* 2002) and exhibit relatively large errors. It is conceivable that dimerization fulfills a function in regulating TF activity in the cell. To investigate this aspect, the TF dimer was further characterized.

To determine the dissociation constant of TF more accurately, the single tryptophan residue at position 151 in the TF sequence was used as an endogenous fluorescent probe. The indole ring of tryptophan exhibits fluorescence when excited at around 280 nm to 295 nm, and this fluorescence is often environmentally sensitive (Lakowicz 1999). A fluorescence emission spectrum of 4 µM unmodified wild type TF is shown in Figure 11 a, displaying an emission maximum at 345 nm. Emission spectra of TF at concentrations ranging from 0.1 to 15 µM were acquired at an excitation wavelength of 295 nm (Figure 11 b) and normalized to TF concentration. A substantial increase in molar fluorescence emitted at 345 nm was observed with increasing TF concentrations. At concentrations above 5 µM, a decrease in fluorescence was observed, probably as a result of an inner filter effect.

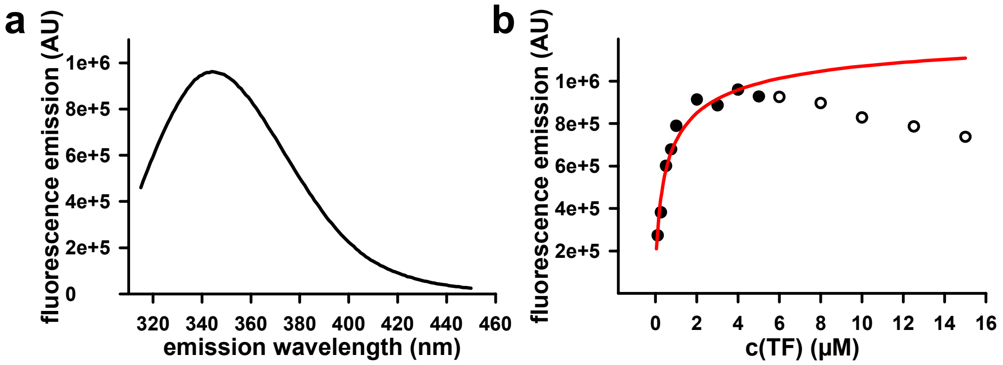

Figure 11: TF tryptophan fluorescence changes upon dimerization.

a. Fluorescence emission spectrum of unlabeled wild type TF excited at 295 nm. **b.** Fluorescence emission at 345 nm of TF *vs.* TF concentration. The data points are represented as circles, the result from the non-linear curve fit with a K_D of 0.9 µM is shown as a red line. Open circles represent data points at concentration where a considerable inner-filter leads to reduction in signal, which were not considered in the analysis.

The molar fluorescence was plotted against TF concentration and analyzed by non-linear curve fitting (see Materials and Methods). The data points for concentrations above 5 µM were not utilized. The analysis yielded a reasonable fit (Figure 11 b) with a dissociation constant of 0.9 µM for the TF dimer. Virtually identical K_D values were obtained for the various TF cysteine mutants as well as for the TF FRK/AAA mutant (see below), indicating that these molecules do not differ from WT TF in their ability to form homo-dimers.

To confirm the dimerization results obtained by the analysis of TF tryptophan fluorescence, steady state fluorescence anisotropy measurements of TF labeled with CPM at position 326 (TF-C) were conducted. Fluorescence anisotropy is correlated to the molecular weight of a molecule by the rotational diffusion coefficient. Large molecules rotate slower than small ones, thereby exhibiting higher fluorescence anisotropy. Additionally, steady state fluorescence anisotropy may also depend on the environment of the fluorophore. If the steady state anisotropy of fluorescently labeled TF is measured at varying total TF concentrations, any change in anisotropy reflects a change in molecular mass of the TF-molecule and / or fluorophore environment associated with dimerization.

250 nM TF-C was incubated with unlabeled TF at concentrations ranging from 0 to 45 µM and the steady state fluorescence anisotropy of the sample was measured. 250 nM TF-C displayed an anisotropy of $r = 0.27$. With increasing TF concentration, an increase in anisotropy was observed reaching a plateau at $r = 0.3$ (Figure 12). Anisotropy was plotted against total TF concentration, and the data points were fitted to the equilibrium equation for dissociation of the TF dimer (Figure 12). A value of 0.9 µM was

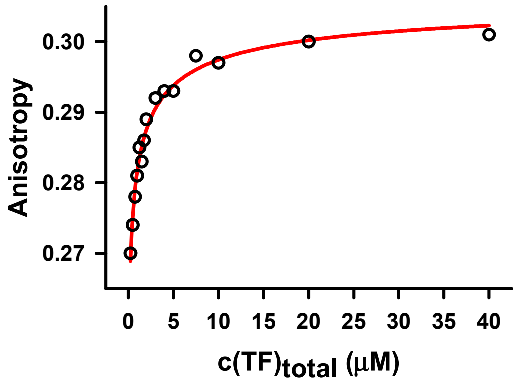

Figure 12: TF dimerization can be monitored with fluorescence anisotropy.

Fluorescence anisotropy of 250 nM CPM-labeled TF was measured in the presence of varying amounts of unlabeled TF. An increase in anisotropy is observed with increasing TF-concentrations (open circles). A reasonable fit to the TF-dimer equilibrium equation was obtained with a K_D of 0.9 µM (red line). in good agreement with the K_D obtained from endogenous tryptophan fluorescence.

determined for the dissociation constant, virtually identical to that found by the analysis of TF tryptophan fluorescence.

To obtain insights into the arrangement of the TF-dimer, TF single cysteine mutants R14C, T150C and E326C were labeled with either CPM serving as a donor or fluorescein serving as an acceptor in resonance energy transfer measurements. 250 nM donor-labeled TF was mixed with 1 µM acceptor-labeled or unlabeled TF, and emission spectra were acquired at an excitation wavelength of 396 nm. For each of the three different donor-labeled versions of TF, the donor fluorescence (at around 460 nm) was normalized to the fluorescence observed in the absence of acceptor, *i.e.* in a control sample containing unlabeled instead of donor-labeled TF (Figure 13 a – c). To rule out that acceptor fluorescence contributes to the emission at 460 nm, samples containing 1 µM acceptor-labeled TF were analyzed under the same conditions in the absence of donor. Virtually no fluorescence emission at 460 nm was observed in the absence of donor-labeled TF (Figure 13 d).

From the decrease in donor fluorescence that was observed in the presence of acceptor, E_{FRET} was calculated. Figure 13 e shows the transfer efficiencies observed for the different donor-acceptor combinations in the inter-molecular FRET measurements. The highest transfer efficiency was observed when both donor and acceptor were attached at position 326 in each TF molecule. Energy transfer was least efficient when both probes were at position 14. This suggests that, in the dimer, the regions of the TF molecule comprising the tips are closest to each other, whereas the amino-terminal domains of the two protomers are distant.

The distances corresponding to the observed FRET efficiencies were calculated using a Förster distance of 47 Å for the donor-acceptor pair used in these experiments. The FRET efficiency was corrected for incomplete dimer formation and for formation of homodimers of donor-labeled TF at the concentrations used in these experiments (see Materials and Methods). The distances are summarized in Figure 14 .

The program *FRETsg* (Schroder & Grubmuller 2004) was utilized in order to interpret the information obtained from inter-molecular FRET measurements. This program finds all configurations that obey the given distances for an arbitrary number of distance distributions between an arbitrary number of points in three-dimensional space. This is achieved by assigning a harmonic potential to each distance and minimizing the energy for the sum of all potentials. Since the optimum configuration for a given data set may not be unique, the minimization is repeated multiple times starting from random initial

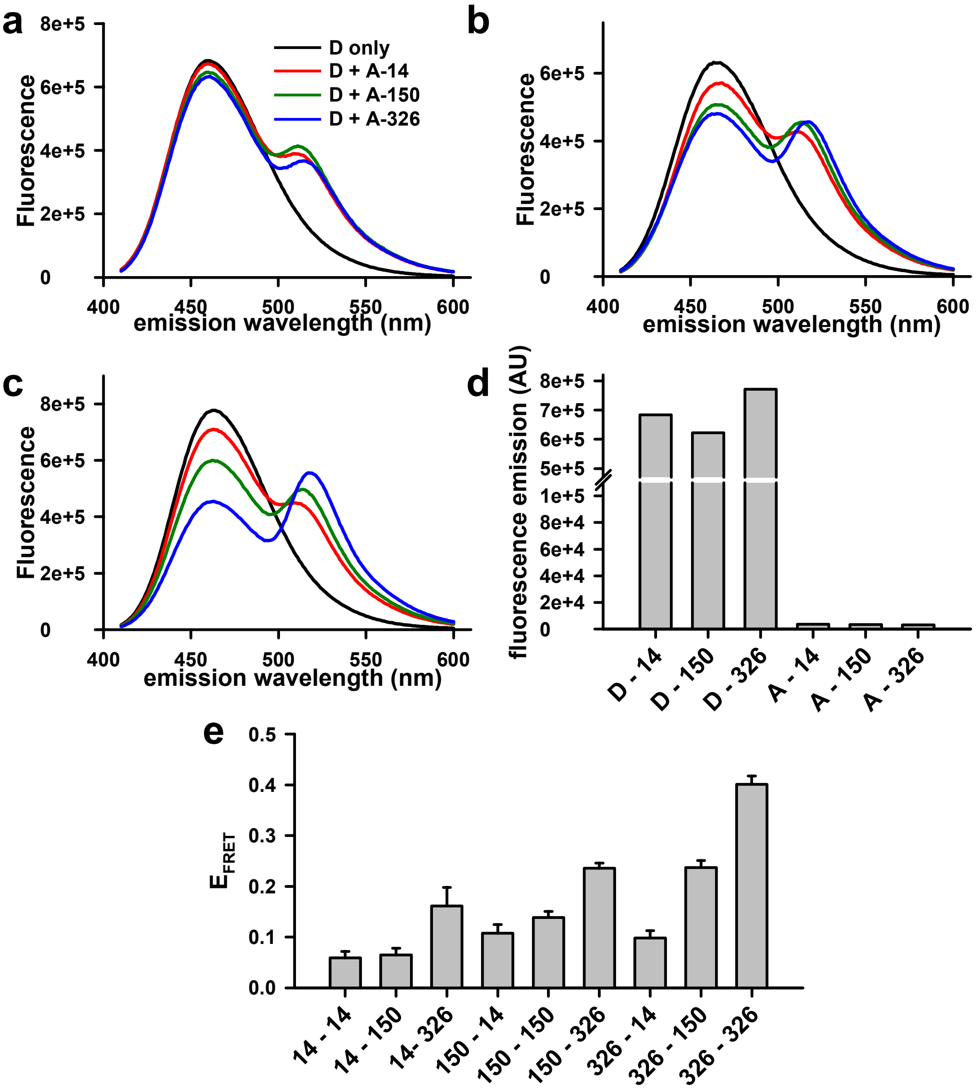

Figure 13: Inter-molecular FRET measurements with single-labeled TF.

a. – c. Fluorescence emission spectra of 250 nM donor-labeled TF with 1 µM unlabeled (black lines) or acceptor-labeled TF. The acceptor was coupled to position 14 (red lines), 150 (green lines) or 326 (blue lines). The samples were excited at 396 nm. Donor positions are 14 (**a**), 150 (**b**) and 326 (**c**). **d.** Intensities of fluorescence emission of 250 nM donor-labeled (D) and 1 µM acceptor labeled (A) TF at 460 nm. The numbers on the x axis indicate the position of the label within the TF sequence. Samples were excited at 396 nm. As can be observed, the acceptor does not exhibit any significant fluorescence emission at 460 nm. **e.** Observed FRET efficiencies for the different combinations of donor- and acceptor-labeled TF. Numbers on the x axis indicate the positions of donor and acceptor, respectively. E_{FRET} represents the average of at least three independent experiments, with standard deviations shown.

configurations. When this analysis was applied to the distances derived from intra- and inter-molecular FRET-measurements, all random initial configurations converged into very similar models, in which the long axes of the protomers were placed at nearly perpendicular angles, with the regions between the tips facing each other. A representation of such a model is given in Figure 14 b.

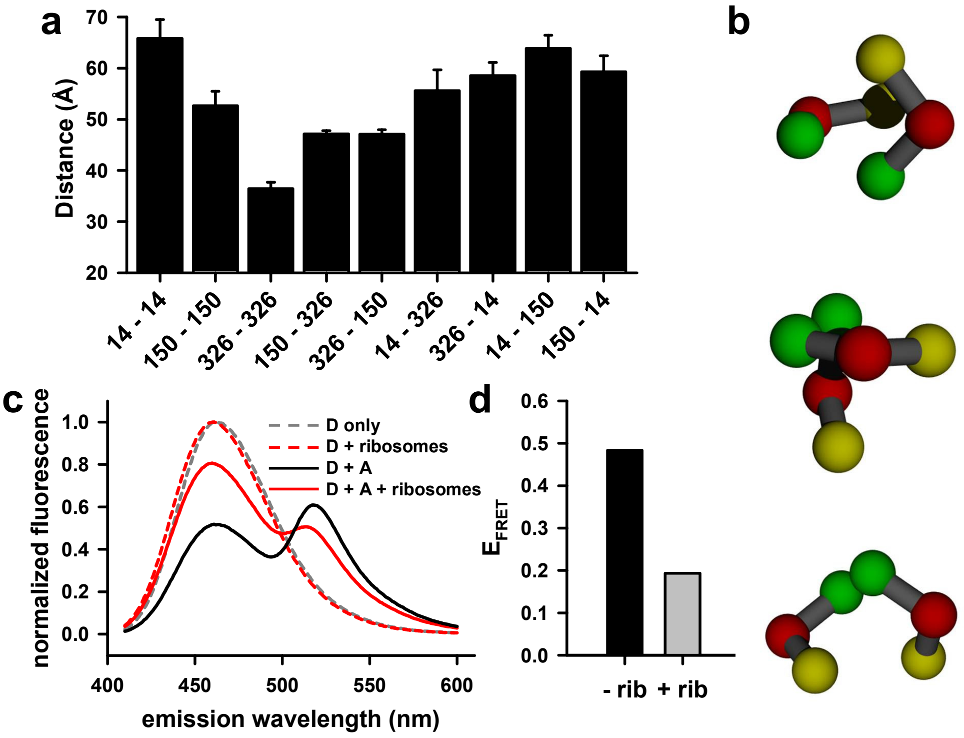

Figure 14: Characterization of the TF-dimer by inter-molecular FRET measurements.

a. Inter-molecular distances between different positions in the TF dimer. Distances were calculated from E_{FRET} (see Materials and Methods). The similarity between the values of reciprocal combinations of donor and acceptor confirms the calculated distances. Measurements correspond to averages of at least three experiments, with standard deviations. **b.** Representation of a model of the TF dimer generated with *FRETsg* from the distances shown in (**a**). The probe positions are represented as colored spheres (amino-terminal-domain: red, PPIase-head: yellow; tip 1: green), which are connected by sticks within the same TF molecule. The three images are different views of the same model, illustrating that the protomers are oriented at nearly perpendicular angles, with the tips of the substrate binding crevice facing towards each other. Models were generated and rendered with POVray. **c.** Fluorescence emission spectra of single donor- and acceptor-labeled TF in the absence (black line) and presence (red line) of 2 µM ribosomes. The respective spectra in the absence of acceptor are represented as broken lines. Presence of ribosomes leads to a marked increase in donor fluorescence. **d.** Inter-molecular FRET efficiencies in the absence (black bar) and presence (grey bar) of ribosomes. E_{FRET} was calculated from the spectra shown in (**c**). The transfer efficiency is strongly decreased in the presence of ribosomes.

The effect of ribosome binding on the oligomeric state of TF was investigated by performing the inter-molecular FRET experiments in the presence of 2 µM ribosomes. Under these conditions, a fraction $f_{bound} \approx 0.6$ of TF is expected to be ribosome-bound (assuming a K_D of 0.9 µM for the TF-ribosome complex, see below). Fluorescence emission spectra of the 326 – 326 donor-acceptor pair in the absence and presence of ribosomes are shown in Figure 14 c. E_{FRET} was markedly reduced in the presence of ribosomes (Figure 14 d), indicating a decrease in TF dimer concentration. The observed decrease in E_{FRET} from 0.48 to 0.19 (~40% of the initial value) correlates well with the fraction of TF that is ribosome-bound under these conditions. The results are in agreement with published observations that TF associates with ribosomes in a 1:1 stoichiometry and that it is the monomer rather than the dimer that exists as the ribosome-bound form.

The results of the inter-molecular FRET-measurements demonstrate that, in solution, TF forms homo-dimers that dissociate with a K_D of 0.9 µM. The protomers within the TF dimer are oriented in an almost perpendicular fashion, with the tips surrounding the hydrophobic crevice oriented towards each other. Furthermore, these results support the notion that the ribosome-bound TF species is a monomer.

IV.3 Translation of FL results in increased recruitment of TF to the ribosome

It has been reported that the dynamic interaction of TF with the ribosome can be resolved by fluorescence spectroscopy (Maier *et al.* 2003). This was achieved by introducing the environmentally sensitive BADAN fluorophore at position 14 in TF (TF-B). Upon binding of TF-B to the ribosome, a decrease in fluorescence was observed. When excess unlabeled WT TF was added, this effect was reversed due to displacement of ribosome-bound labeled TF. The TF FRK/AAA mutant is deficient in ribosome binding, and the corresponding BADAN-derivative did not display the change in fluorescence observed for WT TF-B upon incubation with ribosomes. Also, the mutant protein failed to act as an efficient competitor in the displacement of ribosome-bound TF-B. The association and dissociation of TF-ribosome complexes have been shown to take place on a time scale that is amenable to manual mixing experiments.

To investigate whether the interaction of TF with ribosomes actively engaged in translation can be monitored, a recently developed cell-free coupled transcription/translation system was used (Shimizu *et al.* 2001). Reconstituted from purified *E. coli* ribosomes present at 250 nM and purified recombinant proteins, it provides a well defined protein synthesis system. Importantly, the amount of contaminating TF is negligible (Shimizu *et al.* 2001) (and data not shown).

The system was supplemented with 250 nM TF-B and allowed to equilibrate at 30 °C. Transcription/translation was initiated by the addition of the plasmid pLuc encoding firefly luciferase (FL), a previously characterized TF substrate, and fluorescence was followed over time. Following a lag-phase of ~3 min after the addition of plasmid, TF-B fluorescence started to decrease and reached a steady level corresponding to ~65% of the initial fluorescence after ~25 min (Figure 15). No such decrease was observed when the system was supplemented with an equal amount of the BADAN-labeled TF FRK/AAA mutant (Figure 15).

In a parallel experiment containing ^{35}S-labeled methionine (^{35}S-Met), aliquots were withdrawn at various intervals and the total amount of FL produced in the system was quantitated by SDS-PAGE and phosphorimaging. Full-length FL was detected after ~20 min, and accumulated at a constant rate when the BADAN emission had reached a steady level (Figure 15). The linear accumulation of full-length FL progressed beyond 60 min under the experimental conditions.

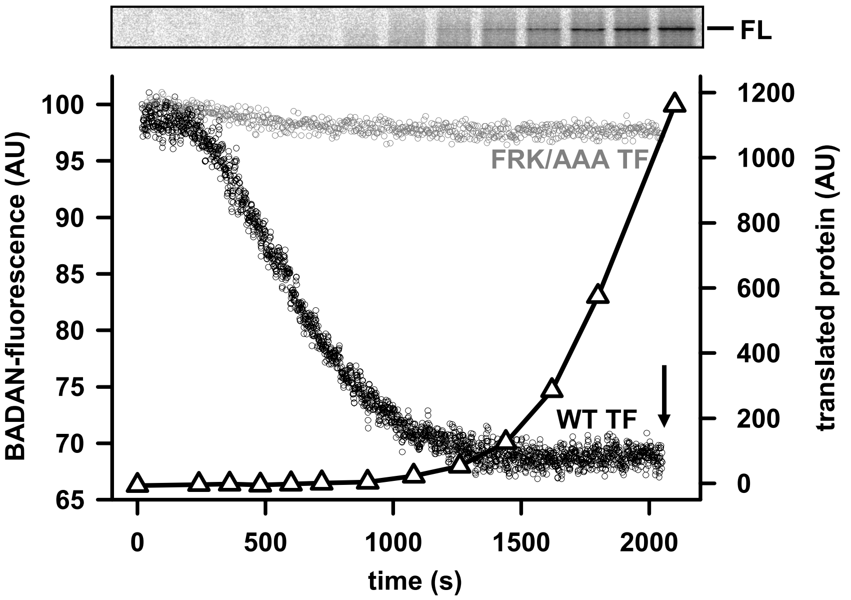

Figure 15: TF recruitment to translating ribosomes can be monitored in real time.

The reconstituted translation system was supplemented with 250 nM TF-B, and fluorescence emission was followed over time (black open circles). No such decrease was observed when the FRK/AAA mutant of TF-B, unable to efficiently bind ribosomes, was used (grey open circles). The production of full-length luciferase was quantitated by ^{35}S-Methionine incorporation and autoradiography of the band corresponding to the full-length protein (FL) (open triangles; autoradiograph in the top panel). TF-B fluorescence reached a plateau when protein production was taking place at a steady level. The arrow indicates the point of time at which competition experiments were conducted (see below).

These findings indicate that the decrease in BADAN fluorescence reflects an increase in the fraction of TF-B that is bound to the ribosome, *i.e.* increased recruitment of TF-B to ribosomes is observed as they become engaged in translation. Once all the available ribosomes in the system are translating, TF-B recruitment and protein synthesis reach a steady state, reflected by constant fluorescence and protein accumulation (Figure 15).

Steady state fluorescence anisotropy has been successfully used to monitor the binding of fluorescently-labeled proteins to ribosomal subunits and entire ribosomes. Therefore, it may be suitable to monitor TF association with ribosomes if the TF is labeled with a fluorescent dye suitable for anisotropy measurements. In the above reactions, if free TF is shifted towards the ribosome-bound form as a result of translation, the steady state anisotropy would be expected to increase with kinetics similar to those observed for the BADAN-labeled TF.

For steady state anisotropy measurements, TF was labeled with CPM at position 326 (TF-C). This fluorophore has been used successfully to monitor the assembly of the *E. coli* protein S21 into ribosomes (Odom *et al.* 1984). Translation reactions containing TF-C were set up and the steady state fluorescence anisotropy of TF-C was measured over time. An increase in anisotropy was observed from ~0.29 to ~0.33 in a sigmoidal fashion (Figure 16) very similar to the change in BADAN fluorescence (compare with Figure 15). This indicates that an increased fraction of the TF-C indeed associated with ribosome-nascent chain complexes upon translation. The CPM-labeled FRK/AAA-mutant did not exhibit such a pronounced increase in anisotropy (Figure 16).

As discussed above, TF undergoes a significant conformational change upon binding to the ribosome. Recruitment to ribosomes upon translation should thus be reflected by a decrease in intra-molecular FRET efficiency. For intra-molecular FRET measurements, two parallel translation reactions similar to the above were set up, except that the labeled TF in one of them contained the fluorescence donor only (TF-C) and the

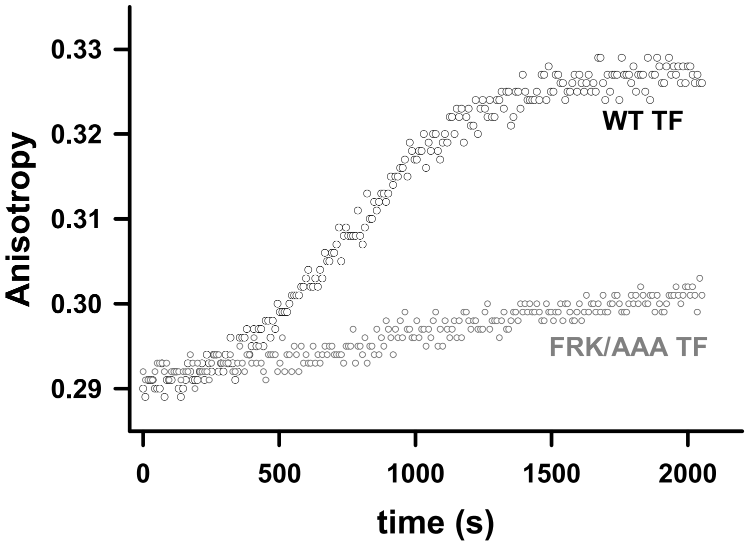

Figure 16: TF-ribosome recruitment during translation causes an increase in steady state fluorescence anisotropy.

The steady state fluorescence anisotropy of TF-C was followed over time during FL translation. An increase in anisotropy from 0.29 to 0.33 was observed, with kinetics very similar to those of TF-B recruitment to translating ribosomes (compare with Figure 15). A significantly less pronounced increase was observed when the FRK/AAA mutant of TF-C, unable to efficiently bind ribosomes, was utilized (grey circles). This result provides an independent confirmation that, upon translation, an increased fraction of TF becomes ribosome-associated.

other one contained both donor and acceptor (TF-CF). A kinetic change with very similar characteristics to the sigmoidal curve of TF-BADAN fluorescence and steady state fluorescence anisotropy was observed for the TF-CF reaction, except that donor emission increased (Figure 17). When E_{FRET} was calculated from the TF-C and TF-CF traces (see Materials and Methods), a clear decrease in energy transfer was observed between the donor and the acceptor (Figure 17). This suggested that the equilibrium between compact and open TF molecules shifted towards the open conformation as ribosomes became engaged in translation.

TF forms homo-dimers in solution, and dimer formation can be monitored by inter-molecular FRET when the protomers are individually labeled with donor and acceptor. In the presence of ribosomes, dimer dissociation is promoted, resulting in lower FRET efficiencies (see above). When FL is translated in the reconstituted system supplemented with the appropriate TF versions for inter-molecular FRET measurements, a

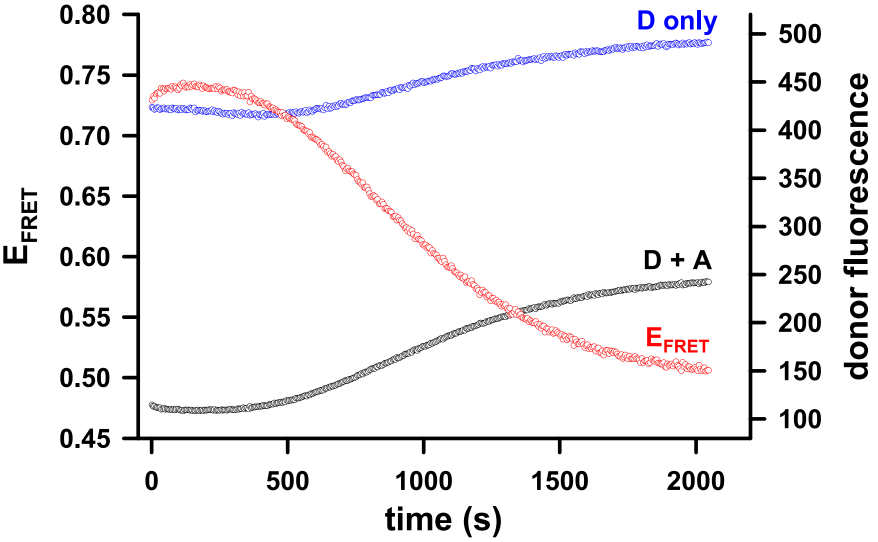

Figure 17: Increased TF recruitment to translating ribosomes is reflected by a conformational change within the molecule.

In an experiment analogous to the one described in Figure 16, the fluorescence emission of donor-only labeled (blue circles) and double-labeled (black circles) TF version R14C T150C was followed during FL translation in the reconstituted system. The intra-molecular FRET efficiency (red circles) was observed to decrease with kinetics similar to those of ribosome-recruitment (compare with Figure 15), indicating that ribosome recruitment is associated with a conformational change within TF, leading to a more extended structure than that in free solution.

decrease in E_{FRET} is observed (Figure 18). This decrease argues that the monomer-dimer equilibrium is shifted towards the monomeric form by increased TF recruitment to the translating ribosome, consistent with the observation that the ribosome-bound form of TF is a monomer.

Taken together, an increased recruitment of TF to the ribosome is observed upon translation of FL in the reconstituted system, as indicated by a decrease in BADAN-fluorescence and an increase in steady state fluorescence anisotropy. Since the corresponding FRK/AAA derivatives of TF do not exhibit such behavior, these phenomena can directly be attributed to ribosome binding. Ribosome recruitment is also reflected by an increased fraction of TF being shifted to a more open conformation, as revealed by intra-molecular FRET measurements. Inter-molecular FRET measurements indicated that ribosome recruitment upon translation is concomitant with stabilization of the monomeric form of TF.

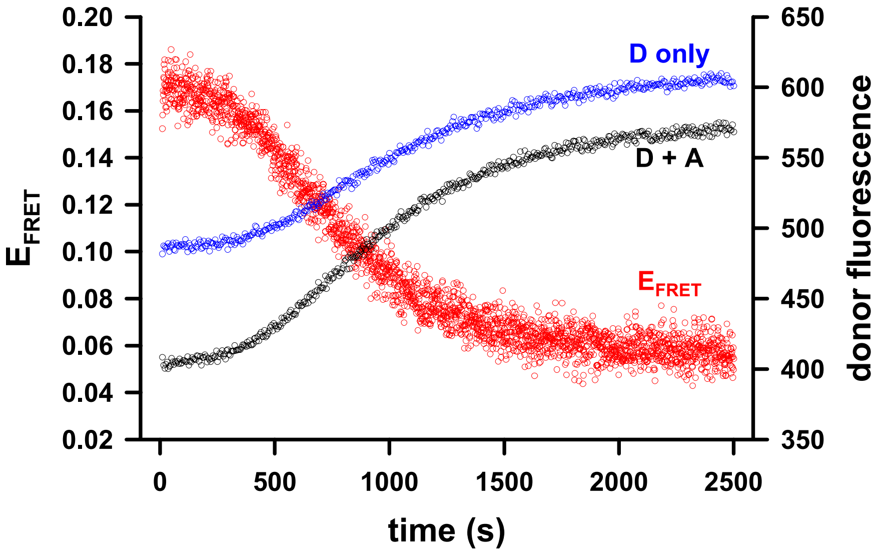

IV.4 Translation results in increased affinity of TF for the ribosome-nascent chain complex

During translation in the reconstituted system, the concentrations of TF and ribosomes remain constant throughout the course of the reaction (250 nM each). Therefore, the increased recruitment to ribosomes engaged in translation must be due to TF having a higher affinity for ribosome-nascent chain complexes than for vacant ribosomes. Thus, it was investigated by what magnitude the K_D of the TF-ribosome complex decreases when ribosomes transit from the vacant to the translating state.

The interaction of TF with vacant ribosomes was characterized by steady state fluorescence anisotropy. To determine the K_D of TF ribosomes complexes in the absence of translation, 250 nM TF-C was incubated with ribosomes at concentrations ranging from 0 to 8 µM, and the steady state fluorescence anisotropy was measured. With increasing concentrations of ribosomes, the anisotropy increased from 0.27 to 0.36 (Figure 19), indicating that TF indeed associated with ribosomes in a saturatable fashion.

Importantly, the anisotropy value in the presence of 250 nM ribosomes is similar to the one of 250 nM TF-C in the translation system before translation was initiated. Also, after assembly into ribosomes, the *E. coli* protein S21 labeled with the same chromophore utilized here, displays an anisotropy value of 0.36 (Odom *et al.* 1984), identical to the one

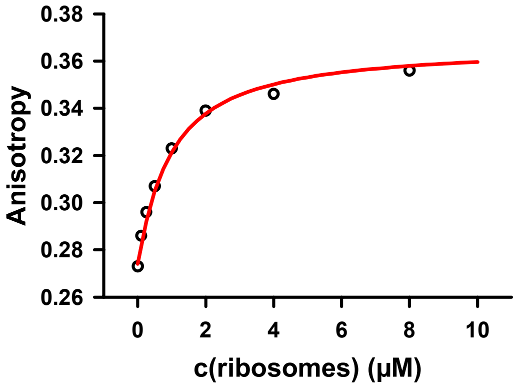

Figure 19: Binding of TF-C to vacant ribosomes is reflected by an increase in steady state fluorescence anisotropy.

250 nM TF-C was incubated with ribosomes at various concentrations, and the steady state fluorescence anisotropy was measured (open circles). An increase in anisotropy was observed with increasing ribosome concentration. The data points were fitted to the equilibrium equation for TF-ribosome dissociation (see Materials and Methods). A reasonable fit (red line) was obtained with a K_D of 0.84 µM, consistent with published values (Maier *et al.* 2003).

that was observed for TF-C at saturating ribosome concentration. Anisotropy was plotted against ribosome-concentration, and the data points were fitted as described in Materials and Methods with the K_D as a variable parameter. A good fit was obtained with a dissociation constant of 0.84 µM (Figure 19).

In an analogous experiment, the fluorescence emission of TF-B was measured in the presence of 0 to 4 µM ribosomes. The data were analyzed in a similar way as those obtained from the anisotropy measurements, yielding a K_D of ~0.9 µM for the dissociation of TF-ribosome complexes (see Materials and Methods), in excellent agreement with what has been observed in the fluorescence anisotropy measurements.

Using the experimentally derived dissociation constant, the fraction of TF that is present in a complex with the ribosome (f_{bound}) at a given ribosomal concentration was calculated. The fluorescence of TF-B measured at different ribosome concentrations can be expressed as a linear function of f_{bound} (see Materials and Methods). The value of the slope then is equivalent to the maximum relative change in fluorescence that is observed when all of the TF-B is associated with ribosomes. This was found to be $\Delta F_{rel}^{max} = -0.51$.

The correlation between BADAN fluorescence and ribosome binding can be used to calculate f_{bound} and to estimate the K_D from the relative decrease in BADAN fluorescence that is observed in the translation system upon FL synthesis (see Materials and Methods). During FL translation, a decrease in TF-B fluorescence to 65% of the initial value was observed ($\Delta F_{rel}^{obs} = -0.35$), corresponding to f_{bound} = 0.71. The concentrations of both TF-B and ribosomes in the translation system were 250 nM each. From these values, the K_D of the TF-ribosome nascent chain complex can be estimated (see Materials and Methods). An apparent K_D of ~30 nM was found for the TF-B ribosome complex during FL translation, compared to ~900 nM for the complex with vacant ribosomes (see above).

In titration experiments, steady state fluorescence anisotropies of 0.27 and 0.36 were determined for free and ribosome-bound TF-C, respectively (Figure 19). From measurements using TF-B, it was estimated that a fraction of f_{bound} = 0.71 of TF is associated with ribosome-nascent chain complexes. With the anisotropies for free and ribosome-bound TF-C, an anisotropy of ~0.33 would be expected during translation of FL (see Materials and Methods). This is indeed what was observed (see Figure 16), confirming the K_D determined from TF-B fluorescence by an independent method.

IV.5 Kinetic analysis of TF-ribosome complex dissociation

The displacement of TF-B from ribosome complexes by competition with excess unlabeled WT TF can be resolved kinetically (Maier *et al.* 2003). This was found to be a rather slow process with a rate constant of 0.036 s^{-1} at 20 ºC, which corresponds to a $t_{1/2}$ of 19 s (Maier *et al.* 2003). A similar experiment was set up at 30 °C. 250 nM TF was incubated with 2 µM ribosomes until an equilibrium was reached. The ribosome bound TF-B was then displaced by the addition of 20 µM WT TF. The $t_{1/2}$ was determined to be 10.3 ± 2.2 s under these experimental conditions (Figure 20), which is consistent with the reported value if the difference in temperature is taken into account.

In a similar way, the kinetics of TF relaxation from its open, ribosome bound conformation back to its compact conformation were determined by kinetically resolving the changes in intra-molecular energy transfer efficiency. Ribosome complexes were formed with either TF-C or TF-CF, and 20 µM WT TF were subsequently added. The change in donor fluorescence was followed over time and E_{FRET} was calculated. The FRET efficiency returned to its baseline with kinetics very similar to those observed for ribosome dissociation (Figure 20), with a $t_{1/2}$ of 8.6 ± 2.3 s.

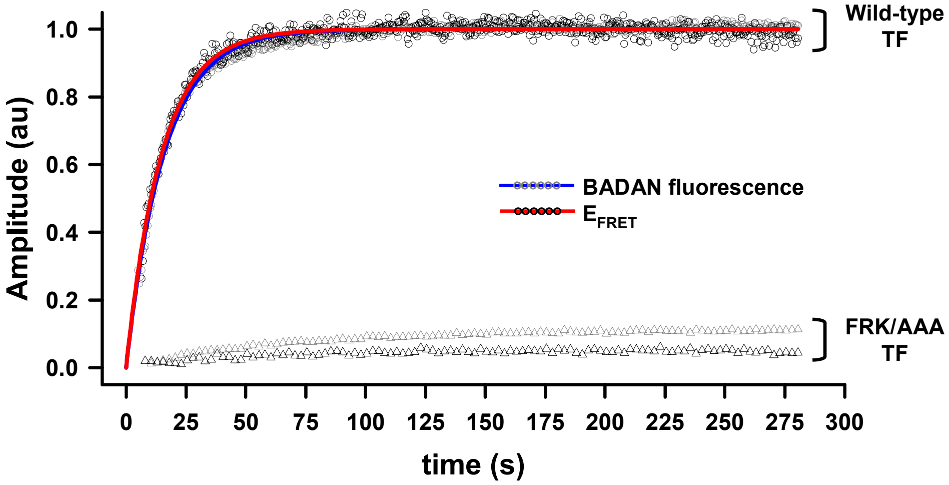

Figure 20: TF dissociation from vacant ribosomes and intra-molecular compaction occur with very similar kinetics.

Displacement of TF-B (grey circles) or intramolecular compaction (as measured by E_{FRET} from the TF-C/TF-CF combination; black circles) from pre-formed complexes with vacant ribosomes was achieved by the addition of excess unlabeled TF (20 µM). Analysis with a single exponential fit yielded very similar half times for ribosome dissociation (blue line; $t_{1/2}$ = 10.3 ± 2.2 s) and intra-molecular compaction (red line; $t_{1/2}$ = 8.6 ± 2.3 s). No such kinetics were observed in analogous experiments with the TF FRK/AAA mutant as the competitor (open gray triangles for TF-B and open black triangles for TF-C/TF-CF). The amplitudes of change in TF-B fluorescence and intra-molecular FRET efficiency were normalized to unity.

Additionally, the change in steady state fluorescence anisotropy of TF-C upon displacement from the ribosomal complex was characterized kinetically in an analogous experiment. The half-time of the anisotropy change was determined to be $t_{1/2} = 10.5 \pm 2.3$ s (data not shown). In none of the competition experiments was efficient displacement observed when the FRK/AAA TF mutant was used as the competitor (Figure 20).

Taken together, displacement of TF from vacant ribosomes at 30 °C occurs with a half-time of ~10 s, demonstrated by two independent methods, namely fluorescence emission of an environmentally sensitive probe and steady state fluorescence anisotropy. The TF conformational change, measured by intra-molecular FRET, also occurs with a very similar half time. This indicates that under these conditions, detachment of TF from ribosomes and its molecular compaction occur simultaneously.

Since it was possible to monitor TF-ribosome interactions with regard to ribosome detachment and TF intra-molecular compaction in a time-resolved manner, the effect of ongoing translation on the kinetics of these processes was examined next. Reactions with the reconstituted *in vitro* translation system were set up containing the various labeled TF molecules as above. Translation of FL was initiated by the addition of plasmid, and excess unlabeled TF was added once the reactions had reached the steady state (35 min after the start of each reaction, arrow in Figure 15). For the experiment that monitored TF-B dissociation from the ribosome by BADAN fluorescence, the change in fluorescence occurred with a $t_{1/2}$ of 11.2 ± 0.9 s (Figure 21). This indicates that, upon translation, the dynamic interaction of TF with the ribosome remains essentially unaltered with respect to ribosome detachment.

In contrast, the experiment that reported TF conformational compaction by intra-molecular FRET revealed kinetics considerably slower than those of ribosome dissociation, with a $t_{1/2}$ of 36.6 ± 3.5 s (Figure 21). Thus, during translation, the processes of ribosome departure and molecular compaction no longer occurred concomitantly. Additionally, the decrease in steady state fluorescence anisotropy of TF-C upon displacement from translating ribosomes was also significantly slower, with an observed $t_{1/2}$ of 46.7 ± 1.34 s (data not shown). As expected, the FRK/AAA TF mutant was unable to act as a competitor in any of these reactions (Figure 21).

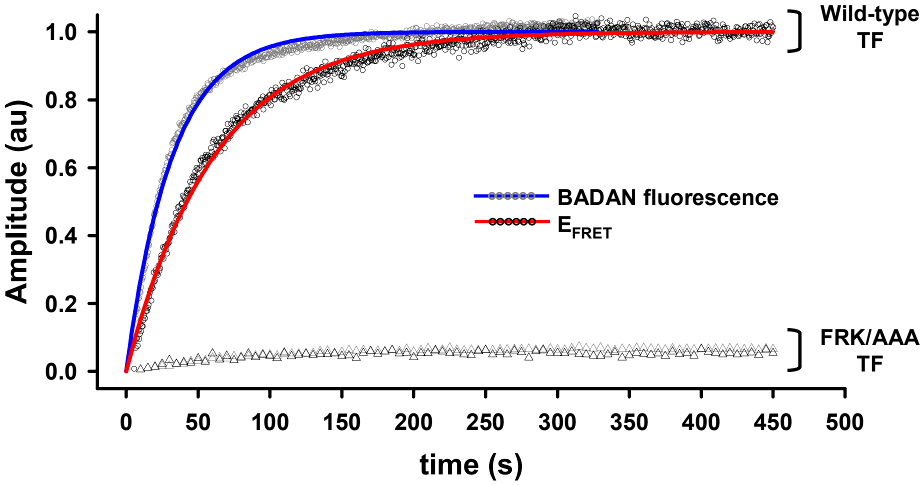

Figure 21: Interaction of TF with nascent luciferase chains leads to a deceleration of intra-molecular compaction.

Ribosome displacement (measured by TF-B-fluorescence; grey circles) and intra-molecular compaction (E_{FRET}; black circles) no longer occurred concomitantly when TF was displaced from ribosomes actively engaged in FL translation. Single exponential curve fitting revealed that ribosome release (blue line) occurred with $t_{1/2}$ of 11.2 ± 0.9 s, whereas intra-molecular compaction (red line) was markedly delayed, with a $t_{1/2}$ of 36.6 ± 3.5 s. No efficient competition was observed with the TF FRK/AAA mutant as competitor (grey and black triangles for ribosome release and intra-molecular compaction, respectively). The amplitudes of fluorescence and intra-molecular FRET change were normalized to unity.

In summary, a kinetic difference is observed between TF ribosome-displacement and intra-molecular compaction when measured in the presence of translation. The delay in intra-molecular compaction compared to ribosome-detachment that is observed with translating, but not vacant, ribosomes argues that TF remains associated with the nascent chain after leaving the ribosome, thereby being kept in a more open conformation. The fact that the TF FRK/AAA mutant, as a competitor, failed to promote TF intra-molecular compaction indicates that ribosome binding is a pre-requisite for TF-substrate interaction.

IV.6 TF interacts with its substrate after ribosome departure and does not rebind post-translationally

In the competition experiments described above, the competitor must bind to the ribosome in order to displace labeled TF from the ribosome, as indicated by the fact that the FRK/AAA mutant fails to act as an efficient competitor of labeled TF. If TF remains bound to the nascent chain post-translationally, it would be expected that TF molecular compaction still occurs more slowly than ribosome dissociation once both TF and the nascent chain are released from the ribosome. Such a post-translational scenario was mimicked in the translation system by fast depletion of Mg^{2+} by means of a chelating agent. This was achieved by the addition of EDTA, which efficiently leads to disruption of the ribosome-nascent chain complex (Michalski *et al.* 1973). To obtain a homogenous population of ribosome-bound nascent chains, FL was translated from a template lacking a stop codon. This prevents the release of the nascent chain and results in stalling of translation and accumulation of ribosome-nascent chain complexes.

To verify that under these conditions the majority of the polypeptide chains produced was kept in a ribosome-bound state, stalled radio-labeled FL nascent chains were produced in the presence of ^{35}S-methionine and analyzed by fractionating ribosomes. In a control reaction, FL was translated from plasmid pLuc, which encodes FL followed by a stop codon. The accumulation and distribution of radio-labeled full-length FL were analyzed by SDS-PAGE and autoradiography.

When comparing the total reactions (Figure 22, lanes “T”), it was found that considerably less material was produced when the template lacked a stop codon. The reactions were subjected to high speed centrifugation at ~200,000 *g* to sediment ribosomes. As expected, the majority of full-length FL (arrowhead in Figure 22) translated from plasmid pLuc was recovered in the post-ribosomal supernatant. In contrast, very little full-length FL was detected in the corresponding fraction of the reaction producing stalled FL (Figure 22, lanes “S200”), whereas most of it was present in the ribosomal pellet (“P200” in Figure 22). A smear of radioactive material is visible above the full-length FL band in the ribosomal pellet fraction of both reactions (“P200” in Figure 22). This material probably corresponds to peptidyl-tRNA species of translated FL, since it co-fractionates with ribosomes and converts into a full-length FL band upon treatment with RNase A (“P200*” in Figure 22). These findings indicate that efficient stalling was achieved in the translation system with a DNA-template lacking a stop codon.

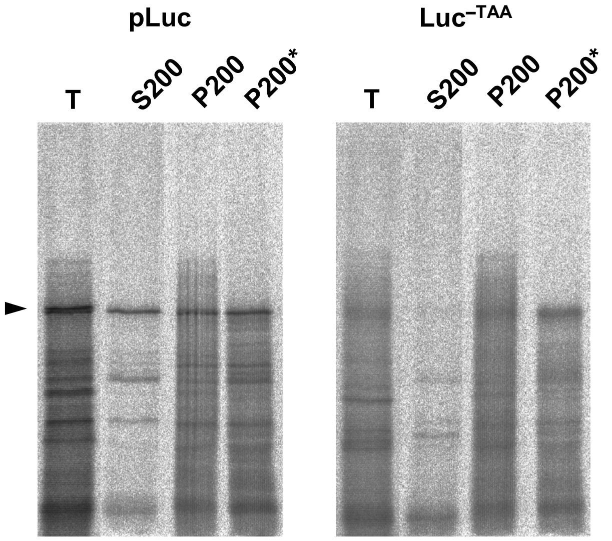

Figure 22: Efficient stalling of nascent chains on the ribosome can be achieved by omission of the stop codon from the FL open reading frame.

Radiolabeled FL was translated in the reconstituted system either from plasmid pLuc (left panel) or from a PCR product encoding the same protein but lacking a stop codon after the FL open reading frame (right panel). The total reaction (T) was subjected to low speed centrifugation, and the low speed supernatant was subjected to high speed centrifugation, yielding a post-ribosomal supernatant (S200) and a ribosomal pellet (P200). After dissolving the ribosomal pellet, a fraction was treated with RNase A to digest tRNA (P200*). FL chains were visualized by autoradiography. When translated from a stop codon-free template (Luc^{-TAA}), the amount of full-length FL (arrowhead) was considerably less, and the protein was found almost exclusively in the ribosomal pellet fraction (P200).

Next, the dynamics of TF-substrate interaction were analyzed kinetically under the above conditions, which mimic a post-translational scenario. Ribosome-bound FL nascent chains were accumulated as described above. Then, excess EDTA was added and ribosome detachment as well as intra-molecular compaction were measured over time (Figure 23). TF dissociation from ribosomes occurred with a half-time of 14.1 ± 0.1 s, whereas the half-time of molecular compaction was 21.2 ± 1.1 s. The slower half-time of intra-molecular compaction compared to ribosome dissociation supports the notion that TF-substrate association is sustained even after TF and its substrate have departed from the ribosome. After disruption of the ribosome-nascent chain complex, TF does not rebind to the substrate, indicating that only in the context of the ribosome, efficient substrate interaction takes place.

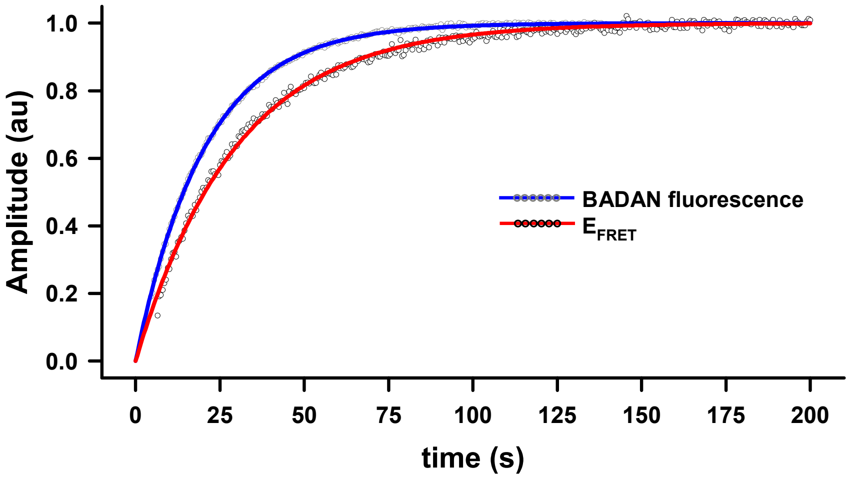

Figure 23: TF stays associated with the nascent chain post-translationally.

After accumulation of FL nascent chains, ribosome-nascent chain complexes were disrupted by depletion of Mg^{2+}, mimicking a post-translational scenario. TF-ribosome release was monitored by TF-B fluorescence (grey circles, blue line), TF intra-molecular compaction was monitored by E_{FRET} (black circles, red line). The amplitudes of both processes were normalized to unity. Under these conditions, the TF conformational change was delayed compared to ribosome release, similar to what was observed in competition experiments with excess unlabeled TF.

IV.7 The properties of the nascent chain modulate its interaction with TF

In competition experiments, TF intra-molecular compaction is markedly delayed with respect to ribosome departure when ribosomes are engaged in FL translation, whereas these processes occur concomitantly when TF is displaced from vacant ribosomes. This suggests that TF remains bound to the nascent chain after leaving the ribosome. To investigate whether this is a general feature of most nascent chains or whether the properties of the substrate confer different modes of binding to TF, model nascent chains in addition to luciferase were analyzed as above.

Different constructs encoding eukaryotic and prokaryotic proteins (see Figure 24) were translated, and the kinetics of TF ribosome dissociation and molecular compaction were determined in competition experiments as described. All proteins tested displayed the characteristic TF ribosome recruitment and conformational change associated with translation (data not shown). However, the kinetics of TF molecular compaction displayed

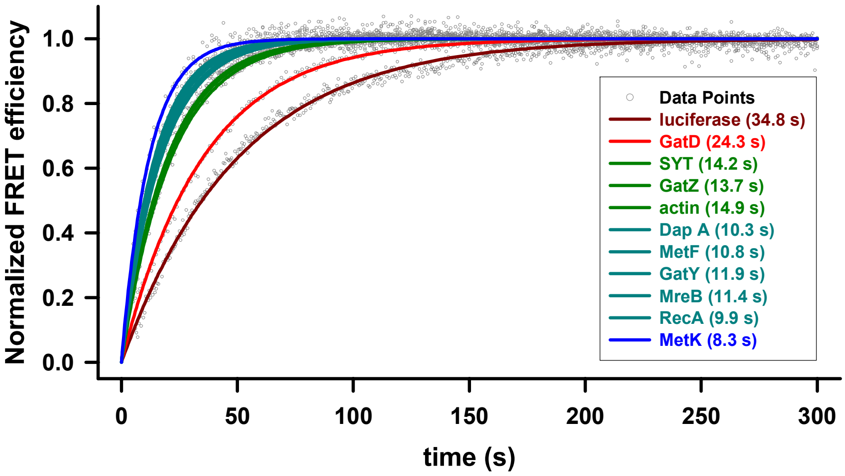

Figure 24: The nature of the nascent chain determines the kinetics of TF molecular compaction.

Various proteins from eukaryotic and prokaryotic origins were translated in the reconstituted system, and the kinetics of TF molecular compaction upon competition with excess unlabeled TF were monitored by intra-molecular FRET. Kinetics with different half times were observed for the various substrate proteins (indicated by name in the inset). Whereas molecular compaction was relatively slow for luciferase (dark red, $t_{1/2} \approx 35$ s) and the bacterial protein GatD (red, ~25 s), other proteins showed intermediate half times (green, SYT, GatZ and actin). For some proteins, ribosome release and TF molecular compaction occur with virtually the same kinetics (turquoise and blue; DapA, MetF, GatY, MreB, RecA and MetK).

significant differences among translated proteins, with $t_{1/2}$ values ranging from ~10 to ~35 s (Figure 24). For most of the nascent chains, dissociation of TF from ribosomes translating these proteins occurred with kinetics similar to those of molecular compaction. However, as was found for FL, molecular compaction occurred considerably more slowly than ribosome release for the *E. coli* protein galactitol-1-phosphate 5-dehydrogenase (GatD) ($t_{1/2}$ = 24.3 s).The half time of change in intra-molecular FRET efficiency was also mildly increased for the *E. coli* proteins threonyl-tRNA synthetase (SYT), tagatose 6-phosphate kinase (GatZ) and *S. cerevisiae* actin ($t_{1/2} \approx 14$ s).

These results suggest that TF remains bound to certain polypeptides for varying lengths of time upon leaving the ribosome, whereas nascent chain release and ribosome departure occur concomitantly for others.

IV.8 Hydrophobic motifs in the substrate determine TF displacement kinetics

The results obtained from competition experiments during translation of various model substrates indicate that there are certain characteristics of the nascent chain that modulate TF-substrate interactions. Since TF is involved in very early steps during protein folding, when the polypeptide chain has not acquired considerable amounts of structure, it is conceivable that these characteristics can be revealed by analysis of the primary structure of the emerging nascent chain. Chaperones interact with their substrates mainly *via* hydrophobic interactions. Thus, the different model substrates tested were analyzed for the presence of hydrophobic motifs within their sequences.

One measure of hydrophobicity of a chemical moiety is the free energy of transfer (ΔG) from water to n-octanol, with lower values corresponding to higher hydrophobicities. Such a hydrophobicity (or hydropathy) scale for amino acid side chains within a peptide was developed by Roseman (Roseman 1988) (see Materials and Methods). Employing this scale, the substrates used in the above experiment were analyzed by calculating the mean hydrophobicity over a window of 15 residues along their sequence (Figure 25). It was found that the number of motifs with high hydrophobicity ($\Delta G \leq -0.5$ kcal/mol) correlated

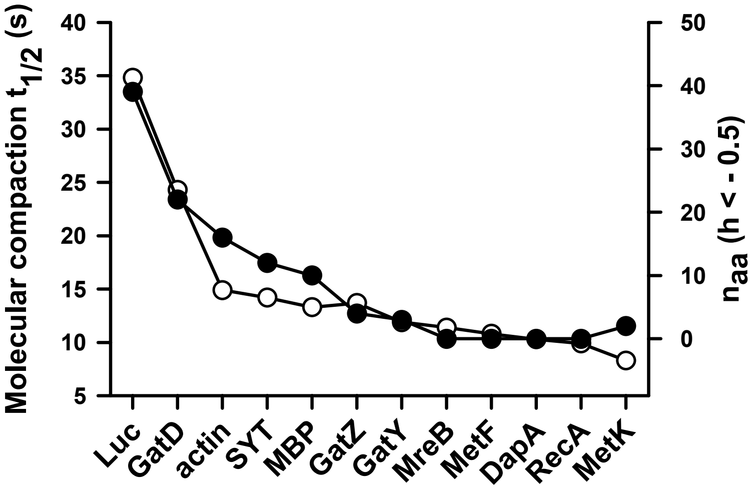

Figure 25: The half-times of TF molecular compaction correlate with the occurrence of motifs of high mean hydrophobicity within the substrate.

The substrates shown in Figure 24 were analyzed in terms of their mean hydrophobicity over a window of 15 residues using the Roseman hydropathy scale (Roseman 1988). Closed circles indicate the number of amino acids (n_{aa}) which were assigned a hydrophobicity of -0.5 kJ/mol or less (right y axis). Open circles represent the half time of TF intra-molecular compaction observed when the respective substrate was translated in the presence of TF (left y axis), which correlates well with the extent of hydrophobic motifs in the substrate.

well with the $t_{1/2}$ values of TF molecular compaction (Figure 25). Importantly, this correlation was maintained independently of the scale used to measure the hydrophobicity of amino acid side chains.

Increasing or decreasing the window size used to calculate mean hydrophobicity resulted in a gradual loss of correlation, which suggests that the optimal TF interaction motif is ~15 amino acid residues in length. The length of the long axis of the proposed substrate binding crevice of TF in the crystal structure is 65 Å (Ferbitz *et al.* 2004), which is sufficient to accommodate a peptide of 18 residues in a fully extended conformation. Thus, a motif of 15 amino acids on an extended substrate polypeptide binding to the TF crevice would be consistent with the dimensions from the structural data available.

To confirm the notion that the occurrence of strongly hydrophobic motifs in the substrate is correlated with the time that the substrate remains bound to TF, individual sub-domains of FL were analyzed for their interaction with TF. The FL crystal structure reveals a two-domain arrangement composed of a complex amino-terminal domain encompassing the first 436 residues and a small carboxyl-terminal domain topologically independent from the rest of the molecule. Sequence analysis showed that motifs with high hydrophobicity clustered in two regions of the amino-terminal domain, and that the carboxyl-terminal part did not contain any such motifs (Figure 26 a).

Contributions of the different FL regions towards TF binding were dissected by generating linear DNA fragments for the translation of three regions of FL independently: one amino-terminal and one middle fragment containing each a cluster of putative TF interaction motifs, and the motif-free carboxyl-terminal region (Figure 26 a). TF was efficiently recruited to the ribosome upon translation of each fragment. TF intra-molecular compaction occurred with similar kinetics as ribosome displacement when the carboxyl-terminal FL fragment was translated (Figure 26 d), but the former was markedly delayed when either the amino-terminal or the middle fragment were translated (Figure 26 b, c). This further strengthens the notion that the interaction between TF and its nascent chain substrate is prolonged when the substrate contains regions of high mean hydrophobicity.

Taken together, the results indicate that the interaction of TF with its substrate, the nascent chain, is modulated by the properties of the substrate itself. The occurrence of segments with high mean hydrophobicity within the nascent chain leads to prolonged interaction with TF.

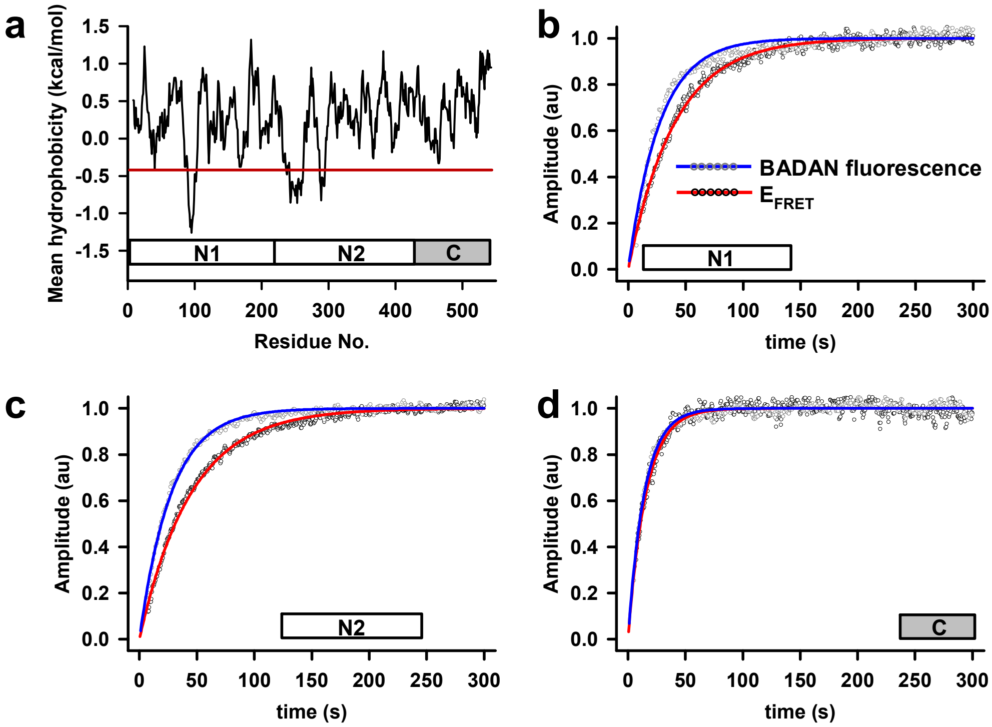

Figure 26: FL regions containing motifs of high mean hydrophobicity exhibit prolonged interaction with TF.

a. Hydrophobicity plot of FL. The boxes indicate the position of sub-domain borders separating the amino-terminal domain (N1), the middle domain (N2) and the carboxyl-terminal domain (C). Motifs of high mean hydrophobicity occur in fragments N1 and N2, whereas the small, topologically independent carboxyl-terminal fragment is motif-free. **b – d.** Comparison of TF ribosome dissociation (grey circles, blue lines) and molecular compaction (black circles, red lines) kinetics. N1, N2 or C were translated individually in the reconstituted system. Whereas TF molecular compaction is delayed relative to ribosome release for N1 (**b**) and N2 (**c**), these processes occur concomitantly for C (**d**).

IV.9 The ability of a nascent chain to fold co-translationally determines the extent of TF recruitment to the ribosome

The analysis of various model substrate proteins revealed that the presence of motifs of high hydrophobicity within the primary structure of the nascent chain causes a prolonged interaction of TF with its substrate. It is thus conceivable that exposure of hydrophobic motifs on the nascent chain promotes TF recruitment to the translating ribosome, whereas burial of these segments, *i.e.* folding of the substrate, diminishes the affinity of TF for the nascent chain. To investigate whether the folding status of a nascent chain affects the degree of TF recruitment to the ribosome-nascent chain complex, the I27 domain of the muscle protein titin was used as a model substrate. The I27 domain belongs to the IgG structural class, and it folds robustly in a co-translational fashion into an all-beta structure (Marszalek *et al.* 1999).

For translation in the reconstituted system, linear DNA templates encoding amino-terminal fragments of the I27 domain were generated by PCR. Absence of a stop codon in the template DNA resulted in stalled translation of the fragments and accumulation of ribosome-bound nascent chains (data not shown). The shortest I27 domain fragment, consisting of 25 amino acids, would be expected to reside completely within the ribosomal exit tunnel, which is ~100 Å in length and can accommodate 30 to 40 residues of a polypeptide chain in an extended conformation. The longest fragment, stalled at the last codon of the full-length I27 domain, should result in a solvent-exposed nascent chain. However, the carboxyl-terminal third of the polypeptide chain would still be contained within the exit tunnel, and thus the folding of the all-beta I27 domain into its native conformation would be prevented. On the other hand, if the I27 nascent chain were fused to carboxyl-terminal flexible extension sequences, this would allow the full-length domain to emerge from the ribosome and folding would be expected to take place.

The stalled titin I27 fragments were synthesized in the translation system in the presence of 250 nM TF-B. When the accumulation of stalled nascent chains was complete, excess unlabeled TF was added, and the change in fluorescence emission associated with displacement of TF-B from the ribosome was quantitated. The amplitude of the displacement reaction reflected the fraction of TF-B that had been recruited to the stalled ribosome-nascent chain complexes (Figure 27 b).

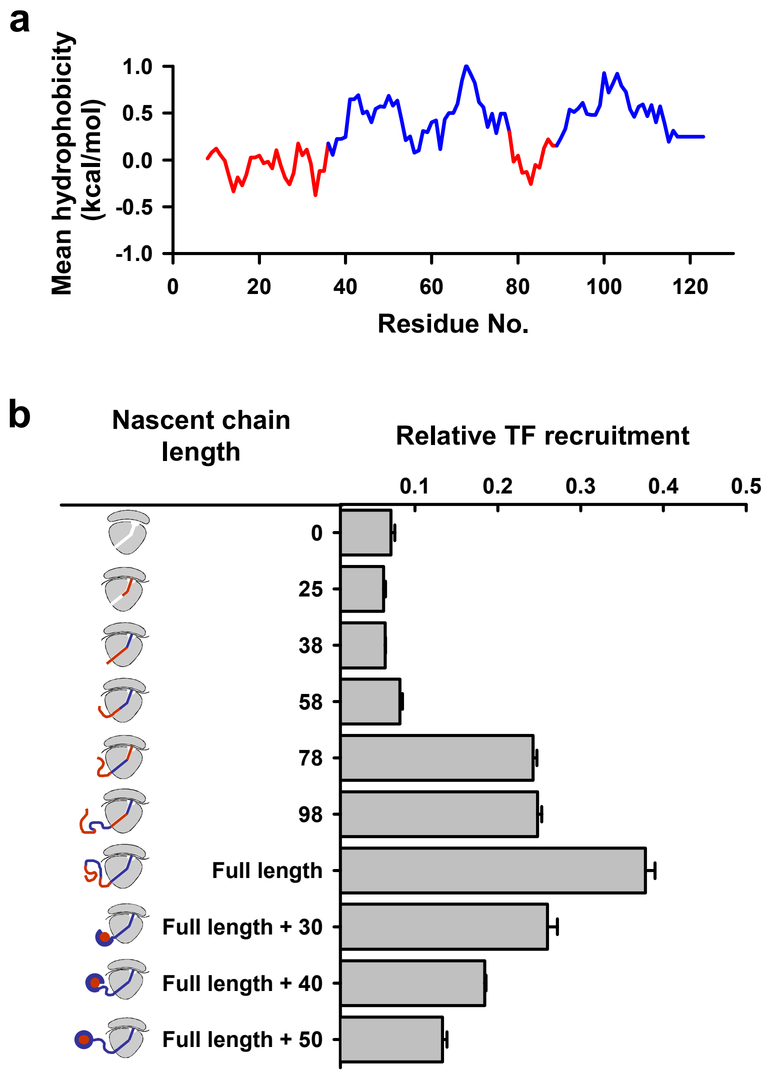

Figure 27: Exposure of hydrophobic motifs on the nascent chain results in increased TF recruitment to ribosome-nascent chain complexes.

a. Hydrophobicity plot of the titin I27 domain. Regions of primary sequence with relative high hydrophobicity are colored in red and more hydrophilic regions are colored in blue. The extreme amino-terminus of the I27 domain is polar due to a His_6 tag at this position. Due to the calculation of mean hydrophobicity over a window of 15 aa, this is not reflected in this diagram. **b.** Amplitude analysis of TF displacement from ribosome-nascent chain complexes. Stalled, ribosome-tethered titin I27 fragments of increasing lengths were accumulated in the presence of TF-B. The histogram shows the amplitudes observed upon competition with excess unlabeled TF (20 µM), reflecting the extent of TF recruitment to ribosome-nascent chain complexes. The diagrams on the left depict the position of the hydrophobic regions along the I27 nascent chain relative to the ribosomal exit tunnel, colored as in (**a**). Circular shapes indicate the acquisition of three-dimensional structure. An increase in TF recruitment was observed when hydrophobic regions on the nascent chain became exposed to the exterior of the ribosome, and TF recruitment was diminished once the nascent chain was allowed to begin acquiring tertiary structure, burying the hydrophobic segments (red) in the interior of the (partially) folded nascent chain.

When the amino-terminal 25 residues of the I27 domain were translated, no increase in TF recruitment to the ribosome was observed. Taking into account that 30 to 40 residues of a peptidyl-tRNA bound to the peptidyl transferase center of the ribosome are shielded from the environment by the ribosomal exit tunnel, this suggests that transition of the ribosome from the vacant to the translating state alone does not provide a high affinity binding site for TF. Similarly, no enhanced recruitment was observed for an I27 domain fragment of 38 residues. I27 stalled at position 58 also did not lead to an increased TF recruitment, although it would be expected that the amino-terminal ~20 residues of the I27 fragment are outside the ribosomal exit-tunnel. The I27 domain utilized in this experiment contains an amino-terminal His_6-tag and is thus rather polar. Therefore, no strong interaction of this segment with TF would be expected.

A more hydrophobic motif is contained within residues 20 to 40 of the I27 domain (Figure 27 a). This region is expected to lie outside the ribosomal exit tunnel when the nascent chain is stalled at position ~80. Indeed, an increase in TF recruitment was observed when I27 was stalled at residue 78 (Figure 27 b). Additional recruitment was seen when the I27 was stalled at position 110 (Figure 27 b). At this nascent chain length, another hydrophobic motif, around position 80 in the I27 sequence (Figure 27 a), emerged from the ribosomal exit tunnel.

To produce ribosome-nascent chain complexes in which the full-length I27 domain has emerged from the ribosomal exit tunnel, a plasmid was constructed encoding the I27 domain followed by a flexible linker of 25 amino acids and the amino-terminus of GFP. From this plasmid, DNA templates for the translation system were generated lacking a stop codon, as described above. The templates encoded the full length I27 domain followed by successive stretches of 30, 40 or 50 residues of downstream sequence, which itself did not contain any hydrophobic motifs. A decrease in TF-ribosome recruitment was observed for these ribosome nascent-chain complexes (Figure 27 b), suggesting that the ribosome-attached I27 domain is able to fold to some extent under these conditions, and loses its ability to interact with TF. Notably, the remaining affinity for the I27 domain even after the full-length protein had emerged from the ribosome (full-length plus 40–50 extra residues), suggests that delayed folding is a fundamental consequence of TF action, even with highly cooperatively folding domains.

To ascertain that the I27 domain indeed is able to fold when allowed to exit the ribosomal tunnel in its entirety, stalled ^{35}S-labeled nascent chains were produced of either the I27 domain alone or the I27 domain followed by the 50 amino acid flexible linker. The samples were treated with Proteinase K (PK) for variable periods before subjected to SDS-PAGE and autoradiography. When the I27 domain is allowed to emerge from the ribosomal exit tunnel completely, as warranted by the 50 residue carboxyl-terminal extension, a high degree of protection from PK digestion (~80%) was observed (Figure 28), indicating acquisition of a compact structure. In contrast, the stalled I27 domain without a linker is degraded considerably more efficiently by the protease (Figure 28). This argues that, with the carboxyl-terminal part of the nascent chain still residing in the ribosomal exit tunnel, the I27 domain is unable to fold.

In summary, the above experiments show that TF recruitment to ribosome-nascent chain complexes is enhanced when the nascent chain presents hydrophobic motifs to the environment outside the ribosomal exit tunnel. Translation *per se* is insufficient to procure a high-affinity binding site for TF on the ribosome. Under conditions that allow co-translational domain folding of the nascent chain, the hydrophobic motifs are buried, resulting in a decreased affinity of TF for these ribosome nascent chain complexes.

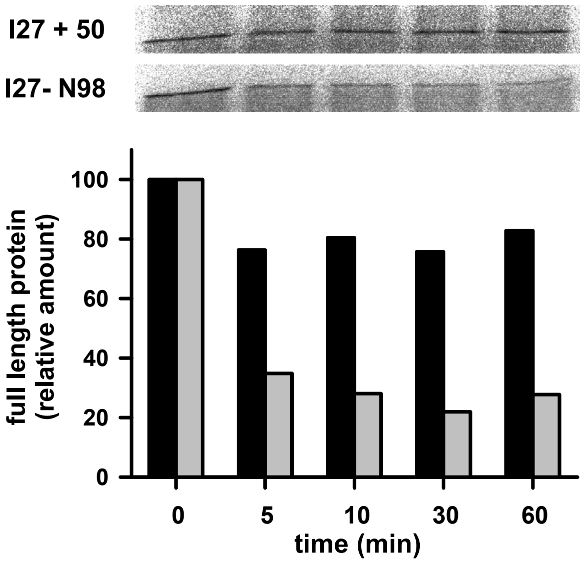

Figure 28: The I27 domain exhibits protease resistance only when the entire domain is allowed to emerge from the ribosomal exit tunnel.

Stalled radiolabeled nascent chains of the titin I27 domain alone (I27-N98) or with a carboxyl-terminal extension of 50 amino acids (I27 + 50) were accumulated in the reconstituted system and subjected of Proteinase K (PK) digestion for increasing lengths of time. The autoradiograph (upper panel) shows that the I27-N98 fragment became degraded over time, whereas the I27 + 50 fragment was stabilized. The band intensities were quantitated, and the amount of protein present before PK treatment (0 min time point) was set 100% (lower panel). Whereas only ~20% of the I27 + 50 fragment was digested, ~80% of the I27-N98 fragment became degraded, suggesting that the I27 + 50 construct was able to acquire tertiary structure, making PK cleavage sites inaccessible.

IV.10 The TF PPIase domain contributes to substrate interaction but is dispensable for the initial binding step

Although crystal structures of TF are available, the identity and localization of the TF substrate binding domain(s) have not been conclusively established. Ferbitz *et al.* proposed that the region in TF surrounded by the two tips and the backbone form a “cradle”, suggesting that substrate binding takes place in this region (Ferbitz *et al.* 2004). However, no functional data are available to support this model.

Proteins displaying PPIase activity, such as TF, aid proteins during their folding and thus must be able to interact with non-native polypeptides. Therefore, it is conceivable that the PPIase domain of TF contributes at least in part towards binding of the nascent chain. In order to explore this possibility, a TF mutant was generated that lacked the entire PPIase domain. Based on the crystal structure, it was decided to genetically delete residues W151 to R243 and to insert a flexible linker to join the adjacent residues (see Figure 29 a). This protein is henceforth referred to as NC.

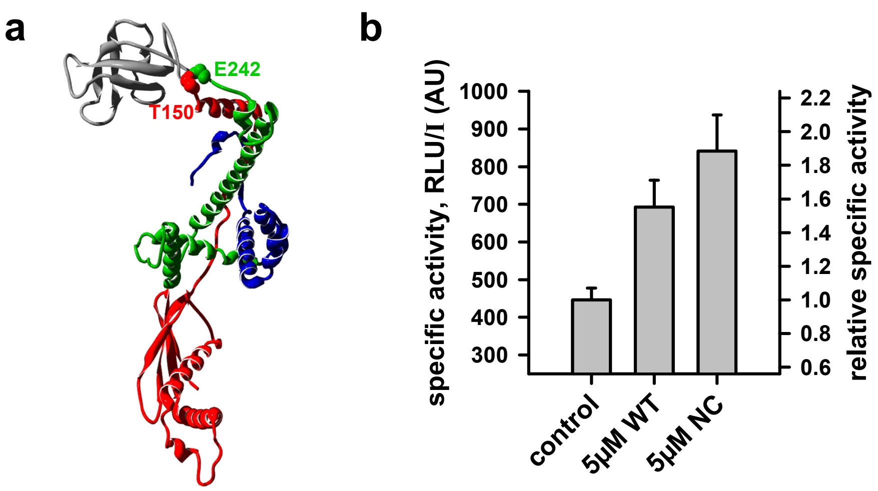

Figure 29: NC is as active as wild type TF in increasing the specific activity of FL translated in the reconstituted system.

a. Ribbon diagram of *E. coli* TF. The PPIase domain (shown in grey) has been replaced with a flexible linker inserted between positions T150 and E242 (red and green, respectively, with the backbone atoms shown in spacefill) in the NC-construct. **b.** Radiolabeled FL was translated in the reconstituted system, which was either unsupplemented (control) or supplemented with 5 µM of either full-length TF (5 µM WT) or NC (5 µM NC). Luciferase activity was measured luminometrically as relative light units (RLU), and the amount of full-length FL was quantitated by autoradiography of band intensities (I), yielding the specific luciferase activity (RLU/I; left axis). Both TF and NC gave rise to a specific FL activity ~1.5- to 2-fold higher than in the unsupplemented sample (right axis).

To establish that the NC protein is functionally active, its ability to increase the specific activity of FL translated in the reconstituted system was investigated. Translation reactions of FL were supplemented with ^{35}S-methionine and 5 µM of either TF or NC. Translation was allowed to proceed for 45 min before the reaction was stopped by addition of chloramphenicol and placement on ice. Luciferase activity was determined by chemiluminescence, and the amount of full-length FL produced was quantified by SDS-PAGE and autoradiography. The specific activity of FL was calculated by dividing the measured activity by the protein amount. The presence of TF led to an increase in FL specific activity by a factor of ~1.6, compared to a ~1.9-fold increase when NC was present at the same concentration (Figure 29 b), in agreement with published findings (Agashe *et al.* 2004). This demonstrates that the truncation mutant NC is at least as active as the full-length protein.

Next, it was investigated whether NC displaces ribosome-bound TF-B during translation as efficiently as TF. Luciferase was translated in the reconstituted system supplemented with 250 nM TF-B. The kinetics obtained in competition experiments using 20 µM of either TF or NC as competitors were indistinguishable (Figure 30). Additionally, in an analogous experiment monitoring the kinetics of TF-conformational change using the TF-C / TF-CF pair, no difference between TF and NC as competitors was observed (Figure 30). Even when the competitor concentration was reduced to 6 and 2 µM, respectively, both competitors yielded virtually the same kinetics of displacement (Figure 30). In summary, no difference was observed between NC and wild type TF regarding their ability to displace labeled TF from ribosome-nascent chain complexes.

To gain further insight into the contributions of the PPIase domain to TF function, cysteine mutants of the NC protein were generated, suitable for labeling with exogenous chromophores. A single cysteine was introduced at position 14. This construct was labeled with BADAN to monitor NC ribosome binding (NC-B). In addition, a double cysteine mutant of NC was generated, introducing cysteines at positions 14 and 150. For intra-molecular FRET measurements, this protein was labeled either with donor only (NC-C) or donor and acceptor (NC-CF).

First, it was verified that the conformation of NC was the same as that of TF as judged by intra-molecular FRET measurements. Fluorescence emission spectra of 250 nM NC-C or NC-CF were acquired in the absence and in the presence of 2 µM ribosomes (Figure 31 a). From the intensity of donor emission at 465 nm, the FRET efficiency was

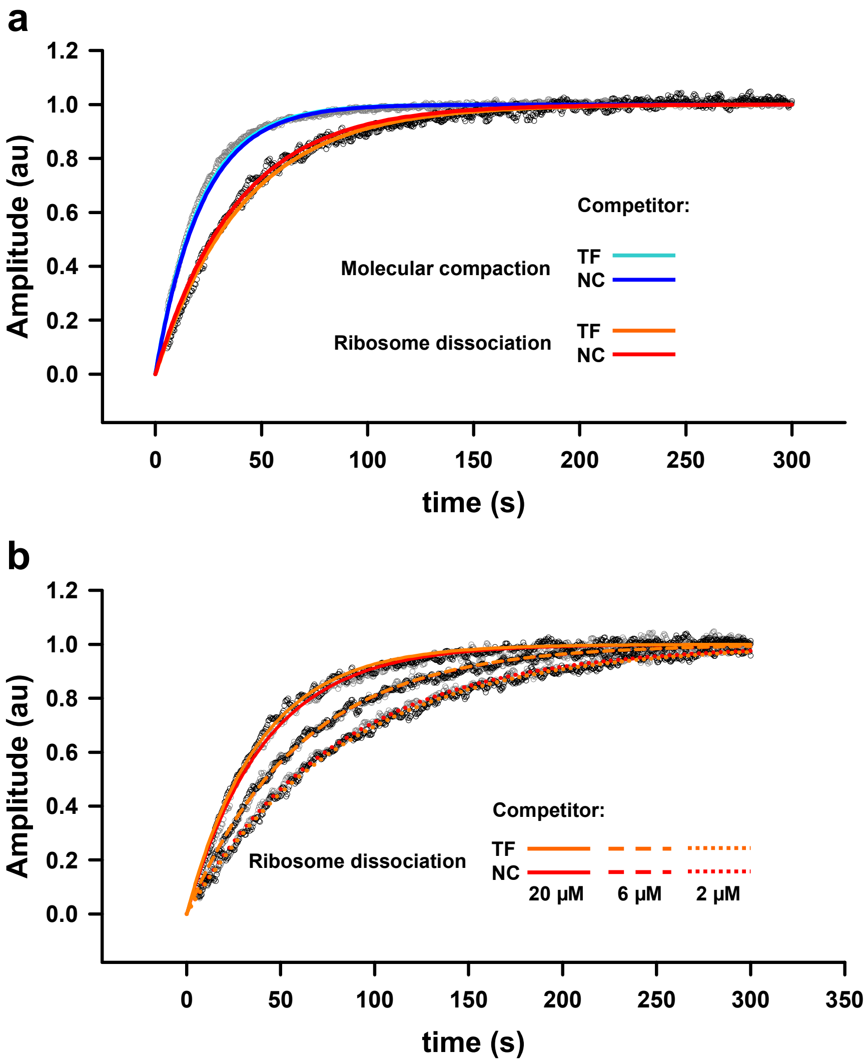

Figure 30: NC is as effective as TF in displacing TF from ribosomes and nascent chains.

a. Kinetics of ribosome-displacement (TF-B fluorescence; grey circles) and TF molecular compaction (intra-molecular FRET; black circles) during FL translation upon competition with 80-fold excess of TF and NC. The kinetics were analyzed by fitting to a single exponential function (turquoise and orange: TF; blue and red: NC). **b.** Titration of competitor concentrations. TF intra-molecular compaction kinetics during FL translation were recorded after addition of TF (grey circles, orange lines) or NC (black circles, red lines). The excess of competitor over labeled TF was 80-fold (solid lines), 24-fold (dashed lines) or 8-fold (dotted lines). At neither concentration of competitor was a difference between TF and NC detected.

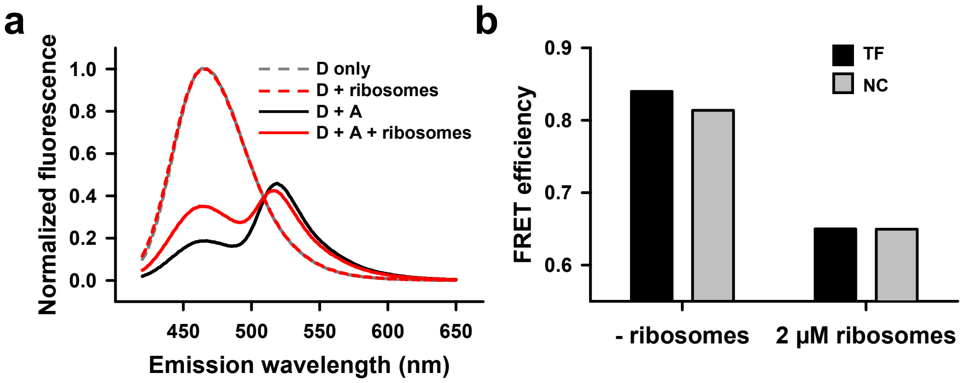

Figure 31: The conformational change in NC upon ribosome binding is very similar to the one observed for TF.

a. Fluorescence emission spectra of double-labeled NC in the absence (black line) and presence (red line) of 2 µM ribosomes. The spectra were normalized to the maximum emission in the absence of acceptor (grey dashed lines). In the presence of ribosomes, an increase in donor fluorescence at ~460 nm and a decrease in acceptor fluorescence at ~510 nm were visible. **b.** Intra-molecular FRET efficiencies of double-labeled TF (black bars) and NC (grey bars) in the absence (left) or presence (right) of 2 µM ribosomes. The FRET efficiencies for NC and TF are very similar in the absence of ribosomes and identical in the presence of ribosomes, indicating that the conformational change observed upon ribosome binding was essentially the same for both molecules.

calculated. In the absence of ribosomes, a FRET-efficiency of 0.81 was measured, similar to what was observed with TF-CF labeled at the corresponding positions (E_{FRET} = 0.84). In the presence of ribosomes, a decrease in FRET-efficiency to 0.65 was observed, corresponding exactly to the value obtained with TF-CF (Figure 31 b) . Thus, regarding the molecular compactness and the conformational change upon ribosome-binding, NC exhibits the same properties as TF.

Next, the recruitment of NC-B to ribosomes translating FL was investigated. Luciferase was translated in the reconstituted system supplemented with 250 nM NC-B. Upon addition of excess unlabeled TF, a change in fluorescence was observed similar to the one obtained with TF-B. However, the half-time of the fluorescence change observed with NC-B was only ~7 sec (Figure 32 b), compared to ~13 sec when TF-B was used. Also, the amplitude of the change in NC-B fluorescence was only one third of that of TF-B. No significant differences in amplitudes or kinetics between TF-B and NC-B were observed in analogous competition experiments with vacant ribosomes (Figure 32 a) . This

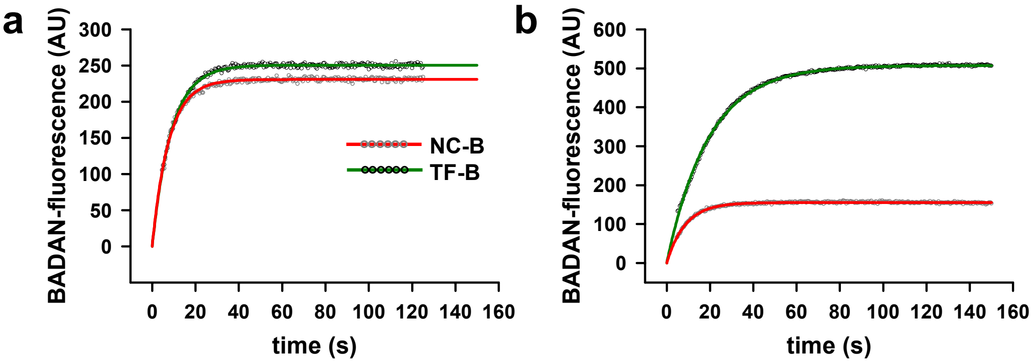

Figure 32: NC has a reduced affinity for nascent chains

a. Displacement kinetics of TF-B (black circles, green line) and NC-B (grey circles, red line) from vacant ribosomes. Excess unlabeled TF was added to preformed complexes of vacant ribosomes and labeled TF versions, and fluorescence was followed over time. No major differences were detected between TF-B and NC-B. **b.** Displacement kinetics of TF-B and NC-B from ribosomes translating FL. The color coding is the same as in (**a**). FL was translated in the presence of TF-B, which was competed out by the addition of excess unlabeled TF. NC-B was displaced more rapidly than TF-B, and the observed amplitude was considerably lower, indicating that less NC-B was recruited to ribosomes translating FL.

indicates that, when compared to TF-B, less NC-B is recruited to ribosomes translating FL, and that NC-B dissociates more rapidly from ribosome-nascent chain complexes. In all competition experiments, no significant difference was observed in regard to whether TF or NC were used as the competitor.

In an experiment analogous to the one described above, the kinetics of intra-molecular FRET change were determined during FL translation. Double labeled TF (TF-CF) or NC (NC-CF) were used, in which donor and acceptor are coupled to identical positions in each molecule (14 and 150). NC-CF was displaced with a half-time of ~23 s (Figure 33), somewhat faster than TF-CF ($t_{1/2} \approx 31$ sec). Thus, the NC-CF protein is displaced more rapidly than the TF-CF, yet, the kinetic difference between ribosome detachment and conformational compaction is preserved.

In summary, the above data indicate that there is no significant difference between the abilities of TF and NC to compete labeled TF from either ribosomes or nascent chains during translation. Thus, the initial binding step to the ribosome nascent chain complex does not seem to depend on the PPIase domain. However, recruitment to ribosome-nascent chain complexes as well as the duration of TF-substrate interaction appear to be enhanced by the PPIase domain, as judged by the analysis of NC-B amplitudes and NC-CF dissociation kinetics.

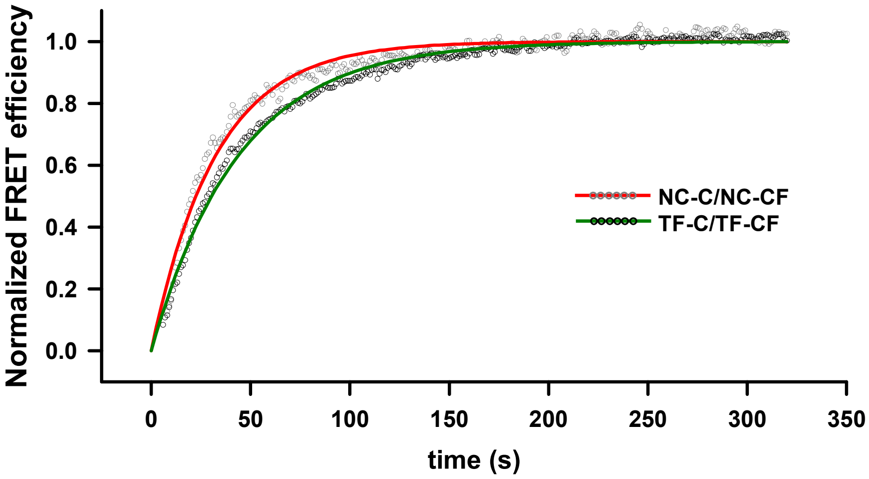

Figure 33: Intra-molecular compaction of NC during translation occurs with slightly faster kinetics that those of wild type TF.

Competition kinetics of intra-molecular compaction as measured by the TF-C/TF-CF pair (black circles, green line) and NC-C/NC-CF pair (grey circles, red line) during FL translation. NC relaxes to its closed conformation with a half time of ~23 s, slightly faster than TF (~31 s). Yet, intra-molecular compaction of NC during translation remained a slower process than ribosome-detachment, similar to the situation with wild type TF (see Figure 32).

IV.11 The ribosomal proteome: Identification of factors that might cooperate with TF or substitute for TF function in a *Δtig* background

IV.11.1 Introduction of a FLAG-His$_6$ epitope tag into genes encoding large ribosomal proteins and assessment of their assembly into intact ribosomes

In addition to TF, other chaperones are involved in aiding nascent proteins to reach their native state in bacteria. A functional overlap between TF and the DnaK/DnaJ/GrpE system has already been demonstrated. Other factors acting in very early stages, possibly at the exit from the ribosome, may still remain to be identified.

The classical way of isolating ribosomes and ribosome associated factors is based upon the considerable sedimentation coefficient of particles as large as ribosomes, which allows their enrichment by successive cycles of centrifugation through relatively dense media such as sucrose solutions. A drawback of this method is that it requires a pronounced dilution of the sample. Ribosome-associated factors that bind with relatively low affinities may therefore not co-migrate with ribosomes through density gradients. In an approach to develop means for ribosome purification other than sedimentation, a "pull-down" method was developed. An affinity tag was genetically introduced into selected ribosomal proteins to allow the isolation of ribosomes and their associated factors in high concentrations. Applied to different strain backgrounds, this technique could prove useful to identify factors that either act in concert with ribosome-associated proteins, such as TF, or compensate for the loss of function in their absence.

As an affinity tag, the FLAG-His$_6$-tag (FH-tag) was chosen. Due to its small size (less than 2.5 kDa including a flexible linker), it seems less likely to interfere with ribosome-structure or function than larger epitopes or proteins, such as streptavidin, MBP or GST. Based on the crystal structure of the large ribosomal subunit from *Deinococcus radiodurans* (pdb code 1nkw, (Harms *et al.* 2001); an X-ray structure of the *E. coli* ribosome was not available at that time), potential target proteins for the introduction of a FH-tag were selected according to their localization within the ribosomal subunit. Proteins localized at the interface of the large and the small ribosomal subunits were excluded from the group of potential candidates because in this region, the tag could interfere with proper subunit assembly, or be inaccessible. Additionally, proteins in close proximity to the ribosomal exit tunnel were not considered suitable for the introduction of an affinity tag, because the presence of extra sequences or binding of an antibody at this position might perturb proper binding of associated factors. Finally, only proteins containing a solvent exposed carboxyl-terminus were regarded as candidates in which the affinity tag would be accessible for recognition by its ligand. For proteins selected as potential targets on the basis of the *D. radiodurans* crystal structure, a high degree of conservation with the *E. coli* homolog was verified. The *E. coli* proteins that were found to match the above criteria were L4, L6, L13, L15, L17, L20 and L22.

Fusion of the FH-tag to the target proteins on the chromosomal level is desirable to ensure that not only a fraction, but all cellular ribosomes contain the FH-tagged protein. *E. coli* ribosomal proteins are encoded by single copy genes, most of which are clustered with other (ribosomal and non-ribosomal protein) genes, resulting in tightly packed operons. It is thus conceivable that introduction of DNA stretches as large as the tet^R gene (necessary to create such chromosomal insertions) could interfere with the function of the targeted operon. Therefore, from the ribosomal proteins that were chosen based on their tertiary and quaternary structure, potential candidates were further selected whose *rpl* genes exhibit favorable genetic features. *rplM* (encoding L13) is located at the very beginning of the L13-operon, *rplQ* (encoding L17) is the last ORF of the alpha-operon. *rplT* (encoding L20) is at the beginning of the L20-operon and is followed by a large stretch of non-coding sequence. *rplV* (encoding L22) is in the middle of the S10 operon without long stretches of non-coding sequences upstream or downstream of the ORF.

Before chromosomal integration of the affinity tag was attempted, expression plasmids were generated for the production of FH-tagged ribosomal proteins L13, L17, L20 and L22. A plasmid encoding L22 could not be generated, probably because altering the cellular levels of L22 disturbs regulatory processes or ribosome assembly, thus interfering with cell survival. Expression of FH-tagged L13 resulted in a marked decrease in growth rate of the *E. coli* BL21(DE3) host cells. However, when FH-tagged ribosomal proteins L17 or L20 were expressed, no abnormal growth was observed. Therefore, only L17FH and L20FH were further analyzed. The positions of the FH-tag within the 50S ribosomal subunit are shown in Figure 34.

FH-tagged ribosomal proteins L17FH and L20FH were expressed from plasmids pL17 and pL20, respectively. In a parallel experiment, *E. coli* enolase was expressed as an untagged, unrelated fully soluble control protein. Cells were lysed, and the cleared lysate (S30) was analyzed by SDS-PAGE and immuno-blotting to verify expression of the tagged ribosomal proteins (see Materials and Methods). When the membrane was probed with an

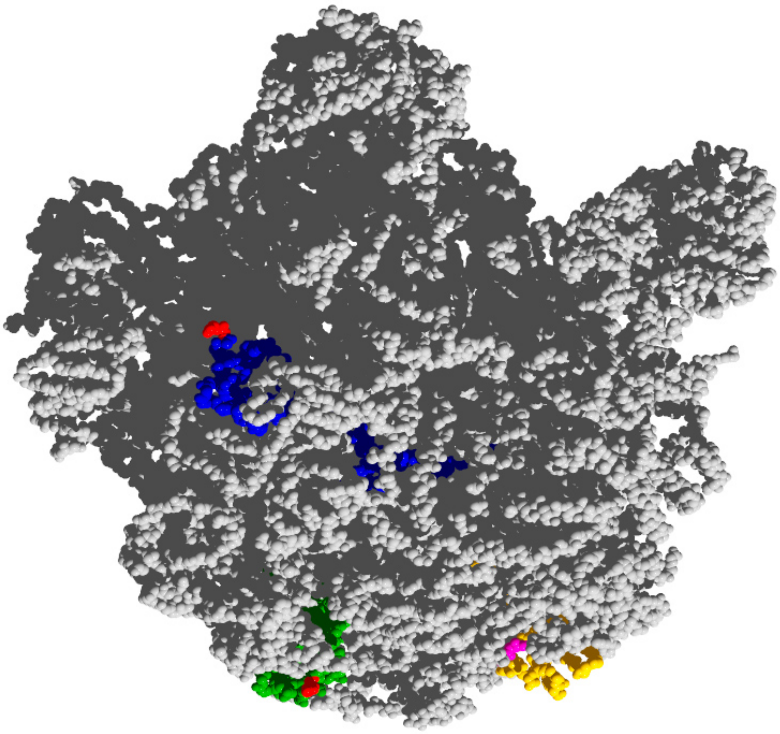

Figure 34: Ribosomal proteins L17 and L20 have solvent exposed carboxyl-termini at a considerable distance from the TF docking site on protein L23

Space-filling representation of the *E. coli* 50S ribosomal subunit. Ribosomal RNA and most proteins are shown in grey. Ribosomal proteins L17 and L20 are colored green and blue, respectively. The carboxyl-terminal residues of these proteins are colored red to indicate the position for placement of the FH-tag. Protein L23 is shown in orange, with the TF docking site (residues 12 – 14) in close proximity to the ribosomal exit tunnel shown in pink. The model was generated with DeepView/Swiss PBB-Viewer based on the coordinates *1vor* (Vila-Sanjurjo *et al.* 2004), and the image was rendered with POVray.

anti-FLAG antibody, no signal was detected in the control sample (Figure 35 a). The FLAG-tagged proteins L17FH and L20FH were detected specifically, with L17FH migrating more slowly than L20FH (Figure 35 a), reflecting the expected small difference in molecular weights (14.4 kDa for L17 *vs.* 13.6 kDa for L20). When the membrane was probed with serum against the ribosomal protein L23, signal was detected in all samples, demonstrating the presence of similar amounts of ribosomes in all three lysates (Figure 35 a).

To assess whether the FH-tagged proteins were incorporated into ribosomes, lysates were prepared from cells expressing plasmid-encoded L17FH, L20FH or enolase. The lysates were subjected to centrifugation through a sucrose cushion, and the ribosomal

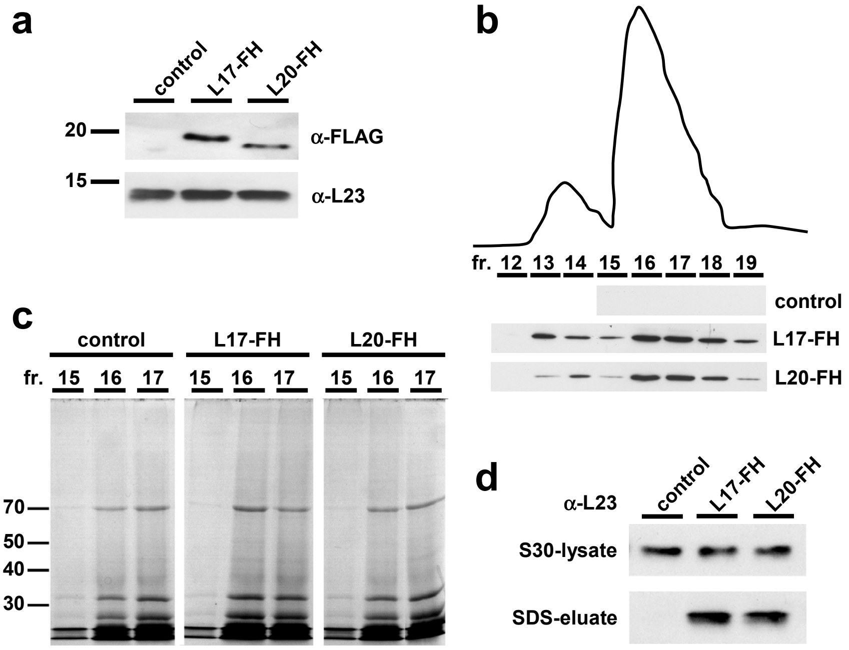

Figure 35: FH-tagged ribosomal proteins L17 and L20 are incorporated into 70S ribosomes.

a. Equivalent amounts of S30 lysates from *E. coli* cells expressing either a control non-ribosomal protein (control) or FH-tagged ribosomal proteins L17 (L17-FH) or L20 (L20-FH) from plasmids were analyzed by immuno-blotting using an anti-FLAG-antibody (upper panel) or anti-L23 anti-serum (lower panel). The FH-tagged proteins were detected specifically with the anti-FLAG antibody. As expected, due to its slightly larger molecular mass, L17-FH migrated slower than L20-FH. **b.** UV absorbance profile of ribosomes separated on a 10-40% sucrose gradient (upper panel). The first peak from the left corresponds to free subunits and the second one to 70S particles. Fraction numbers (fr.) are indicated; the sucrose concentration increases with the fraction number. Immuno-blot analysis of TCA-precipitated gradient fractions using an anti-FLAG antibody (lower panel). Higher signal detected in the immuno-blot correlated with the 50S and 70S peaks in the UV absorbance profile, demonstrating that the FH-tagged proteins L17-FH and L20-FH are incorporated into 50S and 70S ribosomal subunits. As expected, no signal was obtained when ribosomes were prepared from cells expressing a control protein. **c.** Proteins from the 70S peak fractions (fr., indicated) of the sucrose gradient were TCA-precipitated, separated by SDS-PAGE and visualized by Coomassie-blue staining, revealing the expected pattern. Small ribosomal proteins were not resolved by this gel. **d.** Immuno-blot analysis of S30 lysate and SDS-eluted material from anti-FLAG agarose beads from lysates with the indicated over-expressed proteins. L23 was detected in all lysate samples (upper panel). In the eluate fractions, L23 was only detected when L17-FH or L20-FH had been expressed, but not in the control sample, supporting the notion that the tagged proteins were incorporated into large ribosomal subunits.

pellet was recovered. Ribosomes were further separated on 10–40% sucrose gradients. The gradients were fractionated from the top, recording the absorbance at 260 nm. A typical trace of the absorbance is shown in Figure 35 b. Protein from the peak-fractions was precipitated with trichloroacetic acid (TCA), separated by SDS-PAGE and analyzed by Coomassie-blue staining or immuno-blotting and detection with a monoclonal anti-FLAG antibody. The protein pattern visible after Coomassie-blue staining is shown in Figure 35 c. Although the smaller ribosomal proteins were not resolved on this gel system and migrated in the front, the typical ribosomal pattern consisting of the proteins S1 (at ~70 kDa) and other large ribosomal proteins such as L2 and S2 was clearly recognizable. The protein pattern was the same regardless of whether a FH-tagged ribosomal protein or a control protein was expressed (Figure 35 c).

The immuno-blot analysis of the gradient fractions with an anti-FLAG antibody revealed that the FLAG-tagged proteins co-migrate with ribosomes, displaying peaks in fractions 13-14 (free subunits) and fractions 16-17 (70S particles) (Figure 35 b, lower panel). Thus, the plasmid-encoded FLAG-tagged ribosomal proteins L17 and L20 appeared to be incorporated into the large ribosomal subunit and did not disturb assembly of 70S particles. No signal was detected when a control protein was expressed (Figure 35 b).

To assess whether, in the context of the ribosome, the FLAG-tag is bound by an anti-FLAG-antibody, the S30 lysate was incubated with an agarose-based anti-FLAG affinity matrix. After washing away unbound material, the beads were extracted under denaturing conditions in the presence of SDS. The SDS-released material was subjected to SDS-PAGE and immuno-blotting using anti-L23 serum. Whereas L23 was present in all cleared lysates in similar amounts, it could be detected in the eluates from anti-FLAG beads if L17FH or L20FH, but not if enolase had been expressed (Figure 35 d). This demonstrates that ribosomes harboring a FLAG-tag at the carboxyl-terminus of either L17 or L20 can be pulled down specifically with an anti-FLAG affinity matrix.

To increase the specificity of the isolation method, FLAG peptide was used to elute material bound to the anti-FLAG affinity matrix. Cleared lysates from cells expressing L17FH, L20FH or enolase were incubated with anti-FLAG affinity matrix. After washing away unbound material, elution of bound material was achieved with 0.1 mg/ml FLAG peptide in three consecutive steps. After the specific elution, the beads were extracted with SDS-containing buffer to recover non-specifically absorbed material (as well as the antibody light-chains). Figure 36 shows the protein profile of the eluates

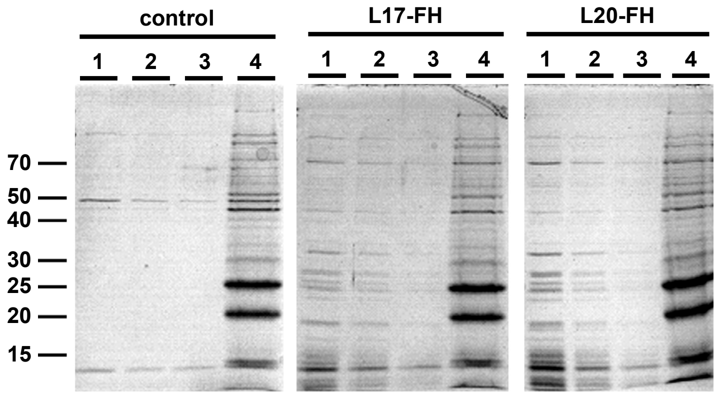

Figure 36: FLAG-tagged ribosomal proteins can be specifically eluted from anti-FLAG affinity matrix using FLAG peptide.

Cleared lysates from *E. coli* cells expressing either enolase as a control non-ribosomal protein or FH-tagged ribosomal proteins L17 or L20 were incubated with anti-FLAG affinity matrix, as indicated. Bound material was eluted in three consecutive steps with FLAG peptide (lanes 1-3). Whereas in the control-sample only small amounts of non-specifically bound enolase were eluted, the typical ribosomal protein pattern was observed in the eluates from cells overexpressing L17-FH or L20-FH. The majority of the ribosomes was recovered in the first two eluate fractions. Extraction of the affinity-matrix with SDS-containing buffer released non-specifically bound material as well as the antibody light-chains (lane 4).

after separation by SDS-PAGE, visualized with Coomassie-blue staining. Most of the bound material was recovered in the first two eluate fractions. The control sample showed some amount of enolase in the eluate fractions, probably due to the high level of overexpression. In both samples containing FH-tagged ribosomal proteins, the typical ribosomal protein pattern was clearly recognizable, indicating that ribosomes containing either L17FH or L20FH could be bound to the anti-FLAG affinity matrix and selectively eluted with FLAG peptide. Some non-specifically binding proteins that were not eluted with the FLAG peptide were visible in the SDS-extract (lane four in Figure 36).

Taken together, the above data show that the introduction of a FH-tag at the carboxyl-terminus of either L17 or L20 did not interfere with ribosome assembly. The FH-tagged proteins were incorporated into 70S ribosomal particles, and the tag mediated binding of 70S ribosomes to an anti-FLAG affinity matrix, which could be selectively eluted with FLAG peptide.

IV.11.2 The FH tag can be introduced into ribosomal protein L17 at the chromosomal level

In the experiments described in the previous section, FH-tagged proteins L17 and L20 were expressed from plasmids in cells containing a wild type chromosomal copy of the respective *rpl* gene. Under these conditions, only a fraction of the ribosomes would be expected to contain the FH-tagged ribosomal protein, since the chromosomally encoded non-tagged version was still expressed in these cells. In order to obtain a homogeneous population of tagged ribosomes, it was necessary to replace the single chromosomal wild type copy of the respective *rpl* gene with the FH-tagged version.

Insertion of DNA sequences into the chromosome of a host organism is usually achieved by homologous recombination. Some organisms, including the yeast *Saccharomyces cerevisiae*, naturally harbor recombination systems, which allow efficient recombination mediated by short homologous sequences. In contrast, *E. coli* and most other bacteria are not amenable to chromosomal replacements that utilize linear DNA, due to high cytosolic exonuclease activity and rather inefficient recombination systems.

In order to circumvent this problem, a method based on the phage λ Red recombinase system has been previously developed (Datsenko & Wanner 2000). Briefly, a helper plasmid was generated that allows the regulated expression of the Red products Gam, Bet and Exo from their corresponding genes γ, β and *exo*. Gam inhibits the host RecBCD exonuclease V, so that Bet and Exo can gain access to DNA ends and promote recombination. After recombination, the helper plasmid, which was designed to be a temperature sensitive replicon, is eliminated by growing the resulting strain at 37 °C. While it has been reported that 36 to 50 nucleotides (nt) of homologous stretches are sufficient for recombination in this system (Datsenko & Wanner 2000), no chromosomal integration of the FH-tag and the tetracycline-resistance gene could be achieved when linear DNA fragments were used that contained stretches of ~50 nt homologous to the host chromosome (data not shown).

To improve the recombination efficiency, the length of the homologous regions was increased. To this end, plasmids were constructed that contained the FH-tag and the resistance gene flanked by ~500 nt of homologous sequence. Using these plasmids as templates, linear DNA fragments were generated by PCR. The PCR product was thoroughly purified to remove any contaminating template DNA and transformed into *E. coli* MC4100 cells expressing the Red recombinase system from a helper plasmid.

No viable mutants could be obtained when the chromosomal tagging of L20 (*rplT*) was attempted, possibly due to disturbance of the L20 operon structure. In contrast, chromosomal integration of the FH-tag with the tetracycline-resistance gene was achieved for the ribosomal protein L17, resulting in an *E. coli* strain with the genotype MC4100 *rplQ::rplQ-FH-tet*^{R} (designated as strain CK1, see Materials and Methods). After two rounds of non-selective colony purification at 37 °C, the strain CK1 exhibited tetracycline resistance and sensitivity towards ampicillin, indicating the integration of the tetracycline-resistance gene into the host chromosome and the loss of the helper plasmid encoding the Red recombinase system.

In order to provide a means of analyzing ribosome-associated factors in different strain backgrounds, it was attempted to transduce the *rplQ-FH-tet*^{R} allele into *E. coli* MC4100 strains devoid of TF (MC4100 *Δtig*), the DnaKJ-system (MC4100 *ΔdnaKdnaJ*) or both (MC4100 *ΔtigΔdnaKdnaJ*) (Genevaux *et al.* 2004) by means of P1 phage transduction (Miller 1992) (see Materials and Methods). No transductants were obtained with strains lacking DnaKJ alone or both DnaKJ and TF. Since it was observed that DnaKJ-deficient strains failed to grow on tetracycline selective medium when transformed with various plasmids that mediate tetracycline resistance in WT or *Δtig* cells (data not shown), it appears likely that the DnaKJ-system is required for proper function of the tetracycline resistance protein. The *rplQ-FH-tet*^{R} allele was, however, successfully transduced into MC4100 *Δtig* cells, resulting in the strain MC4100 *rplQ::rplQ-FH-tet*^{R} *Δtig* (designated as strain CK3).

Next, it was analyzed whether ribosomes from the CK1 and the CK3 strains could be isolated selectively with anti-FLAG affinity matrix. Lysates from CK1 and CK3 cells were prepared in a similar way as described above, except that the cells did not harbor any plasmid and no inducer for protein expression was necessary. Using these lysates, a pull-down with anti-FLAG affinity matrix was performed as described above. Bound material was eluted with 0.5 mg/ml FLAG peptide. The eluate was subjected to SDS-PAGE and proteins were visualized with Coomassie-blue staining (Figure 37). In the control sample prepared from *E. coli* MC4100 cells, lacking any tagged protein, a faint background of non-specific binding proteins was visible. However, in the CK1 as well as in the CK3 samples, the pattern of ribosomal proteins was clearly distinguishable. A protein band migrating at ~60 kDa (arrowhead in Figure 37), that is present in the CK1, but not in the CK3 lysate, most probably represents TF, showing that TF is co-purifying with ribosomes from cells not deleted in this gene.

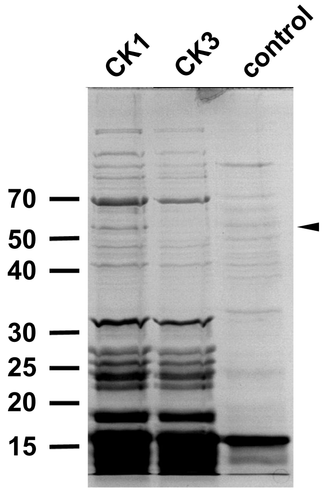

Figure 37: Ribosomes from different strain backgrounds can be isolated by the pull-down procedure developed in this study.

Lysates prepared from *E. coli* strains CK1, CK3 or MC4100 (control) were incubated with an anti-FLAG affinity matrix. Bound material was eluted with FLAG peptide. The eluates from samples CK1 and CK3 showed the typical ribosomal protein pattern in the Coomassie-blue stained SDS-PAGE gel (lanes CK1 and CK3). Weak background was visible in the control sample, where no FLAG-tag was introduced into the ribosomes. The position of the TF band is indicated by the arrowhead, and is clearly absent in the sample corresponding to the strain deleted for this chaperone (CK3).

The above results indicate that L17 is a suitable target for the introduction of an affinity tag into the ribosome. At this position, the tag can be introduced at the chromosomal level without compromising cellular viability. Furthermore, the presence of TF in the eluted material demonstrates that this system is suitable for the co-purification of ribosome-associated factors.

IV.11.3 Additional ribosome-associated proteins can be pulled down under conditions that stabilize ribosome-nascent chain complexes

Many currently utilized antibiotics target the bacterial ribosome. The mechanism by which growth arrest or cell death is mediated, however, differs greatly for these various agents. Two examples of antibiotics that act on the ribosome are chloramphenicol and puromycin, which target the ribosomal peptidyl transferase center. Puromycin mimics the amino-acylated end of the aa-tRNA and participates in peptide bond formation. Its non-hydrolyzable amide bond cannot be cleaved, and the resulting peptidyl-puromycin chain dissociates from the ribosome. Chloramphenicol, on the other hand, acts by occupying the position of the amino acid attached to the A-site tRNA and prevents peptide bond formation. As a result, elongation is arrested and the peptidyl-tRNA is trapped on the ribosome. Thus, chloramphenicol stabilizes ribosome-nascent chain complexes, whereas puromycin leads to (premature) release of the nascent chain.

In addition to the well known ribosome-based function of TF, ribosome-nascent chain complexes may recruit factors that interact with the nascent chain. To explore this possibility, lysates were prepared under conditions that either stabilize or de-stabilize ribosome-nascent chain complexes. Cultures were grown of strains CK1, CK3 and, as a control, MC4100 cells. In mid-log phase, the culture was split in two: One half was treated with chloramphenicol and rapidly chilled on ice, resulting in stabilization of ribosome nascent chain complexes. The other half was treated with puromycin and incubated at 15 °C for an additional 15 min. At this temperature, translation elongation is favored over initiation, which, in combination with puromycin, results in the detachment of nascent chains from translating ribosomes. Chloramphenicol or puromycin were maintained in all buffers in subsequent steps.

Lysates were prepared from all samples and incubated with anti-FLAG affinity matrix. Bound material was eluted with FLAG peptide, and ribosomal RNA was digested by the addition of RNaseA. Eluates were analyzed by SDS-PAGE and Coomassie-blue staining. In the control sample, faint bands of non-specifically bound proteins are visible, without major differences in the band patterns between the chloramphenicol- and the puromycin-treated samples (Figure 38). When lysates of strains CK1 or CK3 were subjected to an anti-FLAG pull-down, the typical ribosomal protein pattern was visible (Figure 38). In the samples prepared from strain CK1 (wild-type for the TF gene), a band migrating at ~60 kDa is visible (arrowhead in Figure 38) that is absent in the samples

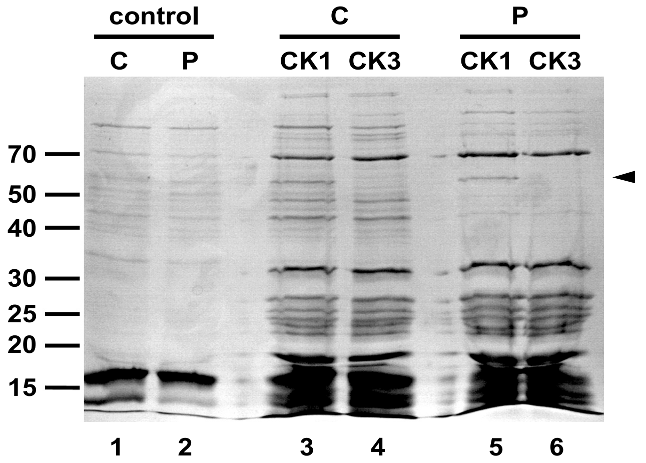

Figure 38: Conditions that stabilize ribosome-nascent chain complexes enhance co-purification of additional ribosome-associated proteins.

Lysates prepared from *E. coli* strains MC4100 (control, lanes 1 and 2), CK1 (lanes 3 and 5) or CK3 (lanes 4 and 6) were subjected to a pull-down using an anti-FLAG affinity matrix, and bound material was eluted with FLAG peptide. Samples in lanes 1, 3 and 4 have been treated with chloramphenicol (C), and the others with puromycin (P). The typical ribosomal protein pattern was detected in all samples from strains CK1 and CK2, but not in the control samples. The arrowhead indicates the position of the TF band. In the chloramphenicol-treated samples, additional protein bands were visible when compared to the puromycin-treated samples, indicating that additional proteins were bound by the stabilized ribosome-nascent chain complex.

derived from strain CK3 (deleted of the *tig* gene), presumably corresponding to TF. In the samples prepared under conditions that favor stabilization of ribosome nascent chain complexes, additional protein bands were present when compared to the puromycin-treated samples. These bands could represent proteins that interact with the nascent chain or whose interaction with the ribosome is enhanced in the presence of nascent chains. Additional bands present in chloramphenicol-stabilized pull-down samples from the strain deleted of TF could represent proteins that are capable of interacting with this the nascent chain in the absence of this chaperone, consistent with the previous observation that GroEL could bind co-translationally to nascent chains in the absence of TF (Ying *et al.* 2005). These bands were not analyzed further in the course of this study.

In summary, the above results show that *E. coli* ribosomes can be successfully purified in a pull-down procedure using a matrix-conjugated anti-FLAG antibody, if an FH-tag is genetically introduced into the ribosomal protein L17. As judged by the growth rate, the tag does not seem to interfere with ribosomal function, even if all of the L17 that is produced contains the tag. In a pilot experiment, it was shown that TF is co-isolated with ribosomes in an pull-down, indicating that ribosome-associated factors can be co-purified using this method. Furthermore, conditions that stabilize ribosome-nascent chain complexes give rise to additional proteins that can be isolated together with ribosomes, some of which may have a function in chaperoning the nascent chain.

V DISCUSSION

V.1 Structural rearrangements within TF upon ribosome binding

Efficient folding of newly synthesized proteins is essential for cellular survival. A number of studies have analyzed protein folding *in vivo*, and have shown that TF, together with other chaperones, plays an important role in this process (Agashe *et al.* 2004; Genevaux *et al.* 2004; Kramer *et al.* 2002; Teter *et al.* 1999; Ullers *et al.* 2004; Vorderwulbecke *et al.* 2004). However, a detailed understanding of the underlying mechanisms by which molecular chaperones operate necessitates biochemical studies *in vitro*. TF binds to the ribosome in the vicinity of the polypeptide exit tunnel (Blaha *et al.* 2003; Kramer *et al.* 2002), where it interacts with nascent polypeptide chains and contributes towards their correct folding. Binding to the ribosome is a pre-requisite for TF to efficiently function in preventing misfolding and ensuring cellular survival (Kramer *et al.* 2002). Thus, characterization of the TF-ribosome interaction in the context of translation is of particular interest.

At the structural level, several crystal structures of the amino-terminal ribosome binding domain of TF (TF-BD) in complex with 50S ribosomal subunits have been solved (Baram *et al.* 2005; Ferbitz *et al.* 2004; Schlunzen *et al.* 2005). Co-crystallization of full-length TF with the 50S ribosomal subunit has not been achieved to date. In the earliest of the available structures, describing a heterologous complex between *E. coli* TF-BD with the 50S ribosomal subunit from the archeon *Haloarcula marismortui* (Ferbitz *et al.* 2004), no major conformational rearrangements within TF-BD were observed. However, only few residues of TF-BD, located in the direct vicinity of the ribosome, could be assigned unambiguously to the experimentally determined electron density. In the two crystal structures of TF-BD in a homologous complex with their bacterial 50S ribosomal subunit counterparts (Baram *et al.* 2005; Schlunzen *et al.* 2005), nearly the entire TF-BD was resolved, revealing the mode of interaction of this domain with the ribosome in atomic detail. Clear structural rearrangements even within the small TF-BD were already observed in these structures. The most prominent difference between free and ribosome-bound TF-BD is a re-orientation of helix $\alpha2$. The rearrangements lead to the formation of additional potential substrate binding sites in TF-BD and enable TF to contact the flexible loop of the ribosomal protein L24, thereby restricting the space available in the TF hydrophobic crevice (Schlunzen *et al.* 2005).

In the present study, the characterization of TF structural rearrangements was carried out with the full-length molecule, utilizing intra-molecular fluorescence resonance energy transfer. The high absorbance of the ribosome in the near UV-region impedes the utilization of intrinsic fluorescent probes within TF. Therefore, fluorescent probes that can be excited outside the absorbance bands of the ribosome were introduced at specific sites within the TF molecule. Positions for the introduction of fluorescent probes were selected based on the crystal structure of full-length TF (Ferbitz *et al.* 2004). In addition to position 14 in the amino-terminal domain, residues 150 in the PPIase domain as well as 326 and 376 in tips 1 and 2, respectively, were selected. FRET measurements revealed that the distances between positions 14 and 150, and 14 and 326 were considerably shorter than the corresponding C_α distances in the TF crystal structure. This suggests that, in solution, TF adopts a conformation that is more compact than the one observed in the crystal structure, particularly along the long axis of the molecule. Perhaps, under the conditions used for crystallization, a conformation of TF is favored that is not the predominant one in solution. It is conceivable that inter-molecular contacts (see Figure S3 in (Ferbitz *et al.* 2004)) or steric constraints in the crystal, *e.g.* exerted by the structurally independent PPIase domain, stabilize a particular conformation. In the present study, a mutant of TF deleted of the PPIase domain, designated NC, was constructed and functionally characterized. It was found that NC behaves similar to TF in a number of ways, indicating its functionality. Crystallization of the NC version of TF was achieved under conditions similar to those applied to crystallize full-length TF (Ferbitz *et al.* 2004). When subjected to X-ray irradiation, the crystals produced a diffraction pattern corresponding to a resolution of ~4 Å (data not shown), and further optimization of the crystallization conditions is currently underway. The NC crystal structure might provide further insights into possible conformations of TF.

TF appears to be structurally flexible based on the variability of the two molecules in the crystallographic asymmetric unit of the full-length TF structure (Ferbitz *et al.* 2004). Additionally, structural flexibility was observed in the crystal structure of a functionally uncharacterized protein from *Mycoplasma pneumoniae* (Schulze-Gahmen *et al.* 2005), which was found to be a structural homolog of TF. The structure of the ribosome-bound amino-terminal domain revealed conformational rearrangements that lead to the exposure of hydrophobic surfaces (Schlunzen *et al.* 2005). In order to probe the structure of full-length TF upon association with ribosomes, distances derived from FRET measurements in the absence and presence of ribosomes were compared. In the presence of ribosomes, a marked decrease in FRET efficiency was observed, consistent with an increased distance between the fluorescent probes within the TF molecule. Thus, TF appears to undergo a conformational change upon binding to the ribosome, resulting in a more extended conformation of the ribosome-bound species when compared to free or dimeric TF. Binding to the ribosome may result in the exposure of surfaces on the TF molecule which are otherwise inaccessible and might contribute to efficient substrate binding.

It has been reported previously that TF forms homo-dimers in solution (Maier, R. *et al.* 2003; Patzelt *et al.* 2002). Using the endogenous single tryptophan at position 151 in *E. coli* TF as an environmentally sensitive fluorescent probe, it was demonstrated in this study that TF forms homo-dimers which dissociate with a K_D of ~0.9 µM. At a cytosolic TF concentration of 40 to 50 µM, compared with ~30 µM ribosomes, under standard growth conditions (Bremer & Dennis 1996; Lill *et al.* 1988), a considerable fraction of TF would be expected to exist as a dimer. Thus, dimer formation *in vivo* may have important regulatory implications. The TF dimer was further characterized in this study by inter-molecular FRET-measurements, attaching either a donor or an acceptor to specific positions within the protomers. The resulting inter-molecular distances were interpreted using the model-building software *FRETsg* (Schröder & Grubmüller 2003). The resulting model revealed that in the TF dimer, the two protomers are oriented in a nearly perpendicular fashion, with the tips facing towards each other. Thus, the putative substrate binding site, which may be constituted by the hydrophobic crevice surrounded by the tips, would be inaccessible in the dimer, preventing inappropriate binding of partially unfolded proteins which otherwise would potentially inhibit post-translational folding in the cytosol.

Based on neutron scattering experiments, it has been reported that the TF homo-dimer is capable of residing on the ribosome (Blaha *et al.* 2003), whereas cross-linking and co-sedimentation data suggested that the monomer is the ribosome-bound species (Patzelt *et al.* 2002). Loss of inter-molecular energy transfer was observed when ribosomes were added to dimeric TF, suggesting that the ribosome-bound TF species is a monomer. The dimer association/dissociation kinetics were found to be fast and not measurable during manual mixing (V.R. Agashe and C.M. Kaiser, unpublished results), indicating that, rather than actively promoting dimer dissociation, the ribosome stabilizes the monomeric form of TF.

The conformational rearrangements within TF observed in the fluorescence measurements suggest the following mechanism of TF regulation: Free TF forms homodimers, in which the main substrate binding domain, *i.e.* the hydrophobic crevice, is occluded. TF monomers are sequestered from the monomer-dimer equilibrium by binding to the ribosome, and the monomeric species is stabilized. Concomitant with ribosome-binding, a conformational change within TF is induced, resulting in a more open conformation, possibly re-aligning its sub-domains and exposing further the substrate binding crevice to the nascent chain as it emerges from the ribosomal exit tunnel.

V.2 Kinetic characterization of the TF-ribosome interaction

It has previously been reported that the environmentally sensitive BADAN fluorophore attached to position 14 of *E. coli* TF exhibits decreased fluorescence upon binding to the ribosome (Maier, R. *et al.* 2003). Utilizing this tool, association and dissociation of BADAN-labeled TF (TF-B) with and from the ribosome have been investigated in real time by fluorescence measurements. In a similar way, the kinetics of the change in intra-molecular FRET efficiency upon interaction with ribosomes were measured. The combination of these methods allowed monitoring of ribosome-binding as well as TF structural changes in real time. When labeled TF was displaced from TF-ribosome complexes by the addition of excess unlabeled TF, it was found that both ribosome detachment and TF intra-molecular compaction occur concomitantly with virtually the same kinetics. Both processes were found to take place with a half time of ~10 s. Thus, as soon as TF is detached from the ribosome, it undergoes a molecular compaction from the extended, ribosome bound conformation to the more compact state observed in solution.

Additionally, steady state fluorescence anisotropy measurements with CPM-labeled TF (TF-C) were successfully used in this study to monitor TF-ribosome interactions. An increase in steady state fluorescence anisotropy of TF-C was observed in the presence of ribosomes. Upon addition of excess unlabeled TF, the anisotropy decreased to a value observed for the TF dimer with kinetics very similar to those described above, thus confirming the kinetic behavior observed with TF-B.

V.3 TF is recruited to translating ribosomes

Previous characterizations of TF-ribosome and TF-substrate interactions were conducted with vacant ribosomes (Maier, R. *et al.* 2003) and free substrate, respectively (Huang *et al.* 2000; Liu *et al.* 2005; Maier, R. *et al.* 2001; Patzelt *et al.* 2001; Suno *et al.* 2004) and thus the mechanisms underlying TF function in its biologically-relevant context of active translation have remained elusive. Free dimeric TF may exhibit certain chaperone properties as measured by prevention of aggregation or refolding of certain denatured model proteins (Kramer *et al.* 2004; Liu *et al.* 2005; Liu & Zhou 2004; Maier, R. *et al.* 2001). However, its role *in vivo*, at least for multi-domain proteins, has been shown to involve a postponement in the acquisition of nascent chain structure relative to translation (Agashe *et al.* 2004). Therefore, its function in chaperoning virtually all nascent chains emerging from the ribosome probably requires the substrate to be presented in the context of the translating ribosome. Characterization of TF ribosome-binding and intra-molecular rearrangements during translation was attempted in an S30-based transcription/translation system with the fluorescence-based tools described above. However, due to the crude composition of the system, high background and poor reproducibility impaired the measurements.

Recently, a protein synthesis system has become available that is reconstituted from purified components (Shimizu *et al.* 2001). All proteins needed for translation, such as initiation, elongation and release factors, as well as the 20 different aminoacyl-tRNA synthetases, were purified individually as His$_6$-tagged recombinant proteins. In addition, the system contains purified tRNAs, amino acids, ribosomes and an energy regenerating system. In contrast to protein synthesis systems based on crude S30 extracts from *E. coli*, this system allows protein synthesis in a well defined environment. Originally developed for rapid and convenient protein production and isolation *in vitro*, this system was applied in the present study to accomplish a real-time analysis of processes occurring during translation.

When luciferase was translated in the reconstituted system, a pronounced increase of TF ribosome-recruitment was observed, as monitored by a decrease in TF-B fluorescence and an increase in steady state fluorescence anisotropy of TF-C. Thus, the affinity of TF is higher for ribosome-nascent chain complexes than for vacant ribosomes. A 30-fold decrease in the K_D of the TF-ribosome complex occurred upon translation of FL. This suggests a regulatory principle for TF function: When protein production in the cell is taking place at a high rate, *e.g.* in *E. coli* cells during mid-log phase, increased amounts of monomeric TF become recruited to the ribosome-nascent chain complexes. Monomerization and conformational opening result in activation of TF. Activated TF is then able to efficiently bind to the nascent chain substrate, protecting it from the entry into non-productive folding pathways and aggregation. If less ribosomes are engaged in translation, *e.g.* during stationary phase, TF is shifted from a ribosome-bound to a free cytosolic form, which readily dimerizes. Dimerization leads to inactivation of TF in terms of substrate binding, providing a cytosolic pool that can be activated when protein synthesis is increased. The regulation of cytosolic TF levels according to the growth rate (Griffiths *et al.* 1995; Guthrie & Wickner 1990; Lill *et al.* 1988; Pedersen *et al.* 1978) is consistent with this model.

A decrease in K_D is the result of changes in the rate constants: A decrease in the off-rate, an increase in the on-rate, or both. The “cradle” model for TF function suggests that TF crouches over the ribosomal exit tunnel, providing a protected environment for domain-wise co-translational folding (Ferbitz *et al.* 2004; Maier, T. *et al.* 2005). This model, based solely on the modeling of full-length TF onto the *H. marismortui* 50S ribosomal subunit, would imply that TF stays associated with the translating ribosome long enough to allow synthesis and co-translational folding of at least an entire protein domain. Based on this model, a decreased off-rate would be expected to account for the increased affinity of TF for the ribosome that was observed upon translation. This aspect was investigated in competition experiments where ribosome-bound labeled TF was displaced from translating ribosomes by the addition of excess unlabeled TF. No difference in the displacement kinetics was observed in the different scenarios with and without translation. Instead, the dynamics of TF-ribosome interaction were found to be unaltered in the presence of translation, indicating that the time that TF resides on the ribosome is not affected by the presence of a nascent chain substrate.

An increased recruitment of TF to translating ribosomes was also reflected by a decrease in the efficiency of intra-molecular FRET. The FRET efficiency measured is an average of the FRET efficiencies for the bound and the free form of TF. Thus, an increase in the fraction of bound TF leads to decreased average FRET efficiency. Upon addition of excess unlabeled wild type TF, a return of the FRET efficiency to the value observed in the absence of ribosomes occurred. Strikingly, the kinetics of ribosome detachment and intra-molecular compaction no longer occurred concomitantly when ribosomes were actively engaged in translation. Instead, the change in intra-molecular FRET efficiency was delayed with respect to ribosome release, with a ~3-fold difference in the $t_{1/2}$ values. This argues that, even after TF has left the translating ribosome, it is kept in its open conformation, presumably by an interaction with the nascent chain. Thus, TF appears to leave the ribosome while still interacting with the elongating polypeptide chain.

This model was supported by data from steady state fluorescence anisotropy measurements, where the change in signal that was observed upon ribosome displacement happened with the similar kinetics as ribosome-release in the case of vacant ribosomes, but is markedly slower when ribosomes are translating. This also indicates that after ribosome dissociation, TF remains associated with a very large molecular weight component, presumably the ribosome-tethered nascent chain.

Importantly, in none of the competition experiments was the TF FRK/AAA mutant (deficient in ribosome binding) found to act as an efficient competitor. This demonstrates that binding to the ribosome is a pre-requisite for efficient substrate binding, consistent with the hypothesis that ribosome binding leads to TF activation. Only then does TF efficiently bind its substrate and remains associated even after departing from the ribosome. Thus, ribosome-binding serves several purposes: Besides creating a high local TF concentration at the ribosomal exit tunnel in close proximity to its substrate, it stabilizes the monomer and induces a conformational change, thereby activating TF.

The delay in intra-molecular compaction over ribosome-dissociation was also observed when the nascent chain was released from the ribosome by disruption of the ribosome-nascent chain complex with EDTA. This further strengthens the notion that beyond ribosome departure of both TF and the nascent chain, similar to a post-translational scenario, TF remains engaged with its substrate. After disruption of the complex, TF is unable to rebind to the substrate regardless of whether it has folded or not. Ribosome-binding is necessary to activate TF and restricts its chaperone activity to ribosome-tethered nascent chains. Other chaperone systems acting downstream of TF may then aid the further folding of the released polypeptide.

V.4 TF regulation by the nascent chain

In vivo experiments have demonstrated that TF and the DnaK system improve the folding yield of certain multi-domain proteins by promoting a post-translational folding mechanism, resulting in a substantial deceleration of folding relative to translation (Agashe *et al.* 2004). The affinity of DnaK for unfolded proteins is regulated by binding and hydrolysis of ATP, resulting in a nucleotide-dependent substrate binding and release. This nucleotide-dependent cycling is regulated by the co-factors DnaJ and GrpE. Although aiding protein folding by a fundamentally different mechanism, GroEL, the Hsp60 chaperonin of *E. coli*, also exhibits a similar ATP-regulated substrate binding and release regulated by its co-factor GroES. In contrast, TF does not contain any nucleotide binding site, nor are any protein co-factors known that co-operate with TF. This poses the question of how TF is regulated.

As discussed in the previous section, efficient binding of substrate requires TF-activation that occurs upon binding of the chaperone to the ribosome in the vicinity of the ribosomal exit tunnel. For efficient folding of newly synthesized proteins, the extent of TF-substrate interaction should depend on the substrate properties: Newly synthesized proteins which cannot readily collapse into a molten globule state and thus expose hydrophobic segments would be expected to interact with TF long enough to prevent aggregation. Yet, TF interaction with proteins which are able to fold rapidly should be limited so that these proteins are not impaired in folding for unnecessarily long periods of time. Absence of any known ATP regulation or regulatory co-factors for TF make it conceivable that certain regulatory features are present on the nascent chain substrates themselves.

At the very early stages in protein maturation, at which TF acts, the nascent chain can be expected to not have acquired significant amounts of structure, but rather be present in an extended form. Thus, primary structure analysis was performed to uncover nascent chain features that dictate TF-substrate interactions. When analyzing the mean hydrophobicity over a window of 15 amino acid residues along the sequence of the nascent chain, motifs of high hydrophobicity were revealed in substrates that cause a delayed intra-molecular compaction of TF. Furthermore, the spread of hydrophobic motifs was found to be tightly correlated with the magnitude of the delay. This correlation was gradually lost when the window size used to calculate the mean hydrophobicity was decreased or increased beyond the 15 residue window. These findings suggest that the extent to which hydrophobic motifs are present in the primary structure of the substrates modulates the affinity of TF for the substrate. The window size for which the optimum correlation was found implies that the TF-binding site on the substrate is composed of a stretch of ~15 residues with high mean hydrophobicity. Significantly, the length of the long axis of the proposed substrate binding crevice of *E. coli* TF in the crystal structure is ~65 Å, which is sufficient to accommodate a peptide of 18 residues in a fully extended conformation (Ferbitz *et al.* 2004).

Most polypeptide chains contain hydrophobic segments which are buried in the hydrophobic core of the native protein structure. During translation, hydrophobic collapse cannot take place unless at least a complete domain has been synthesized. Therefore, virtually all polypeptide chains would expose hydrophobic segments in the course of translation. Indeed, for all model proteins tested, a substantially increased ribosome recruitment of TF was observed upon translation. Only α-synuclein, belonging to the class of natively unfolded proteins (Uversky *et al.* 2000), did not lead to TF-recruitment (V. R. Agashe, unpublished results).

Using the small titin I27 domain as a model substrate that is capable of readily unfolding and refolding (Marszalek *et al.* 1999), the extent of TF recruitment during translation was correlated to the folding properties of the nascent chain substrate. Stalled translation of successively longer amino-terminal fragments of I27 revealed that increased TF recruitment was observed when hydrophobic segments of the nascent chain emerged from the ribosomal exit tunnel and became exposed to the exterior of the ribosome. No significant recruitment was observed when fragments were translated that either resided completely within the exit-tunnel or exposed only a hydrophilic segment outside the tunnel. Co-translational folding of the stalled I27-domain resulted in loss of TF recruitment, consistent with the burial of hydrophobic segments in the interior of the I27 domain. These data also demonstrate that translation *per se* is insufficient to generate a high affinity binding site for TF on the ribosome, *e.g.* by structural rearrangements in the 50S subunit. Rather, the enhanced affinity of TF for ribosome-nascent chain complexes requires both the ribosomal TF binding site on the large subunit as well as a binding motif on the ribosome-tethered nascent chain.

V.5 The TF PPIase domain contributes towards substrate binding, but is not essential for TF function

The role of the central TF PPIase domain in its chaperone activity for nascent chains has so far not been fully understood. The chaperone function of TF is not limited to prolyl-isomerization, and the interaction of TF with nascent chain substrates does not correlate with their proline content (Patzelt *et al.* 2001). Also, eliminating the PPIase activity by point mutations or deletion of the entire domain did not result in reduced TF activity *in vivo* (Genevaux *et al.* 2004; Kramer *et al.* 2004). Yet, all known TF homologs analyzed contain this domain (C.M. Kaiser and J.M. Barral, unpublished). However, the PPIase domain would be expected to interact with non-native proteins to catalyze prolyl-*cis-trans* isomerization and has been shown to bind short hydrophobic peptides (Kramer *et al.* 2004; Patzelt *et al.* 2001). Therefore, it seemed conceivable that the TF PPIase domain contributed to substrate binding.

To analyze the contributions of the PPIase domain during TF function, a deletion mutant (NC) was designed based on the crystal structure of *E. coli* TF (Ferbitz *et al.* 2004) and functionally compared to the full-length protein. Intra-molecular FRET measurements in the absence and presence of ribosomes indicated that the compact shape observed in solution and the conformational change upon ribosome binding are essentially the same for TF and NC. The deletion mutant also exhibited wild type-like properties in its ability to increase the specific activity of luciferase translated in the reconstituted translation system.

As a competitor, NC was indistinguishable from TF in displacement experiments monitoring both ribosome release and intra-molecular compaction. This was observed with vacant as well as with translating ribosomes. Also, the kinetics of ribosome dissociation and intra-molecular compaction of labeled NC in the absence of translation were essentially the same as for TF. Thus, interaction with the ribosome and the initial binding to the substrate are not impaired in the absence of the PPIase domain. In contrast, the recruitment of BADAN-labeled NC to translating ribosomes was diminished and intra-molecular compaction occurred faster than for TF. Yet, the delay of intra-molecular compaction over ribosome dissociation observed in the presence of translation was preserved in the NC mutant. These findings are consistent with the PPIase domain constituting an additional substrate binding site, which is not essential for substrate binding, but further stabilizes the TF-substrate interaction.

V.6 The dynamic cycle of TF function

Taken together, the data presented in the present study indicate that TF operates through a functional cycle in the course of chaperoning nascent chains (Figure 39): Before binding to the (translating) ribosome, TF is present in an equilibrium between the monomeric and the dimeric form, with rapid association and dissociation of the protomers (1). Monomeric TF is withdrawn from the equilibrium by binding to the ribosome (2) and rapidly replenished from the pool of dimers. Ribosome binding results in stabilization of the monomer in the vicinity of the exit-tunnel and induction of a conformational change in TF, which together activate TF for binding to the nascent chain. This activation is enhanced by increased binding to ribosome-nascent chain complexes, presumably through an enhanced on-rate, when compared to the binding to vacant ribosomes. This is reflected

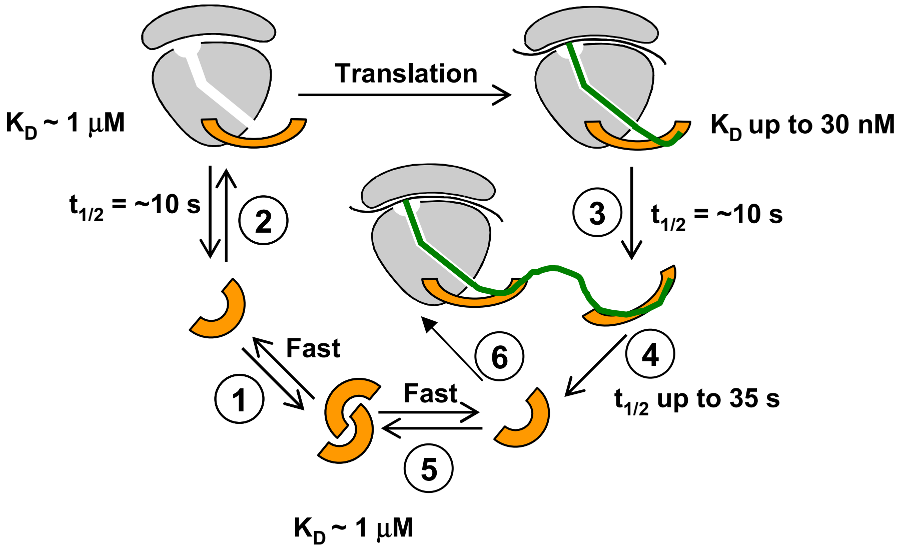

Figure 39: Model of TF function.

TF is represented by an orange shape in a compact and an extended conformation, representing free and ribosome-bound TF, respectively. The ribosome is shown in grey, a nascent chain in green. Monomeric and dimeric TF co-exist in a rapid equilibrium **(1)**. Ribosome binding of the monomer results in TF conformational expansion, activating the TF chaperone function **(2)**. Upon translation, TF interacts simultaneously with the ribosome and the nascent chain, leading to an increased affinity for the ribosome nascent chain complex. Interaction with the substrate preserves the expanded conformation of TF for varying periods of time after ribosome departure **(3)**, depending on the substrate properties. During this period, a second TF molecule may be loaded onto the elongating polypeptide **(4)**. TF dissociates from the nascent chain either co- or post-translationally, undergoes conformational compaction and enters the monomer-dimer equilibrium **(5)**, from which it may be recruited to the translating ribosome again for another cycle of nascent chain chaperoning **(6)**.

by a ~30-fold decrease in K_D. Activated TF then binds to the polypeptide chain emerging from the ribosomal exit tunnel, possibly keeping it in an extended conformation competent for subsequent folding. Hydrophobic segments of the nascent protein, which could promote aggregation, are shielded by the interaction with TF. While staying associated with the nascent chain, TF then dissociates from the ribosome (3). Importantly, the kinetics of this dissociation reaction are similar in the absence and presence of translation, indicating that ribosome dissociation is an intrinsic feature of the system unaffected by the presence of substrate (2 and 3). In contrast, the dissociation from the substrate is decelerated in some cases (4), allowing the ribosome-mediated loading of a second TF-molecule onto the nascent chain (6). Thus two, or possibly more, TF molecules can interact simultaneously with the same nascent chains, consistent with previous evidence (Agashe *et al.* 2004). Finally, TF dissociates from its substrate and enters the monomer-dimer equilibrium (5), which serves to keep a pool of TF that has low affinity for substrate. The substrate is only then allowed to proceed in its folding path, which may be aided by additional chaperones, thus explaining the previously observed TF-mediated delay in folding relative to translation (Agashe *et al.* 2004).

V.7 Factors that work in concert with TF or compensate for its loss of function

The folding of newly synthesized proteins is a crucial process for cellular survival. In the crowded environment of the cytosol, it depends on the aid of molecular chaperones, of which TF is the first to contact the nascent chain in bacteria. However, deletion of the *tig* gene encoding TF does not have major consequences on growth rates or cellular survival under laboratory conditions, suggesting that other factors have overlapping functions. This has already been demonstrated for the DnaK system (Deuerling *et al.* 1999; Teter *et al.* 1999). While the individual deletions of the genes encoding TF and the DnaKJ operon do not result in temperature sensitivity at temperatures up to 37 °C, the combined deletion is lethal at temperatures above 30 °C, demonstrating the functional overlap between the two systems. Other factors may also be involved in guiding newly synthesized cytosolic proteins to their native state, as has been suggested for SecB (Ullers *et al.* 2004). These could potentially be responsible for conferring viability in the absence of TF and the DnaKJ system at temperatures below 30 °C. In this case, they would be expected to associate with ribosome-nascent chain complexes. Thus, co-isolation of factors associated with ribosome-nascent chain complexes could potentially reveal nascent chain associated chaperone functions of hitherto uncharacterized proteins.

The classical way of isolating ribosomes by repeated steps of centrifugation involves large dilutions of the sample, which could result in the loss of factors that bind with low affinities. Therefore, a method was developed in the present study that allows the isolation of ribosomes at high concentrations through a pull-down procedure. To this end, a FLAG-His$_6$ (FH) tag was fused carboxyl-terminally to the *E. coli* ribosomal proteins L17 and L20, encoded by the genes *rplQ* and *rplT*, respectively. Ribosomes harboring either of the FH-tagged proteins were successfully isolated using a commercially available agarose matrix derivatized with an anti-FLAG antibody. The procedure is specific, rapid and avoids strong dilution of the samples prior to elution. Batch sample handling allows the analysis of multiple samples simultaneously.

Chromosomal integration of the FH tag was attempted to guarantee that all ribosomes contained the tagged protein. Whereas attempts to chromosomally tag L20 failed, the tag was successfully fused to ribosomal protein L17 at the chromosomal level, resulting in a strain with the genotype *rplQ-FH-tet*^{R}. In pull-downs from this strain, the TF band was clearly visible, demonstrating that this system is suitable for the co-isolation of ribosome-associated factors.

E. coli strains encoding tagged ribosomal proteins offer a range of possibilities for the identification of factors associated with ribosome-nascent chain complexes. Combination of the *rplQ-FH-tet*^{R} genotype with other genetic modifications can serve to analyze the ribosomal proteome in different strain backgrounds. In this study, it was combined with a deletion of the *tig* gene encoding TF. It was not possible to transduce the *rplQ-FH-tet*^{R} allele into a strain deficient in DnaKJ, probably because the DnaK system is required for functionality of the tetracycline-resistance gene. Transduction of this allele would probably be possible if another resistance marker were utilized. When lysates of these strains were prepared under conditions that either stabilize or destabilize ribosome-nascent chain complexes, marked differences in the protein patterns of the isolated ribosomal samples were observed. Thus, by choosing the appropriate conditions, it is possible to identify factors that specifically co-fractionate with ribosomes when nascent chains are present.

By one-dimensional SDS-PAGE, a variety of different proteins was visible in samples that were prepared under conditions that stabilize ribosome-nascent chain complexes. Two dimensional gel electrophoresis would allow identification of these proteins, so that a ribosomal proteome can be defined under different conditions. It will be of interest to see how this proteome changes in response to circumstances that affect general protein folding, such as elevated temperatures and lack of specific chaperones. In addition, the pattern of ribosome-nascent chain associated proteins can be studied during the translation of any chaperone substrate of interest, since this system is amenable to expression of virtually any model protein.

The tools and methods described here for *in vitro* and *in vivo* work may prove useful for identifying factors that function during the earliest steps of protein biogenesis. The experiments performed throughout this work have provided a detailed and real-time view of the dynamic cycle of Trigger factor function during emergence of the nascent chain from the ribosome.

VI REFERENCES

Agashe, V. R., S. Guha, H. C. Chang, P. Genevaux, M. Hayer-Hartl, M. Stemp, C. Georgopoulos, F. U. Hartl and J. M. Barral (2004). "Function of trigger factor and DnaK in multidomain protein folding: increase in yield at the expense of folding speed." Cell **117**(2): 199-209.

Agashe, V. R., M. C. Shastry and J. B. Udgaonkar (1995). "Initial hydrophobic collapse in the folding of barstar." Nature **377**(6551): 754-7.

Anfinsen, C. B. (1972). "The formation and stabilization of protein structure." Biochem J **128**(4): 737-49.

Anfinsen, C. B. (1973). "Principles that govern the folding of protein chains." Science **181**(96): 223-30.

Auerbach, T., A. Bashan and A. Yonath (2004). "Ribosomal antibiotics: structural basis for resistance, synergism and selectivity." Trends Biotechnol **22**(11): 570-6.

Baldwin, R. L. (1989). "How does protein folding get started?" Trends Biochem Sci **14**(7): 291-4.

Baldwin, R. L. (1995). "The nature of protein folding pathways: the classical versus the new view." J Biomol NMR **5**(2): 103-9.

Baldwin, R. L. (1996). "On-pathway versus off-pathway folding intermediates." Fold Des **1**(1): R1-8.

Baldwin, R. L. and G. D. Rose (1999). "Is protein folding hierarchic? II. Folding intermediates and transition states." Trends Biochem Sci **24**(2): 77-83.

Ban, N., P. Nissen, J. Hansen, P. B. Moore and T. A. Steitz (2000). "The complete atomic structure of the large ribosomal subunit at 2.4 A resolution." Science **289**(5481): 905-20.

Bang, H., A. Pecht, G. Raddatz, T. Scior, W. Solbach, K. Brune and A. Pahl (2000). "Prolyl isomerases in a minimal cell. Catalysis of protein folding by trigger factor from Mycoplasma genitalium." Eur J Biochem **267**(11): 3270-80.

Baram, D., E. Pyetan, A. Sittner, T. Auerbach-Nevo, A. Bashan and A. Yonath (2005). "Structure of trigger factor binding domain in biologically homologous complex with eubacterial ribosome reveals its chaperone action." Proc Natl Acad Sci U S A **102**(34): 12017-22.

Baram, D. and A. Yonath (2005). "From peptide-bond formation to cotranslational folding: dynamic, regulatory and evolutionary aspects." FEBS Lett **579**(4): 948-54.

Barral, J. M., S. A. Broadley, G. Schaffar and F. U. Hartl (2004). "Roles of molecular chaperones in protein misfolding diseases." Semin Cell Dev Biol **15**(1): 17-29.

Beatrix, B., H. Sakai and M. Wiedmann (2000). "The alpha and beta subunit of the nascent polypeptide-associated complex have distinct functions." J Biol Chem **275**(48): 37838-45.

Beckmann, R. P., L. E. Mizzen and W. J. Welch (1990). "Interaction of Hsp 70 with newly synthesized proteins: implications for protein folding and assembly." Science **248**(4957): 850-4.

Ben-Zvi, A. P. and P. Goloubinoff (2001). "Review: mechanisms of disaggregation and refolding of stable protein aggregates by molecular chaperones." J Struct Biol **135**(2): 84-93.

Blaha, G., D. N. Wilson, G. Stoller, G. Fischer, R. Willumeit and K. H. Nierhaus (2003). "Localization of the trigger factor binding site on the ribosomal 50S subunit." J Mol Biol **326**(3): 887-97.

Blobel, G. and D. D. Sabatini (1970). "Controlled proteolysis of nascent polypeptides in rat liver cell fractions. I. Location of the polypeptides within ribosomes." J Cell Biol **45**(1): 130-45.

Bolivar, F., R. L. Rodriguez, P. J. Greene, M. C. Betlach, H. L. Heyneker and H. W. Boyer (1977). "Construction and characterization of new cloning vehicles. II. A multipurpose cloning system." Gene **2**(2): 95-113.

Bradford, M. M. (1976). "A rapid and sensitive method for the quantitation of microgram quantities of protein utilizing the principle of protein-dye binding." Anal Biochem **72**: 248-54.

Braig, K., Z. Otwinowski, R. Hegde, D. C. Boisvert, A. Joachimiak, A. L. Horwich and P. B. Sigler (1994). "The crystal structure of the bacterial chaperonin GroEL at 2.8 A." Nature **371**(6498): 578-86.

Bremer, H. and P. P. Dennis (1996). Modulation of chemical composition and other parameters of the cell by growth rate. Escherichia coli and Salmonella: Cellular and Molecular Biology. F. C. Neidhart. Washington, D. C., ASM Press**:** 1553-1569.

Brockwell, D. J., D. A. Smith and S. E. Radford (2000). "Protein folding mechanisms: new methods and emerging ideas." Curr Opin Struct Biol **10**(1): 16-25.

Brodersen, D. E. and P. Nissen (2005). "The social life of ribosomal proteins." Febs J **272**(9): 2098-108.

Bukau, B., E. Deuerling, C. Pfund and E. A. Craig (2000). "Getting newly synthesized proteins into shape." Cell **101**(2): 119-22.

Bukau, B. and A. L. Horwich (1998). "The Hsp70 and Hsp60 chaperone machines." Cell **92**(3): 351-66.

Callebaut, I. and J. P. Mornon (1995). "Trigger factor, one of the Escherichia coli chaperone proteins, is an original member of the FKBP family." FEBS Lett **374**(2): 211-5.

Chang, H. C., C. M. Kaiser, F. U. Hartl and J. M. Barral (2005). "De novo folding of GFP fusion proteins: high efficiency in eukaryotes but not in bacteria." J Mol Biol **353**(2): 397-409.

Chaudhuri, T. K., G. W. Farr, W. A. Fenton, S. Rospert and A. L. Horwich (2001). "GroEL/GroES-mediated folding of a protein too large to be encapsulated." Cell **107**(2): 235-46.

Crooke, E., L. Brundage, M. Rice and W. Wickner (1988a). "ProOmpA spontaneously folds in a membrane assembly competent state which trigger factor stabilizes." Embo J **7**(6): 1831-5.

Crooke, E., B. Guthrie, S. Lecker, R. Lill and W. Wickner (1988b). "ProOmpA is stabilized for membrane translocation by either purified E. coli trigger factor or canine signal recognition particle." Cell **54**(7): 1003-11.

Crooke, E. and W. Wickner (1987). "Trigger factor: a soluble protein that folds pro-OmpA into a membrane-assembly-competent form." Proc Natl Acad Sci U S A **84**(15): 5216-20.

Daggett, V. and A. Fersht (2003). "The present view of the mechanism of protein folding." Nat Rev Mol Cell Biol **4**(6): 497-502.

Datsenko, K. A. and B. L. Wanner (2000). "One-step inactivation of chromosomal genes in Escherichia coli K-12 using PCR products." Proc Natl Acad Sci U S A **97**(12): 6640-5.

Deuerling, E., H. Patzelt, S. Vorderwulbecke, T. Rauch, G. Kramer, E. Schaffitzel, A. Mogk, A. Schulze-Specking, H. Langen and B. Bukau (2003). "Trigger Factor and DnaK possess overlapping substrate pools and binding specificities." Mol Microbiol **47**(5): 1317-28.

Deuerling, E., A. Schulze-Specking, T. Tomoyasu, A. Mogk and B. Bukau (1999). "Trigger factor and DnaK cooperate in folding of newly synthesized proteins." Nature **400**(6745): 693-6.

Dinner, A. R., A. Sali, L. J. Smith, C. M. Dobson and M. Karplus (2000). "Understanding protein folding via free-energy surfaces from theory and experiment." Trends Biochem Sci **25**(7): 331-9.

Ditzel, L., J. Lowe, D. Stock, K. O. Stetter, H. Huber, R. Huber and S. Steinbacher (1998). "Crystal structure of the thermosome, the archaeal chaperonin and homolog of CCT." Cell **93**(1): 125-38.

Doolittle, R. F. (1995). "The multiplicity of domains in proteins." Annu Rev Biochem **64**: 287-314.

Eggers, D. K., W. J. Welch and W. J. Hansen (1997). "Complexes between nascent polypeptides and their molecular chaperones in the cytosol of mammalian cells." Mol Biol Cell **8**(8): 1559-73.

Ehrnsperger, M., M. Gaestel and J. Buchner (1997). Chaperone function of small heat shock proteins and alpha-crystallin. Molecular chaperones in the life cycle of proteins. A. L. Fink and Y. Goto. New York, Marcel Dekker**:** 533-576.

Ekman, D., A. K. Bjorklund, J. Frey-Skott and A. Elofsson (2005). "Multi-domain proteins in the three kingdoms of life: orphan domains and other unassigned regions." J Mol Biol **348**(1): 231-43.

Ellis, R. J. (2001). "Macromolecular crowding: an important but neglected aspect of the intracellular environment." Curr Opin Struct Biol **11**(1): 114-9.

Ferbitz, L., T. Maier, H. Patzelt, B. Bukau, E. Deuerling and N. Ban (2004). "Trigger factor in complex with the ribosome forms a molecular cradle for nascent proteins." Nature **431**(7008): 590-6.

Ferguson, N., A. P. Capaldi, R. James, C. Kleanthous and S. E. Radford (1999). "Rapid folding with and without populated intermediates in the homologous four-helix proteins Im7 and Im9." J Mol Biol **286**(5): 1597-608.

Ferguson, N. and A. R. Fersht (2003). "Early events in protein folding." Curr Opin Struct Biol **13**(1): 75-81.

Fersht, A. R. (1997). "Nucleation mechanisms in protein folding." Curr Opin Struct Biol **7**(1): 3-9.

Fersht, A. R., A. Matouschek and L. Serrano (1992). "The folding of an enzyme. I. Theory of protein engineering analysis of stability and pathway of protein folding." J Mol Biol **224**(3): 771-82.

Fraser, C. M., J. D. Gocayne, O. White, M. D. Adams, R. A. Clayton, R. D. Fleischmann, C. J. Bult, A. R. Kerlavage, G. Sutton, J. M. Kelley, R. D. Fritchman, J. F. Weidman, K. V. Small, M. Sandusky, J. Fuhrmann, D. Nguyen, T. R. Utterback, D. M. Saudek, C. A. Phillips, J. M. Merrick, J. F. Tomb, B. A. Dougherty, K. F. Bott, P. C. Hu, T. S. Lucier, S. N. Peterson, H. O. Smith, C. A. Hutchison, 3rd and J. C. Venter (1995). "The minimal gene complement of Mycoplasma genitalium." Science **270**(5235): 397-403.

Freedman, R. B., P. Klappa and L. W. Ruddock (2002). "Protein disulfide isomerases exploit synergy between catalytic and specific binding domains." EMBO Rep **3**(2): 136-40.

Frydman, J. (2001). "Folding of newly translated proteins in vivo: the role of molecular chaperones." Annu Rev Biochem **70**: 603-47.

Frydman, J., E. Nimmesgern, K. Ohtsuka and F. U. Hartl (1994). "Folding of nascent polypeptide chains in a high molecular mass assembly with molecular chaperones." Nature **370**(6485): 111-7.

Gautschi, M., H. Lilie, U. Funfschilling, A. Mun, S. Ross, T. Lithgow, P. Rucknagel and S. Rospert (2001). "RAC, a stable ribosome-associated complex in yeast formed by the DnaK-DnaJ homologs Ssz1p and zuotin." Proc Natl Acad Sci U S A **98**(7): 3762-7.

Gautschi, M., A. Mun, S. Ross and S. Rospert (2002). "A functional chaperone triad on the yeast ribosome." Proc Natl Acad Sci U S A **99**(7): 4209-14.

Geissler, S., K. Siegers and E. Schiebel (1998). "A novel protein complex promoting formation of functional alpha- and gamma-tubulin." Embo J **17**(4): 952-66.

Genevaux, P., F. Keppel, F. Schwager, P. S. Langendijk-Genevaux, F. U. Hartl and C. Georgopoulos (2004). "In vivo analysis of the overlapping functions of DnaK and trigger factor." EMBO Rep **5**(2): 195-200.

Gilbert, R. J., P. Fucini, S. Connell, S. D. Fuller, K. H. Nierhaus, C. V. Robinson, C. M. Dobson and D. I. Stuart (2004). "Three-dimensional structures of translating ribosomes by Cryo-EM." Mol Cell **14**(1): 57-66.

Gill, S. C. and P. H. von Hippel (1989). "Calculation of protein extinction coefficients from amino acid sequence data." Anal Biochem **182**(2): 319-26.

Glover, J. R. and S. Lindquist (1998). "Hsp104, Hsp70, and Hsp40: a novel chaperone system that rescues previously aggregated proteins." Cell **94**(1): 73-82.

Grallath, S., J. P. Schwarz, U. M. Bottcher, A. Bracher, F. U. Hartl and K. Siegers (2006). "L25 functions as a conserved ribosomal docking site shared by nascent chain-associated complex and signal-recognition particle." EMBO Rep **7**(1): 78-84.

Griffiths, P. L., R. W. Park and I. F. Connerton (1995). "The gene for Campylobacter trigger factor: evidence for multiple transcription start sites and protein products." Microbiology **141 (Pt 6)**: 1359-67.

Guthrie, B. and W. Wickner (1990). "Trigger factor depletion or overproduction causes defective cell division but does not block protein export." J Bacteriol **172**(10): 5555-62.

Guzman, L. M., D. Belin, M. J. Carson and J. Beckwith (1995). "Tight regulation, modulation, and high-level expression by vectors containing the arabinose PBAD promoter." J Bacteriol **177**(14): 4121-30.

Harms, J., F. Schluenzen, R. Zarivach, A. Bashan, S. Gat, I. Agmon, H. Bartels, F. Franceschi and A. Yonath (2001). "High resolution structure of the large ribosomal subunit from a mesophilic eubacterium." Cell **107**(5): 679-88.

Harrison, C. J., M. Hayer-Hartl, M. Di Liberto, F. Hartl and J. Kuriyan (1997). "Crystal structure of the nucleotide exchange factor GrpE bound to the ATPase domain of the molecular chaperone DnaK." Science **276**(5311): 431-5.

Hartl, F. U. (1996). "Molecular chaperones in cellular protein folding." Nature **381**(6583): 571-9.

Hartl, F. U. and M. Hayer-Hartl (2002). "Molecular chaperones in the cytosol: from nascent chain to folded protein." Science **295**(5561): 1852-8.

Hayer-Hartl, M. K., J. J. Ewbank, T. E. Creighton and F. U. Hartl (1994). "Conformational specificity of the chaperonin GroEL for the compact folding intermediates of alpha-lactalbumin." Embo J **13**(13): 3192-202.

Hesterkamp, T. and B. Bukau (1996). "The Escherichia coli trigger factor." FEBS Lett **389**(1): 32-4.

Hesterkamp, T., E. Deuerling and B. Bukau (1997). "The amino-terminal 118 amino acids of Escherichia coli trigger factor constitute a domain that is necessary and sufficient for binding to ribosomes." J Biol Chem **272**(35): 21865-71.

Hesterkamp, T., S. Hauser, H. Lutcke and B. Bukau (1996). "Escherichia coli trigger factor is a prolyl isomerase that associates with nascent polypeptide chains." Proc Natl Acad Sci U S A **93**(9): 4437-41.

Hoffmann, A., F. Merz, A. Rutkowska, B. Zachmann-Brand, E. Deuerling and B. Bukau (2006). "Trigger factor forms a protective shield for nascent polypeptides at the ribosome." J Biol Chem.

Hohfeld, J. and S. Jentsch (1997). "GrpE-like regulation of the hsc70 chaperone by the anti-apoptotic protein BAG-1." Embo J **16**(20): 6209-16.

Hohfeld, J., Y. Minami and F. U. Hartl (1995). "Hip, a novel cochaperone involved in the eukaryotic Hsc70/Hsp40 reaction cycle." Cell **83**(4): 589-98.

Huang, G. C., Z. Y. Li, J. M. Zhou and G. Fischer (2000). "Assisted folding of D-glyceraldehyde-3-phosphate dehydrogenase by trigger factor." Protein Sci **9**(6): 1254-61.

Huang, P., M. Gautschi, W. Walter, S. Rospert and E. A. Craig (2005). "The Hsp70 Ssz1 modulates the function of the ribosome-associated J-protein Zuo1." Nat Struct Mol Biol **12**(6): 497-504.

Hundley, H., H. Eisenman, W. Walter, T. Evans, Y. Hotokezaka, M. Wiedmann and E. Craig (2002). "The in vivo function of the ribosome-associated Hsp70, Ssz1, does not require its putative peptide-binding domain." Proc Natl Acad Sci U S A **99**(7): 4203-8.

Hundley, H. A., W. Walter, S. Bairstow and E. A. Craig (2005). "Human Mpp11 J protein: ribosome-tethered molecular chaperones are ubiquitous." Science **308**(5724): 1032-4.

Jackson, S. E. and A. R. Fersht (1991). "Folding of chymotrypsin inhibitor 2. 1. Evidence for a two-state transition." Biochemistry **30**(43): 10428-35.

Jamin, M. and R. L. Baldwin (1996). "Refolding and unfolding kinetics of the equilibrium folding intermediate of apomyoglobin." Nat Struct Biol **3**(7): 613-8.

Jenni, S. and N. Ban (2003). "The chemistry of protein synthesis and voyage through the ribosomal tunnel." Curr Opin Struct Biol **13**(2): 212-9.

Jiang, J., K. Prasad, E. M. Lafer and R. Sousa (2005). "Structural basis of interdomain communication in the Hsc70 chaperone." Mol Cell **20**(4): 513-24.

Kabani, M., J. M. Beckerich and J. L. Brodsky (2002). "Nucleotide exchange factor for the yeast Hsp70 molecular chaperone Ssa1p." Mol Cell Biol **22**(13): 4677-89.

Kerner, M. J., D. J. Naylor, Y. Ishihama, T. Maier, H. C. Chang, A. P. Stines, C. Georgopoulos, D. Frishman, M. Hayer-Hartl, M. Mann and F. U. Hartl (2005). "Proteome-wide analysis of chaperonin-dependent protein folding in Escherichia coli." Cell **122**(2): 209-20.

Kim, P. S. and R. L. Baldwin (1982). "Specific intermediates in the folding reactions of small proteins and the mechanism of protein folding." Annu Rev Biochem **51**: 459-89.

Kim, P. S. and R. L. Baldwin (1990). "Intermediates in the folding reactions of small proteins." Annu Rev Biochem **59**: 631-60.

Klumpp, M., W. Baumeister and L. O. Essen (1997). "Structure of the substrate binding domain of the thermosome, an archaeal group II chaperonin." Cell **91**(2): 263-70.

Klunker, D., B. Haas, A. Hirtreiter, L. Figueiredo, D. J. Naylor, G. Pfeifer, V. Muller, U. Deppenmeier, G. Gottschalk, F. U. Hartl and M. Hayer-Hartl (2003). "Coexistence of group I and group II chaperonins in the archaeon Methanosarcina mazei." J Biol Chem **278**(35): 33256-67.

Kramer, G., H. Patzelt, T. Rauch, T. A. Kurz, S. Vorderwulbecke, B. Bukau and E. Deuerling (2004a). "Trigger factor peptidyl-prolyl cis/trans isomerase activity is not essential for the folding of cytosolic proteins in Escherichia coli." J Biol Chem **279**(14): 14165-70.

Kramer, G., T. Rauch, W. Rist, S. Vorderwulbecke, H. Patzelt, A. Schulze-Specking, N. Ban, E. Deuerling and B. Bukau (2002). "L23 protein functions as a chaperone docking site on the ribosome." Nature **419**(6903): 171-4.

Kramer, G., A. Rutkowska, R. D. Wegrzyn, H. Patzelt, T. A. Kurz, F. Merz, T. Rauch, S. Vorderwulbecke, E. Deuerling and B. Bukau (2004b). "Functional dissection of Escherichia coli trigger factor: unraveling the function of individual domains." J Bacteriol **186**(12): 3777-84.

Kristensen, O. and M. Gajhede (2003). "Chaperone binding at the ribosomal exit tunnel." Structure (Camb) **11**(12): 1547-56.

Kummerfeld, S. K. and S. A. Teichmann (2005). "Relative rates of gene fusion and fission in multi-domain proteins." Trends Genet **21**(1): 25-30.

Laemmli, U. K. (1970). "Cleavage of structural proteins during the assembly of the head of bacteriophage T4." Nature **227**(5259): 680-5.

Lakowicz, J. (1999). Principles of Fluorescence Spectroscopy. New York, Kluwer Academic and Plenum Publishers.

Laksanalamai, P., T. A. Whitehead and F. T. Robb (2004). "Minimal protein-folding systems in hyperthermophilic archaea." Nat Rev Microbiol **2**(4): 315-24.

Langer, T., G. Pfeifer, J. Martin, W. Baumeister and F. U. Hartl (1992). "Chaperonin-mediated protein folding: GroES binds to one end of the GroEL cylinder, which accommodates the protein substrate within its central cavity." Embo J **11**(13): 4757-65.

Leroux, M. R. (2001). "Protein folding and molecular chaperones in archaea." Adv Appl Microbiol **50**: 219-77.

Leroux, M. R., M. Fandrich, D. Klunker, K. Siegers, A. N. Lupas, J. R. Brown, E. Schiebel, C. M. Dobson and F. U. Hartl (1999). "MtGimC, a novel archaeal chaperone related to the eukaryotic chaperonin cofactor GimC/prefoldin." Embo J **18**(23): 6730-43.

Levinthal, C. (1969). How to Fold Graciously. Mossbauer Spectroscopy in Biological Systems: Proceedings of a meeting held at Allerton House, Monticello, Illinois. J. T. P. a. M. DeBrunner, E. Illinois, University of Illinois Press**:** 22-24.

Lill, R., E. Crooke, B. Guthrie and W. Wickner (1988). "The "trigger factor cycle" includes ribosomes, presecretory proteins, and the plasma membrane." Cell **54**(7): 1013-8.

Liu, C. P., S. Perrett and J. M. Zhou (2005). "Dimeric trigger factor stably binds folding-competent intermediates and cooperates with the DnaK-DnaJ-GrpE chaperone system to allow refolding." J Biol Chem **280**(14): 13315-20.

Liu, C. P. and J. M. Zhou (2004). "Trigger factor-assisted folding of bovine carbonic anhydrase II." Biochem Biophys Res Commun **313**(3): 509-15.

Lu, J. and C. Deutsch (2005). "Folding zones inside the ribosomal exit tunnel." Nat Struct Mol Biol **12**(12): 1123-9.

Ludlam, A. V., B. A. Moore and Z. Xu (2004). "The crystal structure of ribosomal chaperone trigger factor from Vibrio cholerae." Proc Natl Acad Sci U S A **101**(37): 13436-41.

Lund, P. A. (2001). "Microbial molecular chaperones." Adv Microb Physiol **44**: 93-140.

Maier, R., B. Eckert, C. Scholz, H. Lilie and F. X. Schmid (2003). "Interaction of trigger factor with the ribosome." J Mol Biol **326**(2): 585-92.

Maier, R., C. Scholz and F. X. Schmid (2001). "Dynamic association of trigger factor with protein substrates." J Mol Biol **314**(5): 1181-90.

Maier, T., L. Ferbitz, E. Deuerling and N. Ban (2005). "A cradle for new proteins: trigger factor at the ribosome." Curr Opin Struct Biol **15**(2): 204-12.

Malkin, L. I. and A. Rich (1967). "Partial resistance of nascent polypeptide chains to proteolytic digestion due to ribosomal shielding." J Mol Biol **26**(2): 329-46.

Marszalek, P. E., H. Lu, H. Li, M. Carrion-Vazquez, A. F. Oberhauser, K. Schulten and J. M. Fernandez (1999). "Mechanical unfolding intermediates in titin modules." Nature **402**(6757): 100-3.

Martin, J. and F. U. Hartl (1993). "Protein folding in the cell: molecular chaperones pave the way." Structure **1**(3): 161-4.

Mathews, M. B., N. Sonenberg and J. W. B. Hershey (2000). Origins and principles of translational control. Translational control of gene expression. N. Sonenberg, J. W. B. Hershey and M. B. Mathews. Cold Spring Harbor, New York, Cold Spring Harbor Laboratory Press: 1-31.

Mayer, M. P. and B. Bukau (2005). "Hsp70 chaperones: cellular functions and molecular mechanism." Cell Mol Life Sci **62**(6): 670-84.

Michalski, C. J., B. H. Sells and M. Morrison (1973). "Molecular morphology of ribosomes. Localization of ribosomal proteins in 50-S subunits." Eur J Biochem **33**(3): 481-5.

Michimoto, T., T. Aoki, A. Toh-e and Y. Kikuchi (2000). "Yeast Pdr13p and Zuo1p molecular chaperones are new functional Hsp70 and Hsp40 partners." Gene **257**(1): 131-7.

Miller, J. H. (1992). A Short Course in Bacterial Genetics. Laboratory Manual for Escherichia coli and Related Bacteria. Cold Spring Harbor, Cold Spring Harbor Laboratory Press.

Minton, A. P. (2001). "The influence of macromolecular crowding and macromolecular confinement on biochemical reactions in physiological media." J Biol Chem **276**(14): 10577-80.

Mogk, A. and B. Bukau (2004). "Molecular chaperones: structure of a protein disaggregase." Curr Biol **14**(2): R78-80.

Moore, P. B. and T. A. Steitz (2003). "The structural basis of large ribosomal subunit function." Annu Rev Biochem **72**: 813-50.

Nagata, H., W. J. Hansen, B. Freeman and W. J. Welch (1998). "Mammalian cytosolic DnaJ homologues affect the hsp70 chaperone-substrate reaction cycle, but do not interact directly with nascent or newly synthesized proteins." Biochemistry **37**(19): 6924-38.

Nakatogawa, H. and K. Ito (2001). "Secretion monitor, SecM, undergoes self-translation arrest in the cytosol." Mol Cell **7**(1): 185-92.

Nakatogawa, H. and K. Ito (2002). "The ribosomal exit tunnel functions as a discriminating gate." Cell **108**(5): 629-36.

Narberhaus, F. (2002). "Alpha-crystallin-type heat shock proteins: socializing minichaperones in the context of a multichaperone network." Microbiol Mol Biol Rev **66**(1): 64-93; table of contents.

Naylor, D. J. and F. U. Hartl (2001). "Contribution of molecular chaperones to protein folding in the cytoplasm of prokaryotic and eukaryotic cells." Biochem Soc Symp(68): 45-68.

Nelson, R. J., T. Ziegelhoffer, C. Nicolet, M. Werner-Washburne and E. A. Craig (1992). "The translation machinery and 70 kd heat shock protein cooperate in protein synthesis." Cell **71**(1): 97-105.

Netzer, W. J. and F. U. Hartl (1997). "Recombination of protein domains facilitated by co-translational folding in eukaryotes." Nature **388**(6640): 343-9.

Nicola, A. V., W. Chen and A. Helenius (1999). "Co-translational folding of an alphavirus capsid protein in the cytosol of living cells." Nat Cell Biol **1**(6): 341-5.

Nierhaus, K. H. and D. N. Wilson, Eds. (2004). Protein Synthesis and Ribosome Structure: Translating the genome. Weinheim, Germany, Wiley-VCH.

Nilsson, J. and P. Nissen (2005). "Elongation factors on the ribosome." Curr Opin Struct Biol **15**(3): 349-54.

Nissen, P., J. Hansen, N. Ban, P. B. Moore and T. A. Steitz (2000). "The structural basis of ribosome activity in peptide bond synthesis." Science **289**(5481): 920-30.

Odom, O. W., H.-Y. Deng, E. R. Dabbs and B. Hardesty (1984). "Binding of S21 to the 50S subunit and the effect of the 50S subunit on nonradiative energy transfer between the 3' end of 16S RNA and S21." Biochemistry **23**: 5069-5076.

Ogle, J. M., D. E. Brodersen, W. M. Clemons, Jr., M. J. Tarry, A. P. Carter and V. Ramakrishnan (2001). "Recognition of cognate transfer RNA by the 30S ribosomal subunit." Science **292**(5518): 897-902.

Ogle, J. M., F. V. Murphy, M. J. Tarry and V. Ramakrishnan (2002). "Selection of tRNA by the ribosome requires a transition from an open to a closed form." Cell **111**(5): 721-32.

Ogle, J. M. and V. Ramakrishnan (2005). "Structural insights into translational fidelity." Annu Rev Biochem **74**: 129-77.

Ohman, A., A. Rak, M. Dontsova, M. B. Garber and T. Hard (2003). "NMR structure of the ribosomal protein L23 from Thermus thermophilus." J Biomol NMR **26**(2): 131-7.

Orengo, C. A., D. T. Jones and J. M. Thornton (1994). "Protein superfamilies and domain superfolds." Nature **372**(6507): 631-4.

Paci, E., C. T. Friel, K. Lindorff-Larsen, S. E. Radford, M. Karplus and M. Vendruscolo (2004). "Comparison of the transition state ensembles for folding of Im7 and Im9 determined using all-atom molecular dynamics simulations with phi value restraints." Proteins **54**(3): 513-25.

Patzelt, H., G. Kramer, T. Rauch, H. J. Schonfeld, B. Bukau and E. Deuerling (2002). "Three-state equilibrium of Escherichia coli trigger factor." Biol Chem **383**(10): 1611-9.

Patzelt, H., S. Rudiger, D. Brehmer, G. Kramer, S. Vorderwulbecke, E. Schaffitzel, A. Waitz, T. Hesterkamp, L. Dong, J. Schneider-Mergener, B. Bukau and E. Deuerling (2001). "Binding specificity of Escherichia coli trigger factor." Proc Natl Acad Sci U S A **98**(25): 14244-9.

Pedersen, S., P. L. Bloch, S. Reeh and F. C. Neidhardt (1978). "Patterns of protein synthesis in E. coli: a catalog of the amount of 140 individual proteins at different growth rates." Cell **14**(1): 179-90.

Pfund, C., N. Lopez-Hoyo, T. Ziegelhoffer, B. A. Schilke, P. Lopez-Buesa, W. A. Walter, M. Wiedmann and E. A. Craig (1998). "The molecular chaperone Ssb from Saccharomyces cerevisiae is a component of the ribosome-nascent chain complex." Embo J **17**(14): 3981-9.

Pratt, W. B. and D. O. Toft (2003). "Regulation of signaling protein function and trafficking by the hsp90/hsp70-based chaperone machinery." Exp Biol Med (Maywood) **228**(2): 111-33.

Privalov, P. L. (1996). "Intermediate states in protein folding." J Mol Biol **258**(5): 707-25.

Ptitsyn, O. B. and A. A. Rashin (1975). "A model of myoglobin self-organization." Biophys Chem **3**(1): 1-20.

Radford, S. E. (2000). "Protein folding: progress made and promises ahead." Trends Biochem Sci **25**(12): 611-8.

Radford, S. E., C. M. Dobson and P. A. Evans (1992). "The folding of hen lysozyme involves partially structured intermediates and multiple pathways." Nature **358**(6384): 302-7.

Ramachandran, G. N. and V. Sasisekharan (1968). "Conformation of polypeptides and proteins." Adv Protein Chem **23**: 283-438.

Richter, K. and J. Buchner (2001). "Hsp90: chaperoning signal transduction." J Cell Physiol **188**(3): 281-90.

Riddles, P. W., R. L. Blakeley and B. Zerner (1983). "Reassessment of Ellman's reagent." Methods Enzymol **91**: 49-60.

Roseman, M. A. (1988). "Hydrophilicity of polar amino acid side-chains is markedly reduced by flanking peptide bonds." J Mol Biol **200**(3): 513-22.

Sambrook, J., E. F. Fritsch and T. Maniatis (1989). Molecular Cloning: A Laboratory Manual. Cold Spring Harbor, New York, Cold Spring Harbor Laboratory Press.

Schechter, A. N., R. F. Chen and C. B. Anfinsen (1970). "Kinetics of folding of staphylococcal nuclease." Science **167**(919): 886-7.

Schellman, J. A. (1955). "The stability of hydrogen-bonded peptide structures in aqueous solution." C R Trav Lab Carlsberg [Chim] **29**(14-15): 230-59.

Schiene, C. and G. Fischer (2000). "Enzymes that catalyse the restructuring of proteins." Curr Opin Struct Biol **10**(1): 40-5.

Schiene-Fischer, C., J. Habazettl, F. X. Schmid and G. Fischer (2002). "The hsp70 chaperone DnaK is a secondary amide peptide bond cis-trans isomerase." Nat Struct Biol **9**(6): 419-24.

Schirmer, E. C., J. R. Glover, M. A. Singer and S. Lindquist (1996). "HSP100/Clp proteins: a common mechanism explains diverse functions." Trends Biochem Sci **21**(8): 289-96.

Schluenzen, F., A. Tocilj, R. Zarivach, J. Harms, M. Gluehmann, D. Janell, A. Bashan, H. Bartels, I. Agmon, F. Franceschi and A. Yonath (2000). "Structure of functionally activated small ribosomal subunit at 3.3 angstroms resolution." Cell **102**(5): 615-23.

Schlunzen, F., D. N. Wilson, P. Tian, J. M. Harms, S. J. McInnes, H. A. Hansen, R. Albrecht, J. Buerger, S. M. Wilbanks and P. Fucini (2005). "The binding mode of the trigger factor on the ribosome: implications for protein folding and SRP interaction." Structure (Camb) **13**(11): 1685-94.

Schmid, F. X. (1995). "Protein folding. Prolyl isomerases join the fold." Curr Biol **5**(9): 993-4.

Schmid, F. X. (2001). "Prolyl isomerases." Adv Protein Chem **59**: 243-82.

Schroder, G. F. and H. Grubmuller (2004). "FRETsg: biomolecular structure model building from multiple FRET experiments." Comp Phys Comm **158**: 150-7.

Schröder, G. F. and H. Grubmüller (2003). "FRETsg: Biomolecular Structure Model building from multiple FRET experiments." Comp Phys Comm **158**: 150-157.

Schultz, C. P. (2000). "Illuminating folding intermediates." Nat Struct Biol **7**(1): 7-10.

Schulze-Gahmen, U., S. Aono, S. Chen, H. Yokota, R. Kim and S. H. Kim (2005). "Structure of the hypothetical Mycoplasma protein MPN555 suggests a chaperone function." Acta Crystallogr D Biol Crystallogr **61**(Pt 10): 1343-7.

Schuwirth, B. S., M. A. Borovinskaya, C. W. Hau, W. Zhang, A. Vila-Sanjurjo, J. M. Holton and J. H. Cate (2005). "Structures of the bacterial ribosome at 3.5 A resolution." Science **310**(5749): 827-34.

Shi, X., M. R. Parthun and J. A. Jaehning (1995). "The yeast EGD2 gene encodes a homologue of the alpha NAC subunit of the human nascent-polypeptide-associated complex." Gene **165**(2): 199-202.

Shimizu, Y., A. Inoue, Y. Tomari, T. Suzuki, T. Yokogawa, K. Nishikawa and T. Ueda (2001). "Cell-free translation reconstituted with purified components." Nat Biotechnol **19**(8): 751-5.

Shimizu, Y., T. Kanamori and T. Ueda (2005). "Protein synthesis by pure translation systems." Methods **36**(3): 299-304.

Shinde, U. P., J. J. Liu and M. Inouye (1997). "Protein memory through altered folding mediated by intramolecular chaperones." Nature **389**(6650): 520-2.

Shomura, Y., Z. Dragovic, H. C. Chang, N. Tzvetkov, J. C. Young, J. L. Brodsky, V. Guerriero, F. U. Hartl and A. Bracher (2005). "Regulation of Hsp70 function by HspBP1: structural analysis reveals an alternate mechanism for Hsp70 nucleotide exchange." Mol Cell **17**(3): 367-79.

Siegers, K., B. Bolter, J. P. Schwarz, U. M. Bottcher, S. Guha and F. U. Hartl (2003). "TRiC/CCT cooperates with different upstream chaperones in the folding of distinct protein classes." Embo J **22**(19): 5230-40.

Siegert, R., M. R. Leroux, C. Scheufler, F. U. Hartl and I. Moarefi (2000). "Structure of the molecular chaperone prefoldin: unique interaction of multiple coiled coil tentacles with unfolded proteins." Cell **103**(4): 621-32.

Sondermann, H., C. Scheufler, C. Schneider, J. Hohfeld, F. U. Hartl and I. Moarefi (2001). "Structure of a Bag/Hsc70 complex: convergent functional evolution of Hsp70 nucleotide exchange factors." Science **291**(5508): 1553-7.

Spedding, G. (1990). Isolation and analysis of ribosomes from prokaryotes, eukaryotes, and organelles. Ribosomes and Protein Synthesis - A Practical Approach. G. Spedding. Oxford, IRL. **59:** 1-29.

Steitz, T. A. (2005). "On the structural basis of peptide-bond formation and antibiotic resistance from atomic structures of the large ribosomal subunit." FEBS Lett **579**(4): 955-8.

Sternlicht, H., G. W. Farr, M. L. Sternlicht, J. K. Driscoll, K. Willison and M. B. Yaffe (1993). "The t-complex polypeptide 1 complex is a chaperonin for tubulin and actin in vivo." Proc Natl Acad Sci U S A **90**(20): 9422-6.

Stoller, G., K. P. Rucknagel, K. H. Nierhaus, F. X. Schmid, G. Fischer and J. U. Rahfeld (1995). "A ribosome-associated peptidyl-prolyl cis/trans isomerase identified as the trigger factor." Embo J **14**(20): 4939-48.

Stryer, L. (1968). "Fluorescence spectroscopy of proteins." Science **162**: 526-533.

Suno, R., H. Taguchi, R. Masui, M. Odaka and M. Yoshida (2004). "Trigger factor from Thermus thermophilus is a Zn2+-dependent chaperone." J Biol Chem **279**(8): 6380-4.

Taniuchi, H. and C. B. Anfinsen (1969). "An experimental approach to the study of the folding of staphylococcal nuclease." J Biol Chem **244**(14): 3864-75.

Terada, K., M. Kanazawa, B. Bukau and M. Mori (1997). "The human DnaJ homologue dj2 facilitates mitochondrial protein import and luciferase refolding." J Cell Biol **139**(5): 1089-95.

Teter, S. A., W. A. Houry, D. Ang, T. Tradler, D. Rockabrand, G. Fischer, P. Blum, C. Georgopoulos and F. U. Hartl (1999). "Polypeptide flux through bacterial Hsp70: DnaK cooperates with trigger factor in chaperoning nascent chains." Cell **97**(6): 755-65.

Tomic, S., A. E. Johnson, F. U. Hartl and S. A. Etchells (2006). "Exploring the capacity of trigger factor to function as a shield for ribosome bound polypeptide chains." FEBS Lett **580**(1): 72-6.

Troullier, A., D. Reinstadler, Y. Dupont, D. Naumann and V. Forge (2000). "Transient non-native secondary structures during the refolding of alpha-lactalbumin detected by infrared spectroscopy." Nat Struct Biol **7**(1): 78-86.

Udgaonkar, J. B. and R. L. Baldwin (1990). "Early folding intermediate of ribonuclease A." Proc Natl Acad Sci U S A **87**(21): 8197-201.

Ullers, R. S., J. Luirink, N. Harms, F. Schwager, C. Georgopoulos and P. Genevaux (2004). "SecB is a bona fide generalized chaperone in Escherichia coli." Proc Natl Acad Sci U S A **101**(20): 7583-8.

Uversky, V. N., J. R. Gillespie and A. L. Fink (2000). "Why are "natively unfolded" proteins unstructured under physiologic conditions?" Proteins **41**(3): 415-27.

Vainberg, I. E., S. A. Lewis, H. Rommelaere, C. Ampe, J. Vandekerckhove, H. L. Klein and N. J. Cowan (1998). "Prefoldin, a chaperone that delivers unfolded proteins to cytosolic chaperonin." Cell **93**(5): 863-73.

Valent, Q. A., D. A. Kendall, S. High, R. Kusters, B. Oudega and J. Luirink (1995). "Early events in preprotein recognition in E. coli: interaction of SRP and trigger factor with nascent polypeptides." Embo J **14**(22): 5494-505.

Van Montfort, R., C. Slingsby and E. Vierling (2001). "Structure and function of the small heat shock protein/alpha-crystallin family of molecular chaperones." Adv Protein Chem **59**: 105-56.

Vendruscolo, M. and C. M. Dobson (2005). "Towards complete descriptions of the free-energy landscapes of proteins." Philos Transact A Math Phys Eng Sci **363**(1827): 433-50; discussion 450-2.

Vetsch, M., C. Puorger, T. Spirig, U. Grauschopf, E. U. Weber-Ban and R. Glockshuber (2004). "Pilus chaperones represent a new type of protein-folding catalyst." Nature **431**(7006): 329-33.

Vorderwulbecke, S., G. Kramer, F. Merz, T. A. Kurz, T. Rauch, B. Zachmann-Brand, B. Bukau and E. Deuerling (2004). "Low temperature or GroEL/ES overproduction permits growth of Escherichia coli cells lacking trigger factor and DnaK." FEBS Lett **559**(1-3): 181-7.

Wegrzyn, R. D., D. Hofmann, F. Merz, R. Nikolay, T. Rauch, C. Graf and E. Deuerling (2005). "A conserved motif is prerequisite for the interaction of NAC with ribosomal protein L23 and nascent chains." J Biol Chem.

Weibezahn, J., C. Schlieker, P. Tessarz, A. Mogk and B. Bukau (2005). "Novel insights into the mechanism of chaperone-assisted protein disaggregation." Biol Chem **386**(8): 739-44.

Wiedmann, B., H. Sakai, T. A. Davis and M. Wiedmann (1994). "A protein complex required for signal-sequence-specific sorting and translocation." Nature **370**(6489): 434-40.

Wildegger, G. and T. Kiefhaber (1997). "Three-state model for lysozyme folding: triangular folding mechanism with an energetically trapped intermediate." J Mol Biol **270**(2): 294-304.

Wilkinson, B. and H. F. Gilbert (2004). "Protein disulfide isomerase." Biochim Biophys Acta **1699**(1-2): 35-44.

Wimberly, B. T., D. E. Brodersen, W. M. Clemons, Jr., R. J. Morgan-Warren, A. P. Carter, C. Vonrhein, T. Hartsch and V. Ramakrishnan (2000). "Structure of the 30S ribosomal subunit." Nature **407**(6802): 327-39.

Winter, R. and F. Noll (1998). Methoden der Biophysikalischen Chemie. Stuttgart, Germany, Teubner.

Woolhead, C. A., P. J. McCormick and A. E. Johnson (2004). "Nascent membrane and secretory proteins differ in FRET-detected folding far inside the ribosome and in their exposure to ribosomal proteins." Cell **116**(5): 725-36.

Yaffe, M. B., G. W. Farr, D. Miklos, A. L. Horwich, M. L. Sternlicht and H. Sternlicht (1992). "TCP1 complex is a molecular chaperone in tubulin biogenesis." Nature **358**(6383): 245-8.

Yan, W., B. Schilke, C. Pfund, W. Walter, S. Kim and E. A. Craig (1998). "Zuotin, a ribosome-associated DnaJ molecular chaperone." Embo J **17**(16): 4809-17.

Ying, B. W., H. Taguchi, M. Kondo and T. Ueda (2005). "Co-translational involvement of the chaperonin GroEL in the folding of newly translated polypeptides." J Biol Chem **280**(12): 12035-40.

Yonath, A. (2005). "Ribosomal crystallography: peptide bond formation, chaperone assistance and antibiotics activity." Mol Cells **20**(1): 1-16.

Young, J. C., V. R. Agashe, K. Siegers and F. U. Hartl (2004). "Pathways of chaperone-mediated protein folding in the cytosol." Nat Rev Mol Cell Biol **5**(10): 781-91.

Young, J. C., J. M. Barral and F. Ulrich Hartl (2003). "More than folding: localized functions of cytosolic chaperones." Trends Biochem Sci **28**(10): 541-7.

Young, J. C., I. Moarefi and F. U. Hartl (2001). "Hsp90: a specialized but essential protein-folding tool." J Cell Biol **154**(2): 267-73.

Yusupov, M. M., G. Z. Yusupova, A. Baucom, K. Lieberman, T. N. Earnest, J. H. Cate and H. F. Noller (2001). "Crystal structure of the ribosome at 5.5 A resolution." Science **292**(5518): 883-96.

Yusupova, G. Z., M. M. Yusupov, J. H. Cate and H. F. Noller (2001). "The path of messenger RNA through the ribosome." Cell **106**(2): 233-41.

Zeng, L. L., L. Yu, Z. Y. Li, S. Perrett and J. M. Zhou (2005). "Effect of C-terminal truncation on the molecular chaperone function and dimerization of Escherichia coli trigger factor." Biochimie.

Zhu, X., X. Zhao, W. F. Burkholder, A. Gragerov, C. M. Ogata, M. E. Gottesman and W. A. Hendrickson (1996). "Structural analysis of substrate binding by the molecular chaperone DnaK." Science **272**(5268): 1606-14.

VII APPENDICES

VII.1 Primer sequences and features

Name	Direction	Sequence	
TFP1B	fwd	**ATGCAAGTTTCAGTTGAAACCACTC**	
TFP2	rev	TGCGGTCGACTTA**ATAAACTTCAAACTCTACAGAGTAAG**	*Sal* I
TFP3	rev	TGCGGTCGACTTA**CGCCTGCTGTTTACGCAGAG**	*Sal* I
TFP4	rev	TGCGGTCGACTTA**CGCCTGCTGGTTCATCAG**	*Sal* I
Not-TFC	fwd	ATTTGCGGCCGCCGGT**GAACTGCCGGAACTG**	*Not* I, Gly
XbaI-stop-TFC	rev	GCTCTAGATTA**CGCCTGCTGGTTC**	
SpeNot-TFN	rev	ATTTGGCGGCCGCACTAGTGCC**GGTCGCCTGCTGTTTACG**	*Not* I, *Spe* I, Ala
SpeNot-TFN150C	rev	ATTTGGCGGCCGCACTAGTGCC*ACA***CGCCTGCTGTTTACG**	*Not* I, *Spe* I, Ala, *T150C*

Table A1: Primers utilized for cloning the TF and NC expression contructs. Sequences complementary to the TF-ORF are shown in bold face. Stop codons are red, endonuclease restriction sites introduced by the primers are blue and green, the respective endonuclease is listed in the last column. Underlined residues represent codons that introduce additional amino acids into the TF sequence. In magenta italics, the codon leading to the T150C mutation is highlighted.

Name	Sequence	
T150C fw	ACAGCAG***GCATGC***TGGAAAGAAAAAGACGGCGCTGTTG	*Sph* I
T150C rv	CTTTTTCTTTCCA***GCATGC***CTGCTGTTTACGCAGAGTATCCAG	
E326C fw	TCGGTGG***CAATTGC***AAACAAGCTCTGGAACTGCCGCGAAC	*Mfe* I
E326C rv	GAGCTTGTTT***GCAATTG***CCACCGAAACGCTGTGCAGCCTG	
S376C fw	GAAGAGATG***GCATGC***GCGTACGAAGATCCGAAAGAAGTTATC	*Sph* I
S376C rv	CTTCGTACGC***GCATGC***CATCTCTTCGATCAGGCCTTTCAC	

Table A2: Primers utilized for site-directed mutagenesis on TF. Residues that introduce the mutation are highlighted red. The cysteine-codon is underlined. The endonuclease restriction site introduced by site-directed mutagenesis is shown in italics, the respective endonuclease is listed in the last column.

Name	Direction	Sequence
I27 F- NdeI	fwd	AGGAGATATACATATGCATC
I27 R- SpeI	rev	GGACTAGTCAATTCTTTCACTTTC

Table A3: Primers utilized for the generation of an I27-expression plasmid.
The restriction sites introduced by the primers are underlined. The *Nde* I-site in I27 F-NdeI contains the start-codon for the I27-ORF.

Name	Sequence
LucFwd1	AAGGAGATATACCA**ATGGAAGACGCCAAAAACATAAAG**
LucRev1	TATTCATTA**ATCTCTGGCATGCGAGAATCTGA**
LucFwd2	AAGGAGATATACCAATG**CCTATTTTTGGCAATCAAATC**
LucRev2	TATTCATTA**GTCAACTATGAAGAAGTG**
LucFwd3	AAGGAGATATACCAATG**CGCTTGAAGTCTTTAATTAAATAC**
LucRev3	TATTCATTA**CAATTTGGACTTTCCGCCCTTC**
LucRev3s	ACCACCATA**CAATTTGGACTTTCCGCCCTTC**

Table A4: Sequences of primers utilized to generate linear templates for translation of FL fragments.
Sequences complementary to the pLuc template plasmid are shown in bold face. Stop-codons are in red. Adapter-sequences complementary to the Universal Primer are underlined.

Name	Sequence	translated product
I27-N25	CTTTTCCACTTCTATTAGGCATG	25 aa, stalled
I27-N38	GGCTGTTTCACCAACAAACAC	38 aa, stalled
I27-N58	CTGTCCTTTCAGCTTCCACTG	58 aa, stalled
I27-N78	GATCAGAATATGCTTCTTTCCATC	78 aa, stalled
I27-N98	TTTGGTATTAGCAGCCTGGAAG	f. l., stalled
I27-30	TTCTCCTTTACCGATCGCGGCC	f. l. + 30 aa, stalled
I27-40	AAGAATTGGGACAACTCCAGTG	f. l. + 40 aa, stalled
I27-50	GTGCCCATTAACATCACCATC	f. l. + 50 aa, stalled
I27-30TAA	TTATTCTCCTTTACCGATCGCGGCC	f. l. + 30 aa
I27-40TAA	TTAAAGAATTGGGACAACTCCAGTG	f. l. + 40 aa
I27-50TAA	TTAGTGCCCATTAACATCACCATC	f. l. + 50 aa
T7-uni	GAAATTAATACGACTCACTATAG	(forward primer)

Table A5: Primers utilized to generate linear templates for in vitro translations of I27-fragments.
Stop codons on the primers are in red. All primers except T7-uni are reverse-primers. In the last column, the length of the I27-fragment is listed that is encoded by the PCR-product generated with the respective reverse primer in combination with the T7-uni primer.

Name	Sequence
L13P1	GGAATTCCGCAGTCAGCATGACTATATTGCGCTC
L13P2	GCTCTAGACGCTCGAGGATGTCAAGAACTTGCGGTTGCTGTGC
L13P3	GAGCCAATCAATTCTTGCGGAGCCATGGGCACAGCAACCGCAAGTTCTTGACATC
L13P4	GCTCTAGACTGCCGGAGCAGAAGCCAATTAACGTTTG
L17P1	GGAATTCCAGCCCTGTGGAGCGTATTGCCTAC
L17P2	GCTCTAGACGCTCGAGCTCTGCAGCAGCTTCTGCTTTCTCTGAACG
L17P3	GAGCCAATCAATTCTTGCGGAGCCATGGCGTTCAGAGAAAGCAGAAGCTGCTGCAGAG
L17P4	GCTCTAGAGCTTCAATTCCAGTAATGACAATCGACGGC
L20P1	GGAATTCCCGCGGTCGTGAGATGGCGCACCAG
L20P2	GCTCTAGACGCTCGAGTGCCAGAGCTGCTTTCGCTTTTTCAACCAGAGCGGTG
L20P3	GAGCCAATCAATTCTTGCGGAGCCATGGCACCGCTCTGGTTGAAAAAGCGAAAGCAGCTCTGGCA
L20P4	GCTCTAGAGGCTAATGGCCGCCTTCGCACTGGCAAC
L22P1	CGAGCTCCACGCTGGCGTGGTGTTCGTCCGAC
L22P2	GCTCTAGACGCTCGAGGCGATCGGACACAACCACAGTGATGTGGC
L22P3	GAGCCAATCAATTCTTGCGGAGCCATGGGCCACATCACTGTGGTTGTGTCCGATCGC
L22P4	GCTCTAGACCGCGCCGCCCAGACGGCCGCTAACTTCAAC
tetP1	CTCATGTTTGACAGCTTATCATC
tetP2	CATGCCATGGCTCCGCAAGAATTGATTGGCTC
FHfw	TCGAGGGCAGCGGCGACTACAAGGACGACGATGACAAGGGCAGCGGCCATCATCATCATCATCATTAAGC
FHrv	GGCCGCTTAATGATGATGATGATGATGGCCGCTGCCCTTGTCATCGTCGTCCTTGTAGTCGCCGCTGCCC

***Table A6: Sequences of primers utilized for the introduction of an FH-tag into ribosomal protein genes*.**

L13P1 – L13P4, L17P1 – L17P4, L20P1 – L20P4 and L22P1 – L22P4 were used to amplify ribosomal protein genes with 5'- and 3'-flanking sequences. tetP1 and tetP2 were used to amplify the *tet*^{R}-gene. FHfw and FHrv are oligonucleotides that encode the FH-tag.

VII.2 Plasmid maps and protein sequences

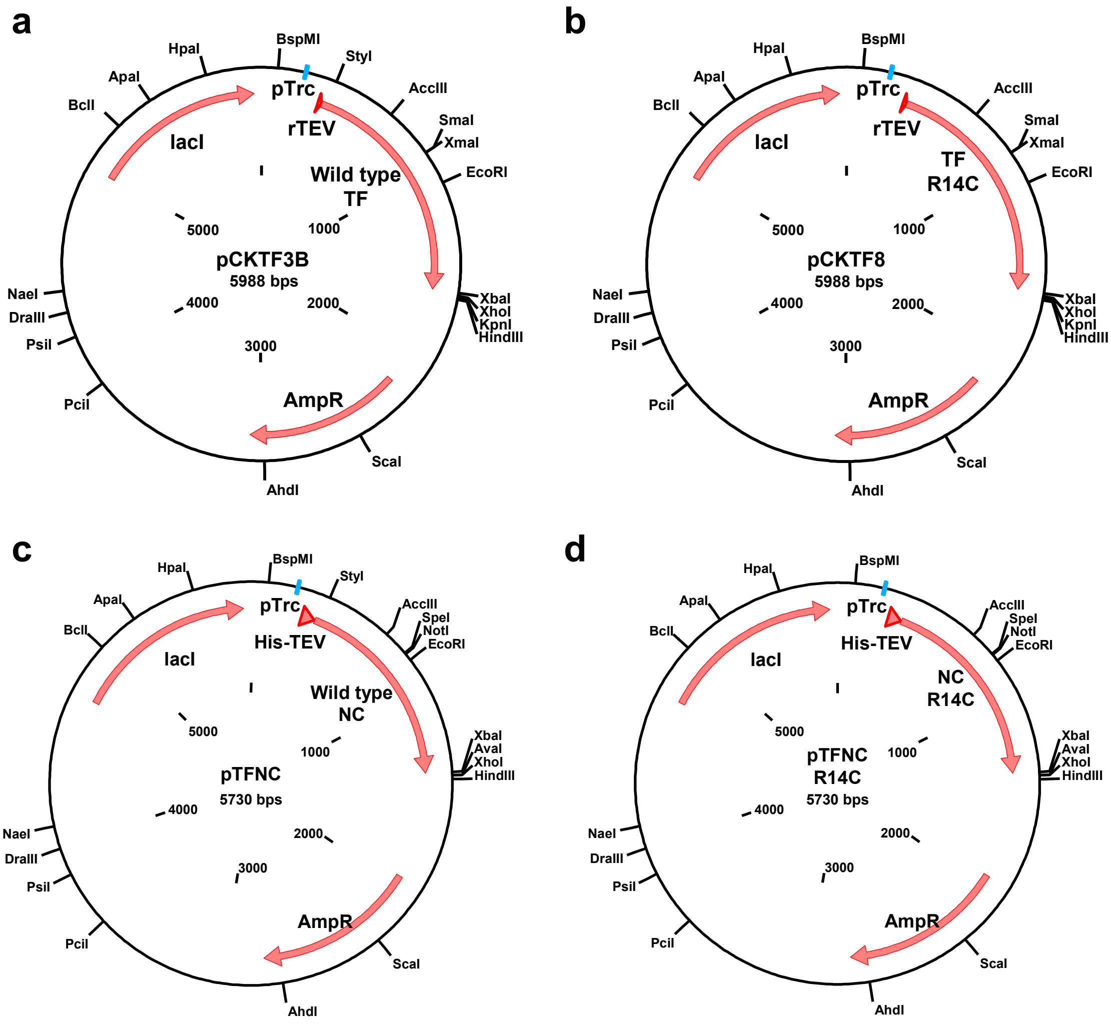
a
BspMI
StyI
HpaI
ApaI
BclI
AccIII
SmaI
XmaI
EcoRI
pTrc
rTEV
lacI
Wild type
TF
5000
1000
pCKTF3B
5988 bps
4000
2000
3000
NaeI
DraIII
PsiI
XbaI
XhoI
KpnI
HindIII
AmpR
PciI
ScaI
AhdI
b
BspMI
HpaI
ApaI
BclI
AccIII
SmaI
XmaI
EcoRI
pTrc
rTEV
lacI
TF
R14C
5000
1000
pCKTF8
5988 bps
4000
2000
3000
NaeI
DraIII
PsiI
XbaI
XhoI
KpnI
HindIII
AmpR
PciI
ScaI
AhdI
c
BspMI
StyI
HpaI
ApaI
BclI
AccIII
SpeI
NotI
EcoRI
pTrc
His-TEV
lacI
Wild type
NC
5000
1000
pTFNC
5730 bps
4000
2000
3000
XbaI
AvaI
XhoI
HindIII
NaeI
DraIII
PsiI
AmpR
PciI
ScaI
AhdI
d
BspMI
HpaI
ApaI
BclI
AccIII
SpeI
NotI
EcoRI
pTrc
His-TEV
lacI
NC
R14C
5000
1000
pTFNC
R14C
5730 bps
4000
2000
3000
XbaI
AvaI
XhoI
HindIII
NaeI
DraIII
PsiI
AmpR
PciI
ScaI
AhdI

Figure A1: Plasmids for recombinant expression of TF-variants.

On the maps of the pPROEX-HTa based plasmids that were used for overproduction of TF-versions for purification, the unique restriction sites listed as well as other important features are listed: His-TEV: His$_6$-tag and TEV-protease recognition site; lacI: Lac-repressor, pTrc: promoter, AmpR: ampicillin resistance.

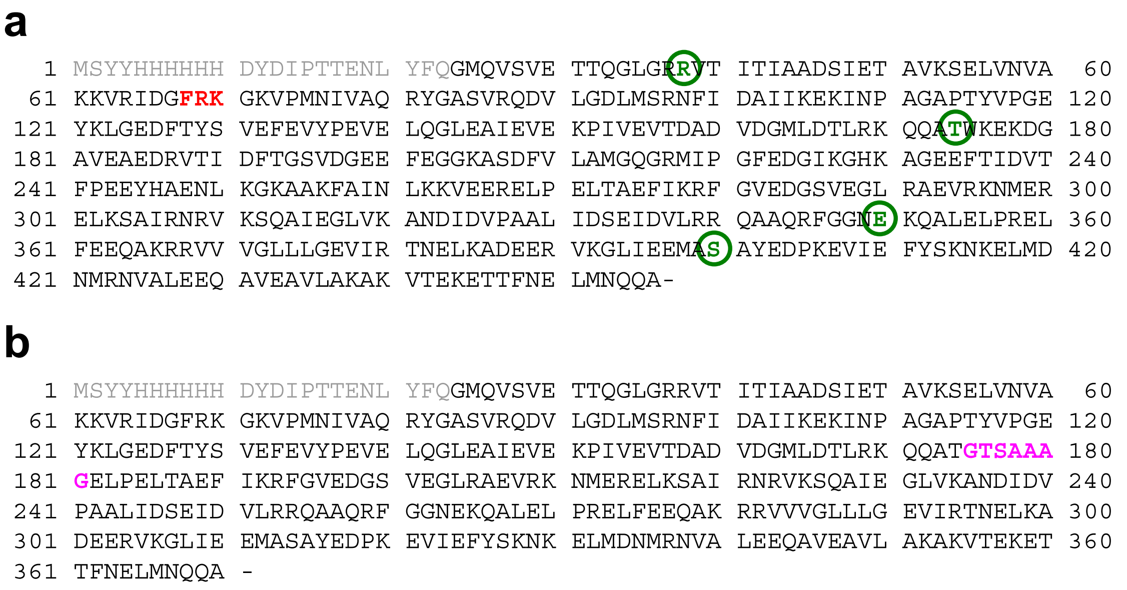

a

```
  1 MSYYHHHHHH DYDIPTTENL YFQGMQVSVE TTQGLGRRVT ITIAADSIET AVKSELVNVA  60
 61 KKVRIDGFRK GKVPMNIVAQ RYGASVRQDV LGDLMSRNFI DAIIKEKINP AGAPTYVPGE 120
121 YKLGEDFTYS VEFEVYPEVE LQGLEAIEVE KPIVEVTDAD VDGMLDTLRK QQATWKEKDG 180
181 AVEAEDRVTI DFTGSVDGEE FEGGKASDFV LAMGQGRMIP GFEDGIKGHK AGEEFTIDVT 240
241 FPEEYHAENL KGKAAKFAIN LKKVEERELP ELTAEFIKRF GVEDGSVEGL RAEVRKNMER 300
301 ELKSAIRNRV KSQAIEGLVK ANDIDVPAAL IDSEIDVLRR QAAQRFGGNE KQALELPREL 360
361 FEEQAKRRVV VGLLLGEVIR TNELKADEER VKGLIEEMAS AYEDPKEVIE FYSKNKELMD 420
421 NMRNVALEEQ AVEAVLAKAK VTEKETTFNE LMNQQA-
```

b

```
  1 MSYYHHHHHH DYDIPTTENL YFQGMQVSVE TTQGLGRRVT ITIAADSIET AVKSELVNVA  60
 61 KKVRIDGFRK GKVPMNIVAQ RYGASVRQDV LGDLMSRNFI DAIIKEKINP AGAPTYVPGE 120
121 YKLGEDFTYS VEFEVYPEVE LQGLEAIEVE KPIVEVTDAD VDGMLDTLRK QQATGTSAAA 180
181 GELPELTAEF IKRFGVEDGS VEGLRAEVRK NMERELKSAI RNRVKSQAIE GLVKANDIDV 240
241 PAALIDSEID VLRRQAAQRF GGNEKQALEL PRELFEEQAK RRVVVGLLLG EVIRTNELKA 300
301 DEERVKGLIE EMASAYEDPK EVIEFYSKNK ELMDNMRNVA LEEQAVEAVL AKAKVTEKET 360
361 TFNELMNQQA -
```

Figure A2: Amino acid sequence of the product translated from TF expression plasmids.

a. Full length TF. The sequence of *E. coli* TF starts at residue 25. The amino-terminal His$_6$-tag and the TEV-protease recognition site (shown in grey) were removed proteolytically after purification of the protein. The residues which have been mutated to cysteines in some of the constructs are shown in green and are encircled. The FRK-motif, which in some of the constructs was mutated to AAA, is shown in red. **b.** Sequence of the NC-version of TF. The residues that constitute the linker that replaces the PPIase domain are highlighted in magenta.

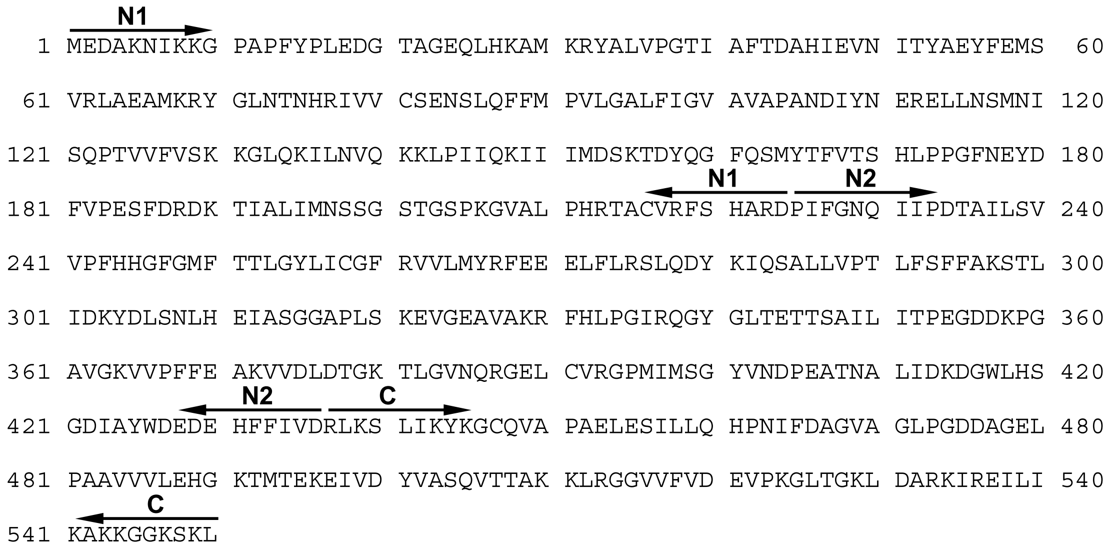
N1
N1
N2
N2
C
C

```
  1 MEDAKNIKKG PAPFYPLEDG TAGEQLHKAM KRYALVPGTI AFTDAHIEVN ITYAEYFEMS  60

 61 VRLAEAMKRY GLNTNHRIVV CSENSLQFFM PVLGALFIGV AVAPANDIYN ERELLNSMNI 120

121 SQPTVVFVSK KGLQKILNVQ KKLPIIQKII IMDSKTDYQG FQSMYTFVTS HLPPGFNEYD 180

181 FVPESFDRDK TIALIMNSSG STGSPKGVAL PHRTACVRFS HARDPIFGNQ IIPDTAILSV 240

241 VPFHHGFGMF TTLGYLICGF RVVLMYRFEE ELFLRSLQDY KIQSALLVPT LFSFFAKSTL 300

301 IDKYDLSNLH EIASGGAPLS KEVGEAVAKR FHLPGIRQGY GLTETTSAIL ITPEGDDKPG 360

361 AVGKVVPFFE AKVVDLDTGK TLGVNQRGEL CVRGPMIMSG YVNDPEATNA LIDKDGWLHS 420

421 GDIAYWDEDE HFFIVDRLKS LIKYKGCQVA PAELESILLQ HPNIFDAGVA GLPGDDAGEL 480

481 PAAVVVLEHG KTMTEKEIVD YVASQVTTAK KLRGGVVFVD EVPKGLTGKL DARKIREILI 540

541 KAKKGGKSKL
```

Figure A3: Amino acid sequence of firefly luciferase.

The boundaries of the three FL domains (N1, N2 and C), which have been translated separately, are indicated by arrows.

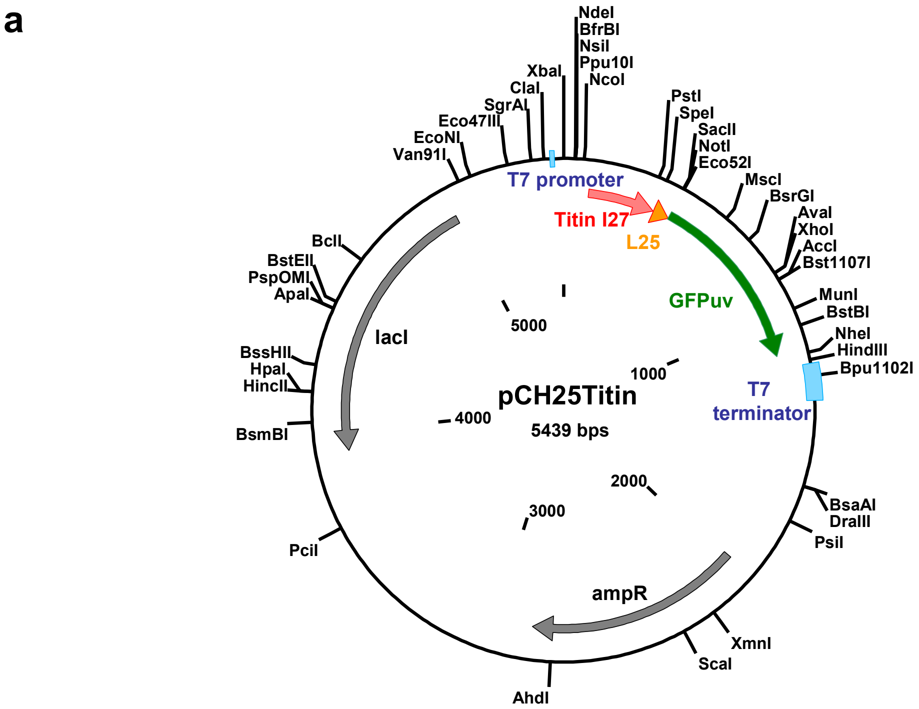
a
NdeI
BfrBI
NsiI
Ppu10I
NcoI
XbaI
ClaI
SgrAI
Eco47III
EcoNI
Van91I
PstI
SpeI
SacII
NotI
Eco52I
MscI
BsrGI
AvaI
XhoI
AccI
Bst1107I
MunI
BstBI
NheI
HindIII
Bpu1102I
T7 promoter
Titin I27
L25
GFPuv
T7
terminator
BclI
BstEII
PspOMI
ApaI
BssHII
HpaI
HincII
BsmBI
lacI
5000
1000
4000
pCH25Titin
5439 bps
2000
3000
PciI
ampR
BsaAI
DraIII
PsiI
XmnI
ScaI
AhdI

b

N25 N38 N58

1 MHHHHHHGSG PWCCCGSACL IEVE**K**PLYGV EVFVGET**A**HF EIELSEPDVH GQWKLKG**Q**PL 60

N78 N98 f.l.

61 AASPDCEIIE DGKKHILI**I**LH NCQLGMTGEV SFQAANT**K**SA ANLKVKE**L**TS GGGGSGGGGS 120

f.l. + 30 f.l. + 40 f.l. + 50

121 GGGGSGGGGS AAAIGKG**E**EL FTGVVPI**L**VE LDGDVNG**H**KF SVSGEGEGDA TYGKLTLKFI 180

Figure A4: Plasmid map of pCH25Titin and amino acid sequence of the translated product.

a. The annotated features in the pCH25Titin plasmid map include the open reading frames of the I27-domain (Titin I27; red) and GFP (GFPuv; green), the linker sequence (L25, orange), the T7-terminator and promoter regions (blue) and the ORFs of the ampicillin resistance gene (ampR) and the LacI-product (lacI; black). **b.** Sequence of the I27-Linker-GFP fusion protein. The arrows start at the residue (shown in bold face) that constitutes the carboxyl-terminal residue of the I27-truncations (see Figure 26).

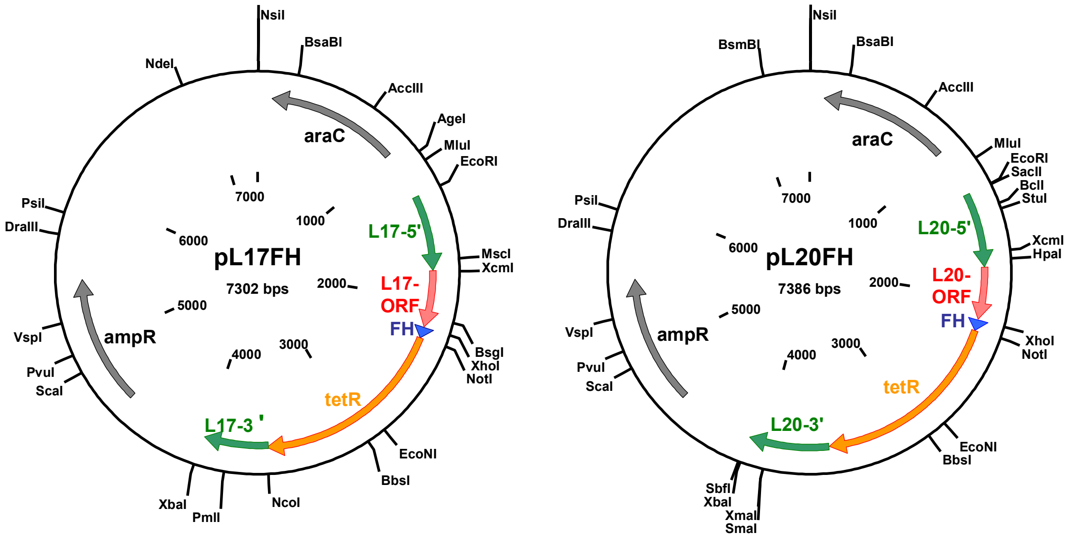
NsiI
BsaBI
NdeI
AccIII
AgeI
MluI
EcoRI
araC
7000
1000
L17-5'
PsiI
DraIII
6000
pL17FH
7302 bps
2000
MscI
XcmI
L17-
ORF
FH
5000
VspI
ampR
4000
3000
BsgI
XhoI
NotI
PvuI
ScaI
tetR
L17-3 '
EcoNI
BbsI
XbaI
PmlI
NcoI
NsiI
BsmBI
BsaBI
AccIII
araC
MluI
EcoRI
SacII
BclI
StuI
7000
1000
L20-5'
PsiI
DraIII
6000
pL20FH
7386 bps
2000
XcmI
HpaI
L20-
ORF
FH
5000
VspI
ampR
4000
3000
XhoI
NotI
PvuI
ScaI
tetR
L20-3'
EcoNI
BbsI
SbfI
XbaI
XmaI
SmaI

Figure A5: Maps pf the plasmids utilized for expression and chromosomal integration of FH-tagged ribosomal protein genes.

Between the *EcoR* I and the *Xba* I site of the plasmids, the following sequences are inserted: ~500 bp of 5'-flanking chromosomal sequence (L17-5' and L20-5'; green) of the respective ORF (L17-ORF and L20-ORF; red), a sequence encoding a FLAG-His$_6$ tag (blue), the ORF encoding the tetracycline resistance protein (tetR, orange) and ~500 bp of the 3'-flanking chromosomal sequence (L17-3' and L20-3'; green) of the respective ORF. The plasmid also contains the ORF for the ampicillin resistance gene (ampR) and the arabinose operon regulatory protein (araC; black).

VII.3 Abbreviations

A	acceptor
aa	amino acid
ADP	adenosine 5'-diphosphate
Amp	ampicillin
APS	ammonium peroxodisulfate
ATP	adenosine 5'-triphosphate
BADAN	6-bromoacetyl-2-dimethyl-aminonaphthalene
BSA	albumin bovine serum
Cam	chloramphenicol
CPM	7-diethylamino-2-(4'-maleimidylphenyl)-4-methylcoumarin
D	donor
DapA	dihydrodipicolinate
DMF	dimethyl-formamide
DMSO	dimethyl-sulfoxide
DNA	deoxyribonucleic acid
DNase	desoxyribonuclease
DTNB	5,5'-dithiobis-(2-nitrobenzoic acid)
DTT	dithiothreitol
E. coli	Escherichia coli
EB	elution buffer
EDTA	ethylenediaminetetraacetic acid
Eno	enolase (2-phosphoglycerate dehydratase)
FL	firefly luciferase
FPLC	Fast Protein Liquid Chromatography
FRET	fluorescence resonance energy transfer
g	acceleration of gravity, 9.81 m/s2
GatD	galactitol-1-phosphate 5-dehydrogenase
GatY	tagatose-1,6-bisphosphate aldolase gatY (TBPA)
GatZ	tagatose 6-phosphate kinase 1
Hsp	heat shock protein
IMAC	Immobilized Metal Affinity Chromatography
IPTG	isopropyl-β-D-1-thiogalactopyranoside
Kan	kanamycin
LB	Luria Bertani
Luc	luciferase
MetF	5,10-methylenetetrahydrofolate
MetK	S-adenosylmethionine synthetase
MreB	Rod shape-determining protein
mRNA	messenger RNA
NAC	nascent chain associated complex
NC	PPIase-deletion mutant of TF
NC-B	BADAN-labeled NC
NC-C	CPM-labeled NC
NC-CF	CPM/fluorescein-labeled NC
NTA	nitrilo-triacetic acid
OAc	acetate

OD	optical density
PAGE	PolyAcrylamide Gel Electrophoresis
PBS	phosphate buffered saline
PCR	Polymerase Chain Reaction
PDB	Protein Data Bank. http://www.rcsb.org/pdb/
PPIase	peptidyl prolyl isomerase
psi	Pound per square inch (6894.76 Pa)
R_0	Förster distance
RAC	ribosome associated complex
RecA	Recombinase A
RNA	ribonucleic acid
RNase A	ribonuclease A
RPL	ribosomal protein of the large subunit
RPS	ribosomal protein of the small subunit
rRNA	ribosomal RNA
S. cerevisiae	Saccharomyces cerevisiae
SAP	shrimp alkaline phosphatase
SDS	sodiumdodecylsulfate
SYT	threonyl-tRNA synthetase (ThrRS)
TCA	trichloroacetic acid
TCEP	tris-(2-carboxyethyl)phosphine
TEMED	N,N,N',N'-tetramethylethylenediamine
Tet	tetracycline
TEV	tobacco etch virus
TF	trigger factor
TF-B	BADAN-labeled TF synthase (DHDPS)
TF-C	CPM-labeled TF reductase
TF-CF	CPM/fluorescein-labeled TF
tig	gene encoding TF
TRiC	TCP1 Ring Complex
Tris-HCl	tris(hydroxymethyl)aminomethane hydrochloride
WT	wild type

VII.4 *Curriculum vitae*

Christian Malte Kaiser
geboren am 4. Dezember 1975 in Hannover

Wissenschaftlicher Werdegang

Okt. 2001 – heute	Experimentelle Doktorarbeit in der Abteilung "Zelluläre Biochemie", Prof. Dr. F. Ulrich Hartl, am Max-Planck-Institut für Biochemie, Martinsried: *Real time observation of TF function on translating ribosomes*

Hochschulstudium

Juni 2001	Diplom Biochemie, Universität Hannover
Nov. 2000 – Mai 2001	Diplomarbeit in der Abteilung "Membranbiochemie", Prof. Dr. D. Oesterhelt, am Max-Planck-Institut für Biochemie, Martinsried: *Untersuchungen am Adhäsin BabA aus dem Humanpathogen Helicobacter pylori*
Okt. 2000	Diplomhauptprüfung Fächer: Biochemie, Biophysikalische Chemie, Pharmakologie
Sept. 1997	Diplomvorprüfung Fächer: Physik, Biologie, Anorganische Chemie, Organische Chemie, Physikalische Chemie, Biochemie
Okt. 1995 – Juni 2001	Studium der Biochemie an der Universität Hannover, Fachbereich Chemie

Hochschulreife

Mai 1995	Allgemeine Hochschulreife, Sophienschule Hannover